OPEN ACCESS

# African Journal of Environmental Science and Technology

December 2021
ISSN 1996-0786
DOI: 10.5897/AJEST
www.academicjournals.org

ACADEMIC JOURNALS
expand your knowledge

## About AJEST

African Journal of Environmental Science and Technology (AJEST) provides rapid publication (monthly) of articles in all areas of the subject such as Biocidal activity of selected plant powders, evaluation of biomass gasifier, green energy, Food technology etc. The Journal welcomes the submission of manuscripts that meet the general criteria of significance and scientific excellence. Papers will be published shortly after acceptance. All articles are peer-reviewed

### Indexing

The African Journal of Environmental Science and Technology is indexed in:
CAB Abstracts, CABI's Global Health Database, Chemical Abstracts (CAS Source Index), China National Knowledge Infrastructure (CNKI), Dimensions Database, Google Scholar, Matrix of Information for The Analysis of Journals (MIAR), Microsoft Academic

AJEST has an h5-index of 14 on Google Scholar Metrics

### Open Access Policy

Open Access is a publication model that enables the dissemination of research articles to the global community without restriction through the internet. All articles published under open access can be accessed by anyone with internet connection.

The African Journal of Environmental Science and Technology is an Open Access journal. Abstracts and full texts of all articles published in this journal are freely accessible to everyone immediately after publication without any form of restriction.

### Article License

# Memberships and Standards

Academic Journals strongly supports the Open Access initiative. Abstracts and full texts of all articles published by Academic Journals are freely accessible to everyone immediately after publication.



Crossref is an association of scholarly publishers that developed Digital Object Identification (DOI) system for the unique identification published materials. Academic Journals is a member of Crossref and uses the DOI system. All articles published by Academic Journals are issued DOI.

Similarity Check powered by iThenticate is an initiative started by CrossRef to help its members actively engage in efforts to prevent scholarly and professional plagiarism. Academic Journals is a member of Similarity Check.

CrossRef Cited-by Linking (formerly Forward Linking) is a service that allows you to discover how your publications are being cited and to incorporate that information into your online publication platform. Academic Journals is a member of CrossRef Cited-by.

Academic Journals is a member of the International Digital Publishing Forum (IDPF). The IDPF is the global trade and standards organization dedicated to the development and promotion of electronic publishing and content consumption.

## Contact


Editorial Office: ajest@academicjournals.org

Help Desk: helpdesk@academicjournals.org

Website: http://www.academicjournals.org/journal/AJEST

Submit manuscript online http://ms.academicjournals.org

Academic Journals
73023 Victoria Island, Lagos, Nigeria
ICEA Building, 17th Floor,
Kenyatta Avenue, Nairobi, Kenya.

# Table of Content

Vol. 15(12), pp. 519-528, December 2021
DOI: 10.5897/AJEST2021.3064
Article Number: 0CCAC4768313
ISSN: 1996-0786

http://www.academicjournals.org/AJEST

ACADEMIC JOURNALS
expand your knowledge

African Journal of Environmental Science and Technology

*Full Length Research Paper*

# An analytical assessment of climate change trends and their impacts on hydropower in Sondu Miriu River Basin, Kenya

**Ochieng Willis Owino*, Oludhe Christopher, Dulo Simeon and Olaka Lydia**

Department of Earth and Climate Sciences, University of Nairobi, Kenya.

Received 3 September, 2021; Accepted 19 October, 2021

**Hydropower is cost effective environment friendly and worldwide proven sustainable energy source. Driven by streamflow stream flows, it is vulnerable to climate change and land use change. The hydropower production from the two-existing run-of-river hydropower projects on the Sondu Miriu River are vulnerable to rainfall variability and requires proper understanding of the climate change trends and policies to support sustainable hydropower development and put in place strategies for building resilience for the local communities. The objective of this paper is to examine climate change trends and their impacts on hydropower in the Sondu Miriu River basin. The methodology involved analysis of downscaled climate data from CORDEX for the period from 1950 to 2100, gridded data from Kenya Meteorological department for a period of 2007 to 2018, river flows data from Water Resources Authority for a period of 2007 to 2018 and hydropower output data from KenGen for a period of 2007 to 2018 to examine the climate change trends within the Sondu Miriu River basin and impacts on hydrology and hydropower. The results indicate that maximum and minimum annual temperature increased by 0.7 and 0.9°C, respectively between 1950 and 2005. Both the maximum and minimum annual temperatures are projected to increase by 1.9°C based on the RCP4.5 and RCP8.5 scenarios between 2006 and 2100 within the Sondu Miriu basin. Annual rainfall increased by 74.8 mm between 1950 and 2005. This is projected to increase by 24.7 and 117.8 mm based on RCP4.5 and RCP8.5 scenarios, respectively. For the period between 2007 and 2018, the observed maximum increased by 5°C while the minimum temperatures decreased by 1°C. The rainfall decreased by 193.14 mm while the mean daily river flows decreased by 0.3 $m^3$/s annually during the same period. This resulted in the decrease of hydropower production by 8.3 GWh in Sondu Miriu HPP between 2007 and 2018 while the production reduced by 14.18 GWh for Sang'oro HPP between 2012 and 2018. Understanding climate change trends within Sondu Miriu River basin should guide the planning for hydropower development projects.**

**Key words:** Climate change, hydropower, Sondu Miriu River basin, downscaling, impacts.

## INTRODUCTION

In the twenty first century, substantial temperature rise is expected because of the projected concentration levels increase of greenhouse gases (GHGs) (Hamududu and Killingtveit, 2012; Kumar et al., 2011; Milly et al., 2005).

*Corresponding author. E-mail: wowino@gmail.com. Tel: +254722861707.

The mean temperature globally is projected through scientific consensus to increase by approximately 3°C by the close of twenty first century because of the current economic and population growth rates. The precipitation levels globally is also expected to accompany this temperature rise by approximately 15% increase (Kumar et al., 2011; Milly, Dunne and Vecchia, 2005). The future global precipitation will affect run-off characteristics and therefore influencing water resources availability (Hamududu and Killingtveit, 2012; Milly et al., 2005). Climate change particularly associated with reduction of rainfall, shortening of rainfall seasons, delayed rainfall onset, increased drought events and rising temperatures are locally perceived to be the main drivers of some changes such as continuous increase in rivers and streams seasonality and progressive reduction in water flows (Kangalawe, 2017).

There is already consensus that water resources availability is expected to be affected globally, regionally, and locally by climate change (Milly et al., 2005). The changes in characteristics of the river flow particularly in timing and quantity usually accompanied by increased reservoirs water losses through evaporation have higher chances to negatively impact on the hydropower generation.

The Eastern African countries except Ethiopia are anticipated to have increase in hydropower generation by 2050 (Hamududu and Killingtveit, 2012). There is expectation of a lot of impacts of climate change on hydropower system operations as well as on the local communities neighbouring the hydropower projects (Harrison et al., 1998). Run-of-river hydropower projects are vulnerable and sensitive to the impacts of climate change such as floods and droughts.

Hydropower constitutes about 38% of the installed electricity generation capacity in Kenya with Sondu-Miriu and Sang'oro hydropower schemes being the most recent to be developed (Kenya Power, 2018). The schemes within the Sondu-Miriu River basin, therefore, offers an opportunity as a case study to learn lessons on integrating climate change adaptation into hydropower developments that results in socioeconomic, environmental, and technical sustainability. As there is still existing potential within Sondu Miriu River basin, this can give guidelines on how to develop future hydropower projects with climate change adaptation fully integrated. Opportunity exists in responding to climate change and awareness enhancement that maintains ecosystem functioning for supporting livelihood and development fundamentally (Shackleton and Shackleton, 2012), and able to motivate new development trajectories (Niang et al., 2014).

The main objective of this paper was to examine climate change trends in Sondu Miriu River basin from 1950 to 2100 and evaluate their impacts on the generation of hydropower in the two-existing run-of-river hydropower projects.

## LITERATURE REVIEW

The design life for hydropower infrastructure is usually more than 100 years and economic design life of 60 years (Kumar et al., 2011). The global energy system is moving towards achieving a less carbon-intensive and sustainable future being a response to the Sustainable Development Goals (SDGs), where a major role is expected to be played by development of hydropower (Zhang et al., 2018).

Electricity supply is projected to affect directly by changing climate through influencing water availability for hydropower generation. Improving the understanding on how water resources availability and temperature are most likely to be impacted on by the changing climate is therefore important (Van Vliet et al., 2016). The general perception that small run-of-river hydropower plants are renewable energy sources associated with little or no environmental impacts has resulted into a global spread of this hydropower technology. Interdisciplinary research progress involving different stakeholders is crucial to harmonize conflicting interests and enable the sustainable development of small run-of-river hydropower plants (Kurigi et al., 2021).

### Climate change and hydrology

During the 21st century, the use of multi-model ensembles in the climate projections has shown that rainfall is projected to increase globally (Milly et al., 2005). Almost all the models project rainfall increases in parts of the tropics (Kumar et al., 2011). The maximum and minimum annual temperatures are also projected to rise by between 0.5 and 3.5°C under the RCP 8.5 with the increase in minimum temperatures being projected to be higher during the cold season of JJAS compared to the MAM and OND rainfall seasons (Olaka et al., 2019). Few studies have examined the possible climate change impacts on hydropower resource potential. Kenya is particularly vulnerable because 38% of installed electricity capacity is based on hydroelectric power.

### Hydropower development in the face of climate change

Climate change impacts on water resources and extreme hydrological events is one of the major challenges for hydropower development (Biao, 2017). Based on the various greenhouse gas emission scenarios, there is evidence that climate change has affected various aspects of water resources and this situation is expected to continue throughout the twenty first century (Shahram et al., 2012). Hydrologic impacts assessment usually relies on spatial downscaling for the translation of large scale GCM projections to the scales that represent more

physical climate change implications (Kopytkovskiy et al., 2015). Hydropower generation and water resources availability are highly influenced by global warming because of increasing global temperatures that alters the rainfall patterns (Shu et al., 2018). Rainfall generally leads to runoff that affects the water availability for use in hydropower generation. The energy system globally is moving towards achievement of sustainable and less carbon-intensive future under the Sustainable Development Goals (SDGs), where development of hydropower will be expected to play a critical role (Zhang et al., 2018).

## Impacts of climate change on hydropower generation

Changes in water resource availability resulting from variations in rainfall, temperature increase, and evaporation rate rise facilitates the escalation of the extreme hydrological events frequency (Qin et al., 2020). It is projected that the fluctuations in streamflow distribution will cause reduction in the net hydropower generation and operation globally under the RCP8.5 scenario near the end of the nineteenth century (Wang et al., 2019; van Vliet et al., 2016). Both the run-of-river and the storage hydropower plants types are affected by spatial and temporal variations in rainfall and temperature, but the storage type of hydropower is stable due to its flexibility provided by its storage capacity while the run-of-river type of hydropower being the most affected due to its sensitivity to any climate change (Hamududu and Killingtveit, 2012; Koch et al., 2011).

Many research projects have been conducted on the climate change impacts on generation of hydropower (Markoff and Cullen, 2008; Madani and Lund, 2010; Hamududu and Killingtveit, 2012; Gaudard et al., 2013; Viola et al., 2015; Arango-Aramburo et al., 2019). On the other hand, only a few research papers on the impacts of hydropower reservoirs on climate change have been published (Wu et al., 2012; Song et al., 2017; Balagizi et al., 2018) because the surface area covered by hydropower reservoirs is low globally (Hunt et al., 2020). The hydropower generation is projected to grow by 75% globally from 2008 to 2050 in the business as usual case while with aggressive actions aimed at reducing the greenhouse gas (GHG) emissions, it could grow by approximately 85% during the same period (Hamududu and Killingtveit, 2017).

Overall, climate change has a possibility of decreasing dry season hydropower potential, while combined effects of deforestation also have the potential of increasing interannual variability. Therefore, incorporation of future climate change and coordination of hydropower reservoir operations should the principle in energy planning for the development of energy portfolios that are more resilient (Arias et al., 2020). For accurate regional quantitative predictions of impacts, analysis of changes in both the temporal distribution of river flows and average river flows is necessary using hydrological models for conversion of climate scenarios time series to runoff scenarios time series (Kumar et al., 2011).

## MATERIALS AND METHODS

### Study area description

Sondu Miriu River basin has got two ROR hydropower projects running. The basin supports various socioeconomic activities within the basin and in the neighbouring basins. It is, therefore, of interest to study the interaction between hydropower development and socioeconomic and environmental activities in this area.

### Study area location and description

Located in the western Kenya, Sondu Miriu River basin is as one of the basins within the Lake Victoria drainage system (Figure 1). There are two run-of-river hydropower projects within the Sondu Miriu basin that draw water from Sondu Miriu River, namely Sang'oro and Sondu Miriu, for generation of hydroelectric power into the Kenya national electricity grid.

The location of Sondu Miriu River basin is geographically confined within latitude 0°17' S and 0°53'S and longitude 34°45'E and 35°45'E. Among the Kenya's river basins draining into Lake Victoria, Sondu Miriu River basin is the fourth largest covering an approximate area of 3,500 $km^2$ (Masese et al., 2012). The main tributaries of the Sondu Miriu River are Yunith and Kapsonoi rivers. Sondu Miriu River originates from the Mau Complex which is an expansive water catchment within Kenya. Diverse development activities and land use types characterize the Sondu Miriu River basin. The development activities and land use include industries, energy, settlements, agriculture, and forestry, among others. The various current existing human activities that have been occurring at different intensities and scales over the years within Sondu Miriu basin have capability to cause a wide range of reaching consequences to several matters in the basin. A number of these issues included general river ecological status, the river system aquatic biodiversity and the various water uses quality. The sedimentation rates that have been observed to be on the increase within Sondu Miriu River have compromised, over the years, the river water quality in the basin (Masese *et al*., 2012).

### Development of climate modelling

Simulation of the present climate to predict the future climate change has resulted into the GCMs development. Despite demonstration of significant skill at hemispheric and continental spatial scales with the incorporation of large proportion of global system complexities, GCMs are not able to represent the local dynamics and features inherently (Xu, 1999). Therefore, for the GCMs to be applied at the local or basin level such as Sondu Miriu River Basin, downscaling techniques for downscaling GCMs outputs are necessary (Xu et al., 2005).

A hierarchy of climate models are applied for the projections of changes in the climate system. These models range from simple to intermediate complexity, comprehensive, and Earth System Models. The simulated changes by these models are done on the basis of a set of anthropogenic (human caused) forcing scenarios. The Representative Concentration Pathways (RCPs) which is a new set of scenarios has been applied for the recent simulations by climate modelling which were carried out under the framework of the Coupled Model Intercomparison Project Phase 5 (CMIP5) by

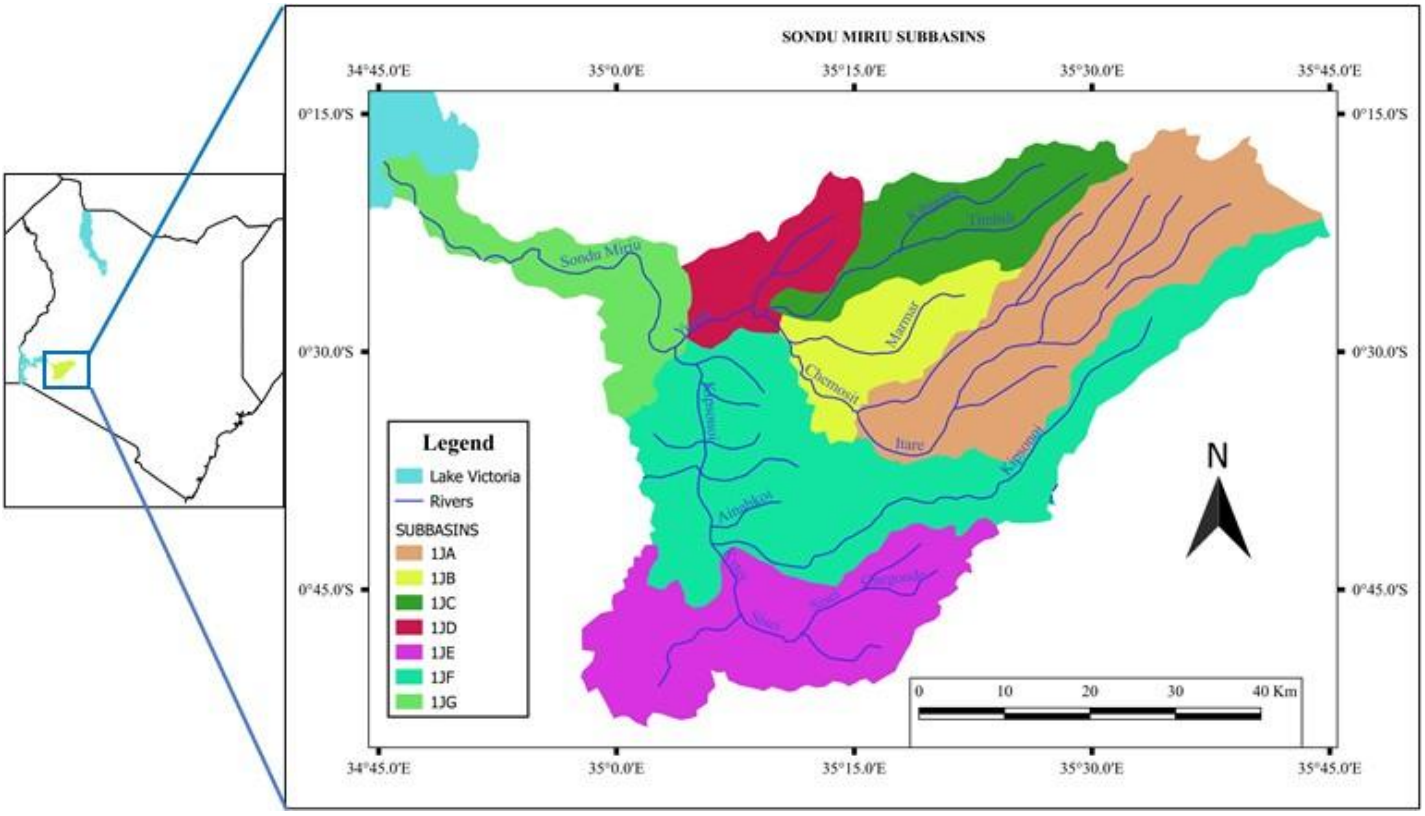


**Figure 1.** Map of Sondu Miriu River basin.
Source: World Resource Institute, 2017

the World Climate Research programme. Many Earth System and comprehensive climate models have taken part in the Coupled Model Intercomparison Project Phase 5, with the results forming the foundation of the climate system projections (IPCC, 2013).

Land use may substantially affect the precipitation and climate regionally (Hunt et al., 2020). These impacts can vary to a larger scale. For instance, precipitation patterns can be affected by converting forest land into agricultural farms (Li et al., 2009; Adnana and Atkinson, 2011; Price, 2011; Hunt et al., 2020), the regional average temperatures can be affected by deforestation (Bonan, 1997; Hunt et al., 2020) alongside other impacts (DeAngelis et al., 2010; Mueller et al., 2016; Chen and Dirmeyer, 2017). Besides land use changes, the regional climate can also be affected by water consumption patterns through evapotranspiration (Hunt and Leal Filho, 2018; Liu et al., 2018; Zou et al., 2018; Hunt et al., 2020). Therefore, water and land management practices have a major influence on climate patterns regionally (Betts, 2001; Tomer and Schilling, 2009). The relationship between climate patterns and land and water management are being proposed as one of the effective regional adaptation measures to manage global warming (Hirsch et al., 2017; Hunt et al., 2020) and to be incorporated into climate models (Li et al., 2018).

**Representative concentration pathways (RCPs)**

The RCPs are scenarios comprising the concentrations and emissions time series of full set of aerosols and greenhouse gases together with gases which are chemically active, including land cover and land use (Moss et al., 2008). Term “representative” implies that every single RCP is only one presentation of the several potential scenarios that can lead to the characteristics of specific radiative forcing. The term “Pathway” puts more emphasis on the trajectory taken during the period to reach the anticipated outcome in addition to the long-term concentration levels (Moss et al., 2010).

The RCPs are references to the concentration pathway section extending to the year 2100, for which the corresponding emission scenarios by the Integrated Assessment Models were produced. The four RCPs that were utilized as the basis for the climate projections and predictions in the latest IPCC Assessment to produce the 5th IPCC Assessment Report were produced from Integrated Assessment Models which were selected from the published literature. The four RCPs included a mitigation scenario leading to forcing levels that are extremely (RCP2.6), stabilization scenarios (RCP4.5 and RCP6), and a scenario considering extremely high greenhouse gas emissions (RCP8.5). Their identification is based on the approximate total radiative forcing such as 2.6 $Wm^{-2}$ for RCP2.6, 4.5 $Wm^{-2}$ for RCP4.5, 6.0 $Wm^{-2}$ for RCP6.0, and 8.5 $Wm^{-2}$ for RCP8.5 (IPCC, 2014).

**Downscaling climate information to regional level**

The necessity for climate change information is a fundamental matter within the climate change discussions. This is especially happening at both the regional and local scale. This information is extremely critical for evaluating the impacts of climate change on the natural systems and human livelihood including coming up with suitable adaptation strategies at both the local and national level

(Giorgi et al., 2009).

Regional climate downscaling (RCD) through the application of both dynamical and statistical tools have been increasingly used in addressing most of the issues relating to climate change. Presently RCD has become a significant methodology for climate change research (Huntingford and Gash, 2005). There has been underutilization of the RCD based products. It is believed that the main reason for this underutilization can be attributed to absence of coordinated framework for evaluating the techniques based on RCD to produce ensemble projections which are of adequate quality that allows for characterization of the underlying uncertainties on climate change projections regionally. These coordinated frameworks exist for global models including the Coupled Model Intercomparison Projects 1-3 (CMIP1-3) or Atmospheric Model Intercomparison Project (AMIP). This has given a lot of benefits to the global climate modelling community immensely from such coordinated activities. The benefits have been in terms of understanding the process, evaluation of the model and generation of the climate change projections. There has been isolation of the studies on RCD which have been continually tied to specific targeted research interests. This has been done to allow for a comprehensive analysis of climate change projections at regional level based on RCD experiments that are not currently available (Giorgi et al., 2009)

Coordinated regional climate downscaling experiment (CORDEX) programme was initiated with an aim of providing a framework for benchmarking for evaluation and possibly improvement of models, on one hand while on the other hand having a set of experiments to provide for exploration to the highest-level possible influence of the various sources of uncertainty. CORDEX, therefore, essentially aims at providing a framework for evaluating and benchmarking model performance (model evaluation framework) as well as designing experiments for producing climate projections suitable for utilization in the studies for impact and adaptation within the framework of climate projection (Giorgi et al., 2009).

Framework for climate projections is currently based on new global model simulations within the CORDEX which were planned to support the IPCC Fifth Assessment Report referred to as CMIP5. These simulations are inclusive of various experiments that range from the 21st century simulations of new GHG scenarios, dekadal prediction experiments and other experiments such as the carbon cycle and the ones aiming at investigations of individual feedback mechanisms (Taylor, 2009).

The methodology applied and the results of the 5-member ensemble simulation of the African climate for the period 1950-2100 using climate modelling system PRECIS carried out over the CORDEX Africa domain suggest that Regional Climate Model (RCM) simulations improve the fit to precipitation and temperature observations in most of the African sub-regions. It should be noted that that the range of RCM projections usually differs from the ones from the GCMs in these regions (Buontempo et al., 2014).

## Climate scenarios

The course spatial scale of GCM outputs for water resources studies is among the primary factors limiting the direct application of climate projections to hydrologic modelling. The development of future projections is usually based on the GCMs at resolutions of hundreds of kilometres which makes them difficult to relate to models at watershed scale (Kopytkovskiy et al., 2015). The climate change projections based on the watershed scale can give indications on the performance of future hydropower generation.

The purpose of climate projection scenarios is to guide researchers in exploring the consequences, which are long term in nature, of the present decisions being made while taking into considerations the inaction within both the socioeconomic and physical systems. The climate projection scenarios provide important reference for emerging research with economic and technological models (Moss et al., 2008). Currently, the research community on climate are applying the four new key scenarios of the Representative Concentration Pathways (RCPs) that give descriptions of a wide range of potential future projections scenarios for the main climate change drivers such as greenhouse gases, land use and air pollutant emissions. The RCP scenarios range from high to low emissions projections (Jubb et al., 2013).

## Data collection

Downscaled climate data from 1950 to 2100, consisting of daily rainfall, minimum temperatures, and maximum temperatures from CORDEX were downloaded from https://cordex.org/data-access/ for the purpose of extracting historical and future climate scenarios for the Sondu Miriu River basin. The gridded daily minimum temperatures, maximum temperatures, and rainfall data for the Sondu Miriu River basin from 2007 to 2018 were obtained from Kenya Meteorological Department (KMD). The daily river flow from and monthly energy generation data from 2007 to 2018 was collected from Water Resources Authority (WRA) and Kenya Electricity Generating Company (KenGen), respectively. The hydropower projects within the Sondu Miriu River basin have been in operation from October 2007.

CORDEX historical and projected climate scenarios were used to compare with the present trends from 1981 to 2018 to facilitate the determination climate change status of over Sondu Miriu River basin. The scenarios were based on the downscaled global circulation models. Scenarios from five models were considered namely Canadian Climate Change Modelling and Analysis (CCCMA), National Centre for Meteorological Research (CNRM), Max Planck Institute for Meteorology (MPI), Model for Interdisciplinary Research on Climate (MIROC), and National Oceanic Atmospheric Observations (NOAA). Ensembles for the five models were used for the analysis of the historical and projected scenarios. The historical scenarios were for the period from 1951 to 2005 while projected scenarios were from 2006 to 2100. The CORDEX projections were used due to their improved fit to observations of precipitation and temperature in most of the African sub regions. CORDEX downscaled projections were based on the Representative Concentration Pathway (RCP) methodology as was adopted by the IPCC for the preparation of the fifth assessment report (IPCC, 2014). For this study, RCP8.5 and RCP4.5 have been adopted as the most likely scenarios. The RCP4.5 represents stabilization scenario while RCP8.5 represents high emission scenario.

## Data analysis

The annual and seasonal trends of climate scenarios (RCP4.5 and RCP 8.5), grided rainfall and temperature data, river flows and electricity output data were determined through trend analysis using Microsoft excel. The data was grouped into annual and seasonal data sets. The data was subjected to curve fitting to capture the trends in climate change and their magnitudes within the Sondu Miriu River basin. Linear curve fitting was adopted to determine the rate of change with time. The curve fitting was performed for all the data sets both annually and seasonally.

The data used for the assessment of climate change impacts on the production of hydropower was from 2008 to 2019 and 2013 to 2019 for Sondu Miriu and Sang'oro, respectively to perform correlation analysis between the climate scenarios and hydropower output. This also considered annual and seasonal changes. Correlation analysis between the observed river flow and observed rainfall was performed to determine the level of influence rainfall over the catchment influences river flow for Sondu Miriu River.

During the same period (2008 – 2018), the observed and projected rainfall and temperature was also compared through correlation analyses and statistical t-test for confidence level to determine the reliability of the climate projection scenarios. T-test was selected as suitable for comparing two groups (flow and rainfall, observed and projected climatic conditions).

## RESULTS AND DISCUSSION

### Historical temperature change over Sondu Miriu River Basin

From 1951 to 2005, there was an annual increase of 0.89 and 0.73°C for minimum and maximum temperatures, respectively. During the same period, the seasonal minimum temperatures increased by 0.81°C for January and February season, 0.83°C for March to May season, 0.85°C June to September season, and 0.96°C for October to December season. The seasonal maximum temperatures also increased by 0.43°C for January and February season, 0.90°C for March to May season, 0.95°C for June to September season and 0.74°C for October to December season. The results have shown that the minimum temperatures have recorded higher rise compared to the maximum temperatures within Sondu Miriu River basin. This is consistent with the findings that the eastern Africa equatorial regions have faced a substantial temperature rise since early 1980s (Anyah and Qiu, 2012) and the Famine Early Warning Systems Network (FEWS NET) reports indicating that over the last 50 years Kenya among other countries has experienced an increase in seasonal mean temperature (Funk et al., 2012).

### Temperature projections over Sondu Miriu River Basin

Within the 21st century, minimum and maximum temperature increases are projected within Sondu Miriu basin. Minimum temperature is expected to rise by about 1.89°C annually the RCP4.5 projection scenario and 4.6°C in the RCP8.5 projection scenario while the maximum temperature in the RCP4.5 projected scenario is projected to increase by 1.85°C annually and in the RCP8.5 projection scenario projected scenario is projected to increase by 4.47°C. In the RCP4.5 projection scenario, seasonal minimum temperatures are projected to increase by 1.86, 1.85, 2.24 and 1.62°C for January to February, March to May, June to September and October to December seasons, respectively while under the RCP8.5 projection scenario the seasonal temperatures are projected to increase by 4.58, 4.23, 5.39 and 4.10°C for January to February, March to May, June to September and October to December seasons, respectively. On the other hand, the seasonal maximum temperatures under the RCP4.5 are projected to increase by 1.76, 1.64, 2.34 and 1.49°C for January to February, March to May, June to September and October to December seasons, respectively while under the RCP8.5 projection scenario the seasonal maximum temperatures are projected to increase by 5.04°C for January and February season, 4.93°C for March to May season, 3.46°C for June to September and 3.71°C for October to December season.

The drier seasons of January to February and June to September are projected to have higher minimum and maximum temperature increase than the long rainfall and short rainfall season under the RCP4.5 projection scenario. This trend applies also to minimum temperatures in the RCP8.5 projection scenario. The first two seasons of the year (January to February and March to May) have higher maximum temperature increase in the RCP8.5 projection scenario than the last two seasons (June to September and October to December) of the year. March to May rainfall season is projected to have higher increase than the October to December rainfall season. Even though the results agree with the earlier findings that minimum temperature increase is projected to be higher for the June to September season than for the long rainfall and short seasons (Olaka et al., 2019), the hot dry (January to February) was omitted in the earlier analysis. Looking at all the four seasons of the year, the cold and dry seasons of the year are projected to experience the highest minimum and maximum increase compared to the rainfall seasons.

Both the minimum and maximum temperatures are projected to increase within the Sondu Miriu River basin within the century. This is expected to enhance the rate of evaporation from open water sources including the main Sondu Miriu River. As a result, the water losses will increase within the basin due to increased water demands from other water users.

### Historical rainfall over Sondu Miriu River Basin

Annual rainfall over Sondu Miriu River basin has increased by about 18.27 mm. The seasonal rainfall has also increased in all the seasons except for the June to September season that has declined. The seasonal rainfall has increased by 1.10 mm for January and February season, 55.55 mm for March to May season, and 36.30 mm for October to December seasons while June to September has decreased by 18.15 mm. Several studies over the eastern Africa region have indicated a decline in rainfall during the March to May and June to September season in the last three to five decades of the 20th century (Funk et al., 2008; Williams and Funk, 2011; Lyon and DeWitt, 2012; Williams et al., 2012; Rowell et al., 2015). The difference in the historical trends is only in the March to May season which may be attributed to spatial variability controlled by a range of physical processes (Rosell and Holmer, 2007; Hession and

Moore, 2011). A study by Rwigi et al. (2016) on the "Assessment of Potential Changes in Hydrologically Relevant Rainfall Statistics over the Sondu River Basin in Kenya Under a Changing Climate" also found out that the observed seasonal rainfall variation in overall indicate a possibility of shifting rainfall patterns where the comparatively dry season of January and February season and short rainfall season of October to December are getting relatively wetter while the long rainfall season of March to May and cold season of June to September are getting relatively drier.

**Projected rainfall over Sondu Miriu River Basin**

The rainfall amount is expected to increase annually within Sondu Miriu River basin in the 21st century by 24.70 mm based on the RCP4.5 projection scenario and by 117.80 mm based on the RCP8.5 projection scenario. This also concurs with the finding of Rwigi et al. (2016) that found out a general tendency of possible increasing rainfall amounts within the Sondu Miriu River basin together with neighbouring basins moving towards future climate periods. Towards 2030 and 2050, more rainfall is projected to be received within Sondu Miriu basin which will be in terms of rainfall days per month having higher probabilities of more wet days per month (Rwigi et al., 2016). The seasonal rainfall is projected to decrease in the June to September by 19.95 mm under the RCP4.5 projection scenario and 40.85 mm under the RCP8.5 projection scenario. The seasonal rainfall is projected to increase by 13.30 mm in the January and February season and by 138.70 mm in the October to December season in the RCP4.5 projection scenario, while for the RCP8.5 projection scenario the projected seasonal increase is by 34.20 mm in the January and February season and 74.10 mm in the October to December season. The March to May seasonal rainfall is projected to decrease by 11.40 mm in the RCP4.5 projection scenario and to increase by 50.35 mm in the RCP8.5 within the 21st century. The findings agree with other recent studies conducted within the region that project rainfall increase within the 21st century including the long rains of March to May season and short rains of October to December season (Moise and Hudson, 2008; Shongwe et al., 2011; Rowell et al., 2015; Olaka et al., 2019). The study also concurs with other studies in the region that the seasonal rainfall for June to September is projected to decline in the 21st century (Patricola and Cook, 2011). A study by Olaka et al. (2019) on "the projected climatic and hydrologic changes to Lake Victoria basin rivers under three RCP emission scenarios for 2015 to 2100 and impacts on the water sector" indicated that the June to September seasonal rainfall is projected to decrease in the RCP8.5 projection scenario but increase in the RCP4.5 projection scenario (Olaka et al., 2019).

**Climate change impacts on hydrology and hydropower generation**

During the period between 2008 and 2019, when the existing two hydropower projects have been in operation within the Sondu Miriu River basin, the annual rainfall has declined. The same trend has been replicated in the seasonal rainfall patterns except the June to September season. The river flow has followed the same pattern with declining annual and seasonal flows except for June to September season. The hydropower output in the two hydropower projects have also followed the same trend whereby the output has been declining annually and in all the seasons except for June to September season. This is an indication that the hydrology and hydropower production will respond to rainfall pattern in the region. This concurs with Olaka et al. (2019) that high variability in projected discharge will have impacts on hydropower production in Sondu Miriu River and this could have the potential to reduce the average electricity production during the drought years (Olaka et al., 2019).

With the rainfall projected to increase within the basin, hydropower generation is expected to remain stable, and this presents an opportunity for more hydropower development within the basin. Generally, the climate change impacts on hydropower output could vary a lot and differ locally, depending on the flow regime change. The impacts of the changing climate are expected to be felt more on the run-of-river hydropower systems compared to other systems with storage (Storage hydropower systems). Since rainfall is projected to increase, storage hydropower systems should be considered to manage the climate variability. A special report on "renewable energy sources and climate change mitigation" by IPCC made a conclusion that the expected overall climate change impacts on existing hydropower generation may be small, or even marginally positive. However, the possibility of substantial variation within countries and even across regions is indicated in results (Berga, 2016).

The correlation between the observed river flows and observed rainfall within the Sondu basin is a strong with an $R^2$ of 0.78, an indication that rainfall data in the basin can be utilised to estimate the streamflow and how it can influence the hydropower production. The strong correlation between the observed rainfall and projected rainfall with $R^2$ of 0.63 for the RCP4.5 projection scenario, and 0.60 for the RCP8.5 projection scenario indicate the reliability of climate change projection scenarios. Therefore, the climate change projections can be used to develop trends that can guide on the future water resource availability for development within the Sondu Miriu River basin.

**Statistical significance**

The statistical test of significance using the t-test has

indicated no significant difference between the streamflow characteristics in Sondu Miriu basin. Based on the period the two run-of-river hydropower projects have been in existence, the t-test for significance indicates no significant difference between the observed and the projected rainfall characteristics within the basin.

## Conclusion

Hydropower development could significantly be undermined by climate change especially for instances where critical resources such as water are threatened, and the incidence and severity of climate extremes such as droughts and floods are increased. The existing hydropower projects in the Sondu Miriu River basin, which are run-of-river type, are vulnerable due to the projected climate variability and climate change in the 21st century. Implementing hydropower projects with storage in the basin can help in adapting to the climate change and climate variability. As the climate change projections indicate that the rainfall is projected to increase as well as temperature, water resources management may be a challenge due to increased evapotranspiration and rainfall variability that may affect the existing run-of-river generation projects in the Sondu Miriu River basin. Putting in place structural and nonstructural measures are required to minimize the impacts. The projected climate change trends can be made use of in determining future availability of water resource within Sondu Miriu River basin for hydropower development by influencing the non-structural and structural measures to be established.

## RECOMMENDATIONS

Both technological and innovative management interventions which are proven through research are required for the management of anticipated changes to minimize the negative impacts climate change may have on the existing hydropower plants in terms of hydropower energy production and future planned hydropower projects in the basin. There should be a close collaboration between the research institutions and the hydropower development institutions interested in the Sondu Miriu River basin to enhance regular updates on climate change trends. This will assist hydropower development institutions in planning appropriately based on the projected climate change trends to minimize any negative impacts that may occur on hydropower generation within the basin. The collaborations should be based on the proposed strategies and backed up by the relevant policy options. The current existing County Development Integrated Plans for the relevant counties should be implemented, monitored, and evaluated based on their effectiveness and improvements suggested to make the better. The research institutions and hydropower development institutions should also actively be involved in the processes for developing policies that are aimed at integrating adaptation into the development of hydropower in particular and energy sector in general at national level and in the relevant counties interacting with Sondu Miriu River basin. Further research is required for understanding the detailed interaction between catchment conservation and management practices and basin climate change characteristics. This will assist in proposing relevant and appropriate strategies and policies to promote climate change adaptation within the Sondu Miriu River basin.

## CONFLICT OF INTERESTS

The authors have not declared any conflict of interests.

### REFERENCES

Adnana NA, Atkinson PM (2011). Exploring the impact of climate and land use changes on streamflow trends in a monsoon catchment. International journal of climatology 31(6):815-831.

Arango-Aramburo S, Turner SW, Daenzer K, Ríos-Ocampo JP, Hejazi MI, Kober T, van der Zwaan B (2019). Climate impacts on hydropower in Colombia: A multi-model assessment of power sector adaptation pathways. Energy Policy 128:179-188.

Arias ME, Farinosi F, Lee E, Livino A, Briscoe J, Moorcroft PR (2020). Impacts of climate change and deforestation on hydropower planning in the Brazilian Amazon. Nature Sustainability 3(6):430-436.

Balagizi CM, Kasereka MM, Cuoco E, Liotta M (2018). Influence of moisture source dynamics and weather patterns on stable isotopes ratios of precipitation in Central-Eastern Africa. Science of the Total Environment 628:1058-1078.

Berga L (2016). The role of hydropower in climate change mitigation and adaptation: a review. Engineering 2(3):313-318.

Betts RA (2001). Biogeophysical impacts of land use on present-day climate: near-surface temperature change and radiative forcing. Atmospheric Science Letters 2(1-4):39-51.

Biao EI (2017). Assessing the impacts of climate change on river discharge dynamics in Oueme River Basin (Benin, West Africa). Hydrology 4(4):47.

Bonan GB (1997). Effects of land use on the climate of the United States. Climatic Change 37(3):449-486.

Buontempo C, Williams K, McSweeney C, Jones R, Mathison C, Wang C (2014). Downscaling a perturbed physics ensemble over the CORDEX Africa domain. In EGU General Assembly Conference Abstracts P. 15909.

Chen L, Dirmeyer PA (2017). Impacts of land-use/land-cover change on afternoon precipitation over North America. Journal of Climate 30(6):2121-2140.

DeAngelis A, Dominguez F, Fan Y, Robock A, Kustu MD, Robinson D (2010). Evidence of enhanced precipitation due to irrigation over the Great Plains of the United States. Journal of Geophysical Research: Atmospheres 115(D15).

Funk C, Dettinger MD, Michaelsen JC, Verdin JP, Brown ME, Barlow M, Hoell A (2008). Warming of the Indian Ocean threatens eastern and southern African food security but could be mitigated by agricultural development. Proceedings of the National Academy of Sciences of the United States of America 105(32):11081-11086.

Funk C, Michaelsen J, Marshall M (2012). Mapping recent decadal climate variations in precipitation and temperature across Eastern Africa and the Sahel. In: Remote Sensing of Drought: Innovative Monitoring Approaches [Wardlow, B.D., M.C. Anderson, and J.P. Verdin (eds.)]. CRC Press, Boca Raton, FL, USA pp. 331-358.

Gaudard L, Gilli M, Romerio F (2013). Climate change impacts on hydropower management. Water resources management

27(15):5143-5156.
Giorgi F, Jones C, Asrar GR (2009). Addressing climate information needs at the regional level: the CORDEX framework. World Meteorological Organization (WMO) Bulletin 58(3):175.
Hamududu B, Killingtveit A (2012). Assessing climate change impacts on global hydropower. Energies 5(2):305-322.
Hamududu B, Killingtveit A (2017). Assessing climate change impacts on global hydropower. In Climate Change and the Future of Sustainability. Apple Academic Press pp. 109-132.
Hession SL, Moore N (2011). A spatial regression analysis of the influence of topography on monthly rainfall in East Africa. International Journal of Climatology 31(10):1440-1456.
Hirsch A., Wilhelm M, Davin EL, Thiery W, Seneviratne SI (2017). Can climate-effective land management reduce regional warming? Journal of Geophysical Research: Atmospheres 122(4):2269-2288.
Hunt JD, Falchetta G, Zakeri B, Nascimento A, Schneider PS., Weber NAB, de Castro NJ (2020). Hydropower impact on the river flow of a humid regional climate. Climatic Change 163(1)379-393.
Hunt JD, Leal FW (2018). Land, Water, and Wind Watershed Cycle: a strategic use of water, land and wind for climate change adaptation. Climatic Change 147(3):427-439.
Huntingford C, Gash J (2005). Climate equity for all. Science *309*(5742):1789-1790.
Intergovernmental Panel on Climate Change (IPCC) (2013). Climate Change 2013 The Physical Science Basis. Contribution of working group I to the fifth assessment report of the intergovernmental panel on climate change (Stocker, T. F., D. Qin, G. K. Plattner, M. Tignor, S. K. Allen, J. Boschung, A. Nauels, Y. Xia, B. Bex, and B. M. Midgley (eds)). Cambridge University Press, Cambridge, United Kingdom and New York, NY, USA, 1535 p.
IPCC (2014). Climate Change (2014). Mitigation of Climate Change. Contribution of Working Group III to the Fifth Assessment Report of the Intergovernmental Panel on Climate Change [Edenhofer, O., R. Pichs-Madruga, Y. Sokona, E. Farahani, S. Kadner, K. Seyboth, A. Adler, I. Baum, S. Brunner, P. Eickemeier, B. Kriemann, J. Savolainen, S. Schlömer, C. von Stechow, T. Zwickel and J.C. Minx (eds.)]. Cambridge University Press, Cambridge, United Kingdom and New York, NY, USA.
Jubb I, Canadell P, Dix M (2013). Representative concentration pathways (RCPs). Australian Government, Department of the Environment.
Kangalawe RY (2017). Climate change impacts on water resource management and community livelihoods in the southern highlands of Tanzania. Climate and Development 9(3):191-201.
Kenya Power (2018). Annual Report and Financial Statements for the Year ended 30th June 2018.
Koch F, Prasch M, Bach, H, Mauser W, Appel F, Weber M (2011). How will hydroelectric power generation develop under climate change scenarios? A case study in the Upper Danube basin. Energies 4(10):1508-1541.
Kopytkovskiy M, Geza M, McCray JE (2015). Climate-change impacts on water resources and hydropower potential in the Upper Colorado River Basin. Journal of Hydrology: Regional Studies 3:473-493.
Kumar A, Schei T, Ahenkorah A, Rodriguez RC, Devernay JM, Freitas M, Hall D (2011). Hydropower. In IPCC Special Report on Renewable Energy Sources and Climate Change Mitigation [O. Edenhofer, R. Pichs-Madruga, Y. Sokona, K. Seyboth, P. Matschoss, S. Kadner, T. Zwickel, P. Eickemeier, G. Hansen, S. Schlomer, C. von Stechow (eds)], Cambridge University Press, Cambridge, United Kingdom and New York, NY, USA.
Kurigi A, Pinheiro AN, Sordo-Ward A, Bejarano MD, Garrote L (2021). Ecological impacts of run-of-river hydropower plants—Current status and future prospects on the brink of energy transition. Renewable and Sustainable Energy Reviews 110833.
Liu T, Yu L, Bu K, Yan F, Zhang S (2018). Seasonal local temperature responses to paddy field expansion from rain-fed farmland in the cold and humid Sanjiang Plain of China. Remote Sensing 10(12):2009.
Lyon B, DeWitt DG (2012). A recent and abrupt decline in the East African long rains. Geophysical Research Letters 39(2):L02702. doi:10.1029/2011GL050337.
Madani K, Lund JR (2010). Estimated impacts of climate warming on California's high-elevation hydropower. Climatic Change 102(3):521-538.
Markoff MS, Cullen AC (2008). Impact of climate change on Pacific Northwest hydropower. Climatic Change 87(3):451-469.
Masese FO, Raburu PO, Kwena F (2012). Threats to the Nyando Wetland. Community Based Approach to the Management of Nyando Wetland, Lake Victoria Basin, Kenya 68 p.
Milly PC, Dunne KA, Vecchia AV (2005). Global pattern of trends in streamflow and water availability in a changing climate. Nature 438(7066):347-350.
Moise AF, Hudson DA (2008). Probabilistic predictions of climate change for Australia and southern Africa using the reliability ensemble average of IPCC CMIP3 model simulations. Journal of Geophysical Research D: Atmospheres 113(15):D15113. doi:10.1029/2007JD009250.
Moss R, Babiker W, Brinkman S, Calvo E, Carter T, Edmonds J, Elgizouli I, Emori S, Erda L, Hibbard K, Jones R (2008). Towards new scenarios for the analysis of emissions: Climate change, impacts and response strategies. Intergovernmental Panel on Climate Change Secretariat (IPCC).
Moss RH, Edmonds JA, Hibbard KA, Manning MR, Rose SK, Van Vuuren DP, Carter TR, Emori S, Kainuma M, Kram T, Meehl GA (2010). The next generation of scenarios for climate change research and assessment. Nature 463(7282):747-756.
Mueller ND, Butler EE, McKinnon KA, Rhines A, Tingley M, Holbrook NM, Huybers P (2016). Cooling of US Midwest summer temperature extremes from cropland intensification. Nature Climate Change 6(3):317-322.
Niang I, Ruppel OC, Abdrabo MA, Essel A, Lennard C, Padgham J, Urquhart P (2014). Africa. In: Climate Change (2014). Impacts, Adaptation, and Vulnerability. Part B: Regional Aspects. Contribution of Working Group II to the Fifth Assessment Report of the Intergovernmental Panel on Climate Change [Barros, V.R., C.B. Field, D.J. Dokken, M.D. Mastrandrea, K.J. Mach, T.E. Bilir, M. Chatterjee, K.L. Ebi, Y.O. Estrada, R.C. Genova, B. Girma, E.S. Kissel, A.N. Levy, S. MacCracken, P.R. Mastrandrea, and L.L. White (eds.)]. Cambridge University Press, Cambridge, United Kingdom and New York, NY, USA pp. 1199-1265.
Olaka LA, Ogutu JO, Said MY, Oludhe C (2019). Projected climatic and hydrologic changes to Lake Victoria Basin Rivers under three RCP emission scenarios for 2015–2100 and impacts on the water sector Water 11(7):1449.
Patricola CM, Cook KH (2011). Sub-Saharan Northern African climate at the end of the twenty-first century: forcing factors and climate change processes. Climate dynamics 37(5-6):1165-1188.
Price K (2011). Effects of watershed topography, soils, land use, and climate on baseflow hydrology in humid regions: A review. Progress in physical geography 35(4):465-492.
Qin P, Xu H, Liu M, Du L, Xiao C, Liu L, Tarroja B (2020). Climate change impacts on Three Gorges Reservoir impoundment and hydropower generation. Journal of Hydrology 580:123922.
Rosell S, Holmer B (2007). Rainfall change and its implications for Belg harvest in South Wollo, Ethiopia. Geografiska Annaler: Series A, Physical Geography 89(4):287-299.
Rowell DP, Booth BB, Nicholson SE, Good P (2015). Reconciling past and future rainfall trends over East Africa. Journal of Climate 28(24):9768-9788.
Rwigi S, Muthama NJ, Opere A, Opijah FJ (2016). Assessment of Potential Changes in Hydrologically Relevant Rainfall Statistics over the Sondu River Basin in Kenya Under a Changing Climate. Journal of Meteorological and Related Sciences 9:2-12.
Shackleton SE, Shackleton CM (2012). Linking poverty, HIV/AIDS and climate change to human and ecosystem vulnerability in southern Africa: consequences for livelihoods and sustainable ecosystem management. International Journal of Sustainable Development and World Ecology 19(3):275-286.
Shahram M, Faridah O, Babak K, Roslan H (2012). Assessing the key factors in climate change studies. International Proceedings of Chemical, Biological and Environmental Engineering (IPCBEE) 28:195-200.
Shongwe ME, van Oldenborgh GJ, van den Hurk B, van Aalst M (2011). Projected changes in mean and extreme precipitation in Africa under global warming. Part II: East Africa. Journal of Climate 24(14):3718-

3733.
Shu J, Qu JJ, Motha R, Xu JC, Dong DF (2018). Impacts of climate change on hydropower development and sustainability: a review. In IOP Conference Series: Earth and Environmental Science. Institute of Physics Publishing.
Song Z, Liang S, Feng L, He T, Song XP, Zhang L (2017). Temperature changes in three gorges reservoir area and linkage with three gorges project. Journal of Geophysical Research: Atmospheres 122(9):4866-4879.
Taylor KE (2009). A summary of the CMIP5 experiment design. http://cmip-pcmdi. llnl. gov/cmip5/docs/Taylor_CMIP5_design. pdf.
Tomer MD, Schilling KE (2009). A simple approach to distinguish land-use and climate-change effects on watershed hydrology. Journal of Hydrology 376(1-2):24-33.
Van Vliet MTH, Van Beek LPH, Eisner S, Flörke M, Wada Y, Bierkens MFP (2016). Multi-model assessment of global hydropower and cooling water discharge potential under climate change. Global Environmental Change 40:156-170.
Viola MR, De Mello CR, Chou SC, Yanagi SN, Gomes JL (2015). Assessing climate change impacts on Upper Grande River basin hydrology, southeast Brazil. International Journal of Climatology 35(6):1054-1068.
Wang H, Xiao W, Wang Y, Zhao Y, Lu F, Yang M, Yang H (2019). Assessment of the impact of climate change on hydropower potential in the Nanliujiang river basin of China. Energy 167:950-959.
Williams AP, Funk C (2011). A westward extension of the warm pool leads to a westward extension of the Walker circulation, drying eastern Africa. Climate Dynamics 37(11-12):2417-2435.
Williams AP, Funk C, Michaelsen J, Rauscher SA, Robertson I, Wils THG, Koprowski M, Eshetu Z, Loader NJ (2012). Recent summer precipitation trends in the Greater Horn of Africa and the emerging role of Indian Ocean Sea surface temperature. Climate Dynamics 39(9-10):2307-2328.
World Resource Institute (2017). https://www.wri.org/resources/data-sets/kenya-gis-data downloaded on 16th January 2017.
Wu J, Gao X, Giorgi F, Chen Z, Yu D (2012). Climate effects of the Three Gorges Reservoir as simulated by a high resolution double nested regional climate model. Quaternary International 282:27-36.
Xu CY (1999). Climate change and hydrologic models: A review of existing gaps and recent research developments. Water Resources Management 13(5):369-382.
Xu CY, Widén E, Halldin S (2005). Modelling hydrological consequences of climate change—progress and challenges. Advances in Atmospheric Sciences 22(6):789-797.
Zhang X, Li HY, Deng ZD, Ringler C, Gao Y, Hejazi MI, Leung LR (2018). Impacts of climate change, policy and Water-Energy-Food nexus on hydropower development. Renewable Energy 116:827-834.
Zou J, Zhan C, Zhao R, Qin P, Hu T, Wang F (2018). Impacts of Water Consumption in the Haihe Plain on the Climate of the Taihang Mountains, North China. Advances in Meteorology 2018.

Vol. 15(12), pp. 529-539, December 2021
DOI: 10.5897/AJEST2021.3071
Article Number: 70B8DD668358
ISSN: 1996-0786

http://www.academicjournals.org/AJEST

ACADEMIC JOURNALS
expand your knowledge

African Journal of Environmental Science and Technology

*Full Length Research Paper*

# Phenology and mechanisms of the early upwelling formation in the southern coast of Senegal

**Malick Wade[1*], Mamadou Thiam[1], Ibrahima Diba[2] and Bouya Diop[1]**

[1]Laboratoire des Sciences de l'Atmosphère et de l'Océan – Matériaux et Dispositifs (LSAO-MED), Université Gaston Berger de Saint-Louis, Sénégal.
[2]Laboratoire d'Océanographie, des Sciences de l'Environnement et du Climat (LOSEC), Université Assane Seck de Ziguinchor, Sénégal.

Received 7 October, 2021; Accepted 9 December, 2021

**Mechanisms of the interannual variability of upwelling onset dates on the Petite-Cote of Senegal are investigated using daily NEMO model data outputs and NOAA ocean surface temperature observations (OISST). We first determined the phenology (onset dates, end dates, duration and occupied area of the upwelling) over the Petite-Côte located in south of the Senegalese coast. Our results show that upwelling in the Petite-Côte starts on average on 03-December (with a standard deviation of 13 days) and ends on average on 13-June (with a standard deviation of 11 days). Upwelling lasts, on average, 6 months in the region. The maximum upwelling intensity is noted on 15-May and the maximum occupied area exhibits a February-May plateau. We then performed a composite analysis based on the earliness of the upwelling setup dates to understand the mechanisms involved. Our results show that for the earliest upwelling years, we note a strengthening of the vertical velocities 3 weeks before the onset of the upwelling but we note especially an abnormal intensification of the coastal jet. The latter seems to be the initiator of the early onset of the upwelling in the region. These reinforcements are associated with a significant decrease in surface temperature (SST) and an intensification of northerly trade winds.**

**Key words:** Upwelling, phenology, Senegalese coast, petite-côte.

## INTRODUCTION

The Senegalese upwelling is the southern part of the Canary Islands upwelling system, which is one of the four major upwelling systems in the world, along with the Benguela in South Africa, California in North America and Peru-Chile (Humboldt) in South America. It consists of an upwelling of deep water towards the surface. Despite a relatively small surface area, less than 1% of the ocean surface, these regions are known for their intense biological productivity. This richness is mainly due to the trade winds that blow parallel to the coast, generating coastal upwelling (Rebert, 1978; Roy, 1989). Coastal and off-shore upwelling result from these northeasterly winds, which drive a zonal Ekman transport under the action of the Coriolis force (Jacox et al., 2018). This transport is indeed divergent, particularly strong at the coast, but also in the ocean interior over a distance depending on latitude (Faye et al., 2015). Mass balance requires compensation by an upward vertical transport of cold and

*Corresponding author. E-mail: malick.wade@ugb.edu.sn. Tel: +221 77 825 93 64. Fax: +221 77 825 93 64.

nutrient-rich waters, which favors the phytoplankton growth (Herbland and Voituriez 1974; Huntsman and Barber, 1977; Bricaud et al., 1987; Van Camp et al., 1991). Indeed, the trade winds are the driving force behind the permanent or seasonal upwellings that develop along the West African coastline, from Morocco to Senegal via Mauritania. The northern trade winds push the waters offshore. According to mass conservation, a vertical flow compensates for this imbalance and brings nutrient-rich deep cold water to the surface. The West African upwelling is very particular (Lathuilière, 2008); among the 4 major upwelling systems, it is probably the less studied. After a major effort in the 1970s, this region has been little studied until fairly recently. Furthermore, the inter-comparison of the 4 upwelling systems shows that the West African Coastal Upwelling is the one that presents both the greatest seasonal variability and the greatest diversity of behavior along the coast. However, the phenology of this system (start date, end date, duration, occupied surface) as well as the behavior of physical parameters before, during and after an upwelling event remain to be studied in depth, especially with data from numerical models that allow a process study. In addition, over the last thirty years, the atmospheric circulation over the tropical Atlantic and the African continent has undergone profound changes, one of the most spectacular consequences was the drought that hit the Sahelian zone from the 1970s (Roy, 1989). These changes can have a significant impact on the marine ecosystem and require a great deal of understanding. This study focuses on the analysis of physical oceanic and atmospheric parameters that initiate the upwelling from the regional circulation model (NEMO) and is part of the general problem of understanding the Senegalese upwelling (especially in the southern part commonly called the Petite Côte, PC) in terms of phenology, variation of basic upwelling parameters (SST, Wind, Currents, Mixing layer, Thermocline) and the effect of possible changes in atmospheric circulation on this part of the Canary Islands system.

Fishing is the main activity of coastal populations. However, the fishing activity depends intrinsically on the intensity of the upwelling (in terms of surface occupied, duration, etc.). In recent years, the fishing activity has decreased dramatically (fishermen often return with low catches) and has important socio-economic consequences (Merem et al., 2019). In the perspective of a good management of the resource and its control, it is important to understand the functioning of the upwelling. In other words, this study will make it possible to understand the inter-annual variability of the Senegalese upwelling in order to be able to prevent possible events of intensification and/or relaxation of the upwelling which is very important for predictability. In this study, we propose to study the following two main questions:

(i) What is on average the duration, the area occupied, the start date, the end date of upwelling in the Petite-Côte?
(ii) What are the physical oceanic and atmospheric parameters that govern the early initiation of upwelling in the Petite-Côte?

## DATA AND METHODS

### Observation

We used the Optimium Interpolation Sea Surface Temperature V2.0 (OISST) ¼° data which can be downloaded at https://psl.noaa.gov/data/gridded/data.noaa.oisst.v2.highres.html. OISST is a daily product of National Oceanic Atmosphere Administration (NOAA); it is an analysis constructed by combining observations from different platforms (satellites, ships, buoys, and Argo floats) on a regular global grid. A spatially complete SST map is produced by interpolation to fill in the gaps. The methodology includes bias adjustment of satellite and ship observations (referenced to buoys) to compensate for platform differences and sensor biases.

There are two types of daily OISSTs, named after the relevant SST satellite sensors. These are the Advanced Very High-Resolution Radiometer (AVHRR) and the Advanced Microwave Scanning Radiometer on the Earth Observing System (AMSR-E). The AVHRR has the longest record (late 1981 to present) of SST measurements from a single sensor design. Infrared instruments, such as AVHRR, can make observations at relatively high resolution but cannot see through clouds. Microwave instruments such as the AMSR-E can measure SST in most weather conditions (with the exception of heavy rain) but not near land.

### ATLTROP025 model interannual simulation

We use also the Nucleus for European Modelling of Ocean (NEMO) model with version 3.6 in this study. It is a general circulation model which, like all OGCMs, tries to solve the primitive Navier-Stokes equations. NEMO was born as part of the new version of Océan PAraléllisé (OPA), (Madec et al., 1998) for ocean dynamics and thermodynamics, Louvain-la-neuve Ice Model (LIM) for atmospheric dynamics and thermodynamics and Tracer in the Ocean Paradigm (TOP) for biogeochemistry (Madec, 2008, 2014). It is then intended to be a flexible tool to study over a wide spatio-temporal spectrum the ocean and its interactions with the other components of the terrestrial climate system (atmosphere, sea ice, biogeochemical tracers etc...). The prognostic variables are the three-dimensional velocity field (u, v, w), sea surface height (linear or not), temperature and salinity. The distribution of the variables is done on a three-dimensional Arakawa C-grid using a vertical z-coordinate (with integer or partial levels), or an s-coordinate (which takes into account the topography), or a combination of both.

The outputs used in this study are daily and cover the period 1990-2015. The regional grid of 1/4° horizontal resolution encompasses the tropical Atlantic (35°S - 35°N, 100°W - 15°E). It has 75 irregular levels on the vertical, 12 levels in the upper 20 m and 24 levels in the first 100 m. This configuration has already been described in detail in Hernandez et al. (2016), a study in which it is shown that the NEMO v3.6 model successfully reproduces the mean state of the tropical Atlantic and sea surface cooling following tropical storms and hurricanes west of the region. Beyond the validation done by Hernandez et al. (2016), we compared the mean state of the NEMO model data with that of the OISST observations. We clearly see that the model is able to reproduce the mean state of the tropical Atlantic (Figure 1).

Lateral boundaries are forced with daily outputs from the

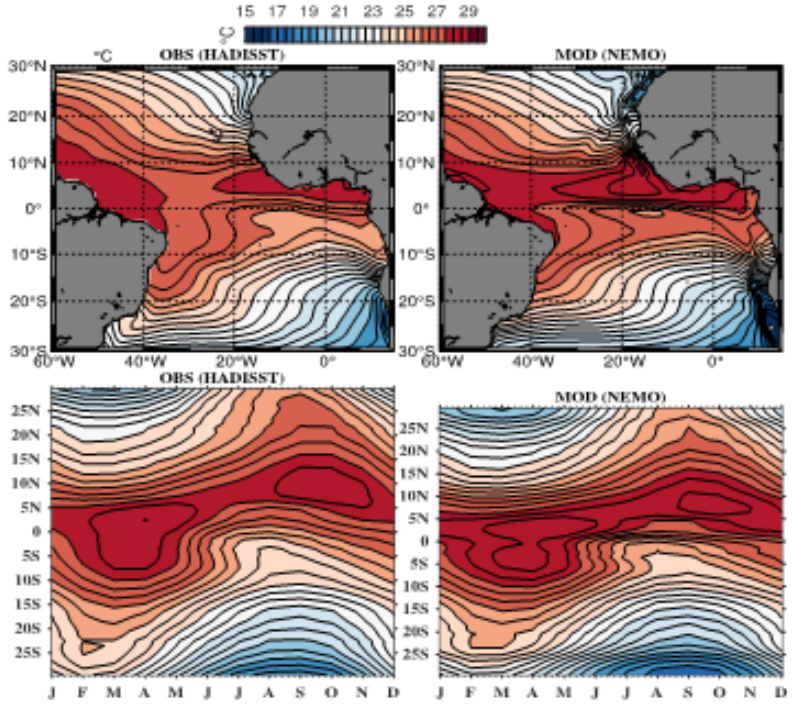


**Figure 1.** Annual mean surface temperature (top) and hovmöller diagram (bottom) of the Atlantic Ocean for the observation and the model.

MERCATOR GLORYS2V3 global reanalysis. Details of the method are given in Madec (2014). At the surface, atmospheric fluxes of momentum, heat, and freshwater are provided by bulk formulas (Large and Yeager, 2009). The model is forced with the DFS5.2 product (Dussin et al., 2014) which is based on the ERA-interim reanalysis (Dee et al., 2011) and consists of 3 h fields of wind speed, temperature, atmospheric humidity, daily longwave, shortwave and precipitation fields.

The model reference experiment is initialized with temperature and salinity climatology provided by World Ocean Atlas (WOA98) from Levitus et al. (1998) and is integrated over the period 1979-2012. For more information, the reader can use the following address http://www.nemo-ocean.eu.

## Methodology

We first calculated the anomalies of the atmospheric and oceanic variables. These anomalies are obtained by removing from the raw value, the seasonal cycle over the whole period. We then calculated all the indices averaged in the study area shown by the black rectangle in Figure 2. We show also in Figure 2, the standard deviation of sea surface temperature and note that its maximum is located along the Senegalese-Mauritanian coasts, which shows a very high variability of the SST in these regions. The annual mean surface winds are superimposed and show mainly a northeast direction.

Several indices have been developed to quantify the upwelling phenomenon. These indices are often based on surface data, especially satellite data, and are essential to characterize the upwelling phenomenon in terms of spatio-temporal intensity. In the literature, four upwelling indices are most often used: an upwelling index based on the SST (Demarcq and Faure, 2000; Caniaux et al., 2011), an upwelling index based on winds and an upwelling index based on chlorophyll.

To characterize the cold tongue in the tropical Atlantic, Caniaux et al. (2011) defined an index based on a temperature threshold. Their SST threshold was chosen based on the contour of the isotherms that characterize the upwelling in the cold tongue area of the equatorial Atlantic. This index expresses the cooling intensity and is defined point by point by subtracting the SST for each grid point from a SST threshold within a domain A. The surface $(S_{PC})$ occupied by the upwelling and the intensity $(TI_{PC})$ of the cooling (considered here as the upwelling index) are given respectively by the following relations:

$$S_{PC} = \int_{A(x)} H_e(24°C - SST\,(x))dA$$

$$TI_{PC} = \frac{1}{S_{PC}} \int_{A(x)} (24°C - SST\,(x))\, H_e(24°C - SST\,(x))dA$$

PC stands for the Petite-Côte, A is the area of the region and $H_e$ the Heaviside function defined as follows:

$$H_e = \begin{cases} 1 & if\ SST < 24°C \\ 0 & elsewhere \end{cases}$$

We adopted the same method in our study (as in Caniaux et al.; 2011) to characterize the coastal upwelling index. The threshold temperature chosen, expressing the limit value of the SST at which we consider that the upwelling has started, is taken at 24°C. Note that this threshold SST value is very sensitive to our results but represents a value that allows us to obtain results comparable to those obtained using other methods (Teisson, 1983). Furthermore,

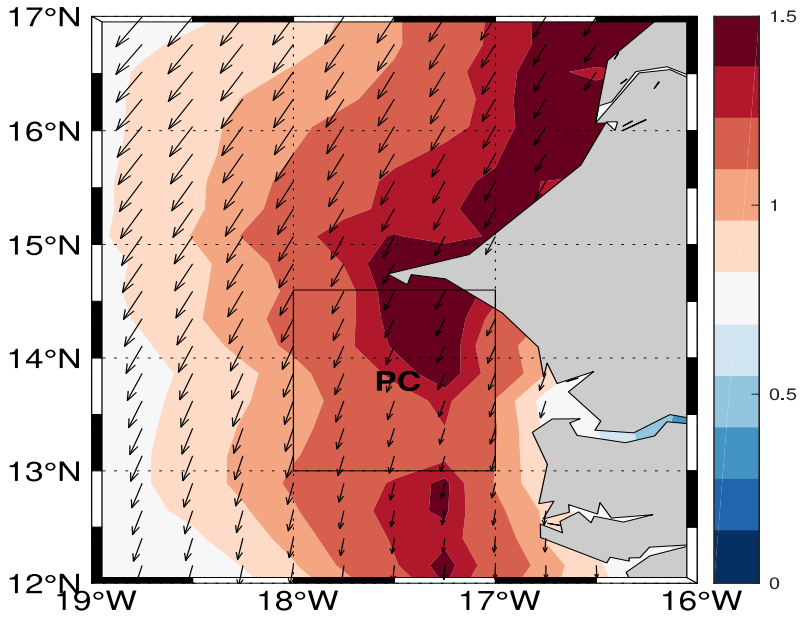


**Figure 2.** Standard deviation of surface temperature from OISST data (color) and annual mean of surface winds (vectors) in the Atlantic Ocean over the period 1990-2015.

the method of Caniaux et al. (2011) is used because it has the advantage of providing, in addition to the start and end dates, the upwelling surface which is important information for understanding the variability of the upwelling in this region.

The start date is obtained, for each year, as the first day when upwelling index is greater than zero and the end dates are obtained as the day when the value of the latter is equal to zero. This is our methodology for characterizing the upwelling phenology (start dates, end dates, surface area, date of maximum area) mentioned in Table 1.

One of the questions we are interested in is the oceanic and atmospheric mechanisms involved during early upwelling years. Thus, we chose to perform a composite analysis based on Table 1. The composite analysis method is a very useful statistical tool to spatially and temporally isolate the average behavior of a large meteorological field with respect to an area of influence that we want to test. This method does not allow to apprehend the complexity of physical processes. In fact, it has certain advantages for extracting signals or interactions from a complex environment. We defined a threshold to characterize the early (late) years by considering the years whose date of onset of the upwelling is less (more) than 1 time the standard deviation below (above) the mean start date. The threshold of 13 days which represents 1 time the standard deviation (Table 1) allows us to isolate early and late upwelling years. Thus, a year is considered as early year if it starts before 21-November and late if it starts after 16-December. The years that do not meet this selection criterion are considered as normal years. From these criteria, we form three groups of samples mentioned in the following Table 2.

We compared our results with the literature and relatively good consistency is found. For example, 2002 and 2006 upwellings are of chosen as case studies years in terms of late upwelling setup (Marin et al., 2009; Polo et al., 2008). Thus, we chose to average 30 days before and 30 days after the onset of upwelling for all atmospheric and oceanic variables to better diagnose the behavior of the parameters for early upwelling years. Finally, for the composite analysis of the different variables, we apply a lanczos filter to the data at intra-seasonal timescale to remove frequencies greater than 90 days.

## RESULTS AND DISCUSSION

### Seasonal cycle of the local atmospheric variables

One of the most important parameters for understanding coastal upwelling is the study of wind speed and direction. Thus, we show in Figure 3, the monthly climatology of wind direction and intensity. From October, the winds begin to intensify and are from North to Northeast in Mauritania but from North to slightly Northwest in the Petite-Côte. From November, the winds are, practically, of North-East sectors along the West African coast and intensify until March. From November, the winds are of North-West sectors in the Senegalese coasts (Figure 3). From April to May, the winds turn to the southeast, weaken in June and have a low intensity or even cancel out over the period from July to September. These results confirm those found by Roy (1989) when he studied the fluctuation and variability of winds along the Senegalese coast over the period 1963-1986 with observation data from weather stations.

On the other hand, the wind frequency map shows that the winds are predominantly northeast from November to March, then predominantly northwest from April to October with a penetration of monsoon winds with a southwest component during the months of June to October (Figure 4). Southeast winds are less frequent in the region and show their weakest maxima in September.

**Table 1.** Phenology of the coastal upwelling in the Petite Côte.

| Year | Mean surface area ($10^4$ km$^2$) | Maximum surface area ($10^4$ km$^2$) | Date of maximum surface area | Upwelling Index $(TI_{PC}, °C)$ | Date of formation | Date of end | Duration (Days) |
|---|---|---|---|---|---|---|---|
| 1991 | 1.6913 | 3.0858 | 31-May-1991 | 0.5534 | 26-Nov-1990 | 28-Jun-1991 | 214 |
| 1992 | 1.4070 | 2.6229 | 25-May-1992 | 0.4959 | 09-Dec-1991 | 12-Jun-1992 | 186 |
| 1993 | 1.4484 | 3.3172 | 18-May-1993 | 0.5014 | 04-Dec-1992 | 11-Jun-1993 | 189 |
| 1994 | 1.7084 | 3.0858 | 20-May-1994 | 0.5726 | 16-Nov-1993 | 22-Jun-1994 | 218 |
| 1995 | 1.3778 | 3.2401 | 12-May-1995 | 0.5096 | 08-Dec-1994 | 12-Jun-1995 | 186 |
| 1996 | 1.3516 | 3.3944 | 10-May-1996 | 0.4767 | 09-Dec-1995 | 01-Jun-1996 | 175 |
| 1997 | 1.5116 | 3.2401 | 25-May-1997 | 0.5288 | 23-Nov-1996 | 14-Jun-1997 | 203 |
| 1998 | 1.5194 | 3.3172 | 19-May-1998 | 0.5178 | 11-Dec-1997 | 21-Jun-1998 | 192 |
| 1999 | 1.4372 | 2.3144 | 13-May-1999 | 0.4959 | 02-Dec-1998 | 04-Jun-1999 | 184 |
| 2000 | 1.4767 | 3.3172 | 20-May-2000 | 0.5370 | 20-Nov-1999 | 18-Jun-2000 | 211 |
| 2001 | 1.4269 | 2.9315 | 14-May-2001 | 0.4932 | 01-Dec-2000 | 31-May-2001 | 181 |
| 2002 | 1.3100 | 3.2401 | 23-May-2002 | 0.4411 | 02-Jan-2002 | 15-Jun-2002 | 164 |
| 2003 | 1.4167 | 3.2401 | 08-May-2003 | 0.5178 | 24-Nov-2002 | 13-Jun-2003 | 201 |
| 2004 | 1.4484 | 2.5458 | 24-May-2004 | 0.4959 | 13-Dec-2003 | 23-Jun-2004 | 193 |
| 2005 | 1.1959 | 3.3172 | 23-Apr-2005 | 0.4438 | 05-Dec-2004 | 17-May-2005 | 163 |
| 2006 | 1.3535 | 3.3172 | 14-May-2006 | 0.4384 | 30-Dec-2005 | 10-Jun-2006 | 162 |
| 2007 | 1.6813 | 3.1629 | 01-Jun-2007 | 0.5397 | 10-Dec-2006 | 08-Jul-2007 | 210 |
| 2008 | 1.4150 | 3.3172 | 21-Apr-2008 | 0.5342 | 26-Nov-2007 | 13-Jun-2008 | 200 |
| 2009 | 1.6414 | 3.1629 | 29-May-2009 | 0.6027 | 02-Nov-2008 | 17-Jun-2009 | 227 |
| 2010 | 1.3098 | 3.0087 | 28-Apr-2010 | 0.4548 | 08-Dec-2009 | 27-May-2010 | 170 |
| 2011 | 1.2724 | 3.2401 | 21-May-2011 | 0.4411 | 23-Dec-2010 | 14-Jun-2011 | 173 |
| 2012 | 1.4444 | 3.3944 | 16-May-2012 | 0.5205 | 23-Nov-2011 | 13-Jun-2012 | 203 |
| 2013 | 1.4977 | 2.7001 | 12-May-2013 | 0.4932 | 02-Dec-2012 | 17-Jun-2013 | 197 |
| 2014 | 1.5222 | 2.8544 | 30-Apr-2014 | 0.5068 | 25-Nov-2013 | 07-Jun-2014 | 194 |
| 2015 | 1.3402 | 3.3172 | 07-May-2015 | 0.4685 | 03-Dec-2014 | 19-Jun-2015 | 198 |
| Mean | 1.4482 | 3.1000 | 15-May | 0.5032 | 03-Dec | 13-Jun | 192 |
| SD | 0.1300 | 0.2800 | 34 | 0.0419 | 13 | 11 | 18 |

## Phenology of upwelling in the Petite-Côte

Figure 5 shows the monthly climatology of the upwelling index and upwelling area calculated from the method of Caniaux et al. (2011). It shows a significant seasonal variation of the index with a maximum noted in March coinciding with the maximum of the average area occupied by the upwelling. Note that the maximum area shows a plateau from January and lasts relatively four months (January to May). On the other hand, the upwelling in the Petie-Côte begins on average on December 3 (with a standard deviation of +/- 13 days) and ends on June 13 (with a standard deviation of +/- 11 days (Figure 5 and Table 2) with a significant daily variance (shaded area). The mean upwelling duration is 192 days (about 6.5 months) and the maximum mean upwelling

**Table 2.** Distribution of early, normal and late upwelling formation in the Petite Côte.

| | |
|---|---|
| **Early upwelling years** | 1994; 2000; 2009 |
| Normal upwelling years | 1991; 1992; 1993; 1995; 1996; 1997; 1998; 1999; 2001; 2003; 2004; 2005; 2007; 2008; 2010; 2012; 2013; 2011; 2015 |
| Late upwelling years | 2002; 2006; 2011 |

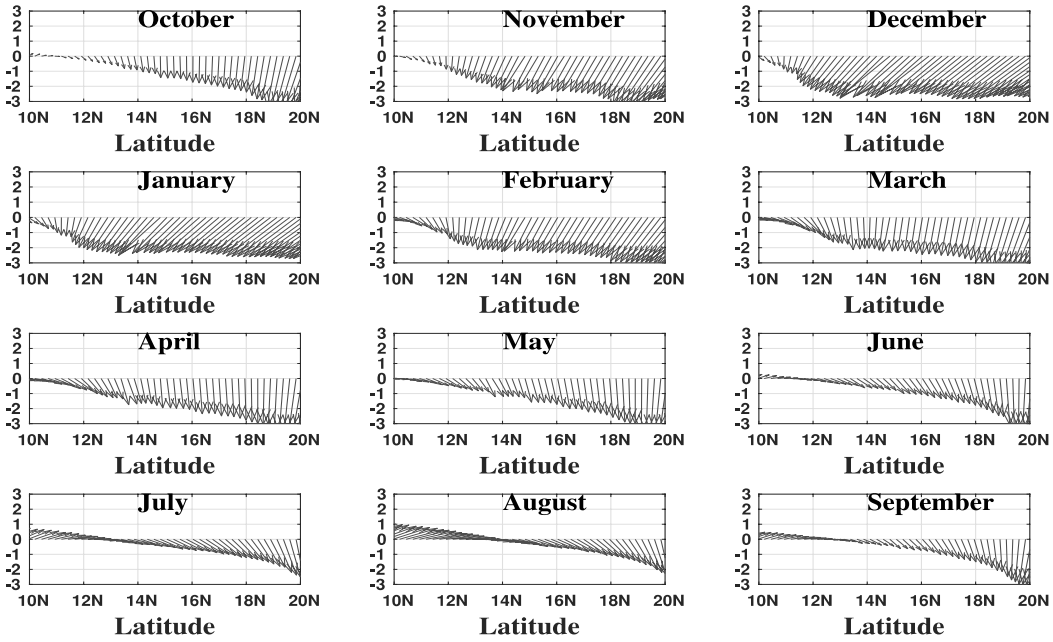


**Figure 3.** Monthly climatology of wind speed and direction along the of West African coasts over the period 1990-2015.

index is 0.5032 coinciding with 15 May. For more information, details are given in Table 2.

On the other hand, a synthesis of Table 2 is shown in Figure 6, highlighting practically all the information on the phenology of upwelling in in the Petite-Côte. Upwelling features show strong interannual variability in the starting dates, duration (in days) and the surface area (in km², the larger the circle, the larger the surface area and vice versa).

Note that, years in which upwelling starts earlier do not necessarily correspond to years of strong upwellings in terms of intensity and surface area. For example, the year 1994 (in which upwelling started earlier, e.g. on November 16, 1993) do show, practically, comparable surface area compared to normal years. Also, a year of late upwelling formation may correspond to a normal year in terms of surface area. However, the duration of the upwelling seems to be often related to the earliness of the upwelling. The earlier the upwelling, the longer the duration. We understand that the interannual variability of the upwelling system in the region is complex and requires extensive analysis. One of the important scientific questions of this paper is to understand the interannual variability of the onset dates of upwelling in the Petite-Côte. We will attempt to answer this question in the following paragraphs.

## Composite analyses

Ensemble averages of atmospheric and oceanic variables were made for early upwelling years, with the starting date for each year as the center (corresponding to lag 0). Days before the upwelling starting date correspond to negative lags: for example, lag -1 corresponds to one day before the upwelling start date and lag +1 corresponds to one day after the upwelling start date and so on.

## Surface temperature

The composite analysis on surface temperature shows that for an early upwelling year, SST anomalies are

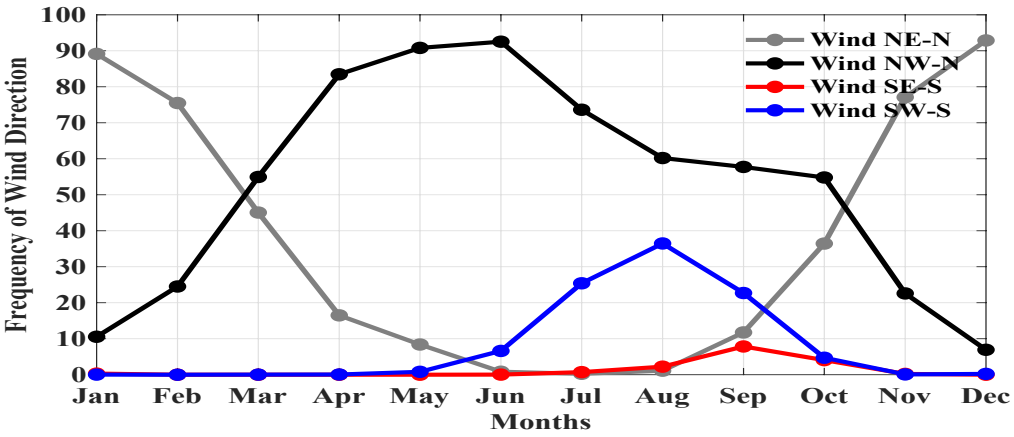


**Figure 4.** Monthly climatology of wind sector frequency on the Petite-Côte Senegalese over the period 1990-2015.

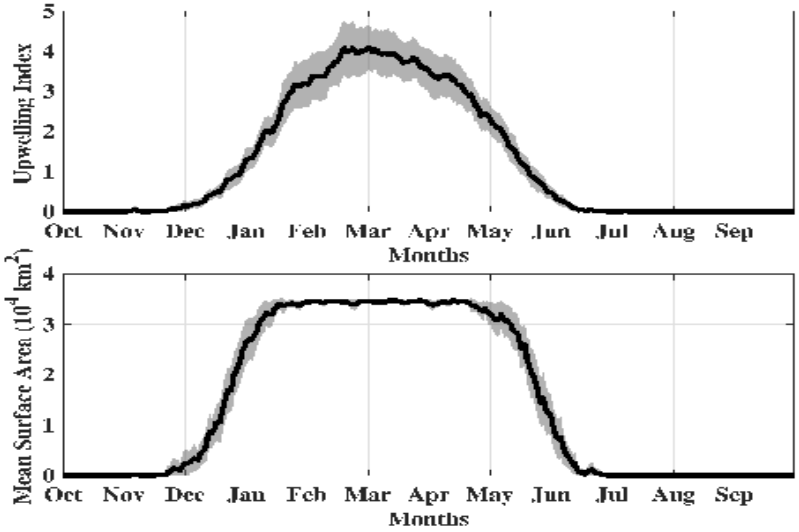


**Figure 5.** Monthly climatology of the index (top) and surface area (bottom) of the upwelling in the Petite-Côte for the period 1990-2015.

abnormally negative and form 14 days before (lag -14) the start of the upwelling corresponding to a strong cooling of the SST in the area (Figure 7). This strong cooling first appears a few tens of kilometers from the coast and occupies virtually the entire Senegalese coastal region several days after the start of the upwelling (Figure 7). The distance between the maximum cooling and the coast confirms that upwelling in this area occurs not at the coast but at some distance from it (Figure 7) and confirms the work of Ndoye et al. (2014) among others.

This cooling is also associated to the strengthening of northeasterly to northerly winds favorable to the upwelling in the Petite-Côte. The cooling values at lag 0 range between -0.2°C and -0.3°C. The wind pattern may play an important role in the early initiation of the upwelling. Indeed, according to Ekman's theory, winds parallel to the coast are more efficient to produce upwelling under the effect of Ekman transport. However, on the Petite-Côte, the winds are often parallel to the coast (purely from the North) and therefore favorable to upwelling which is the case in lag 2.

## Currents

The pattern of the vertical velocity for an early upwelling year is shown in Figure 8. Positive anomalies of vertical velocity are observed before the onset of the upwelling. Upwelled waters start 3 weeks (lag -22) before the onset

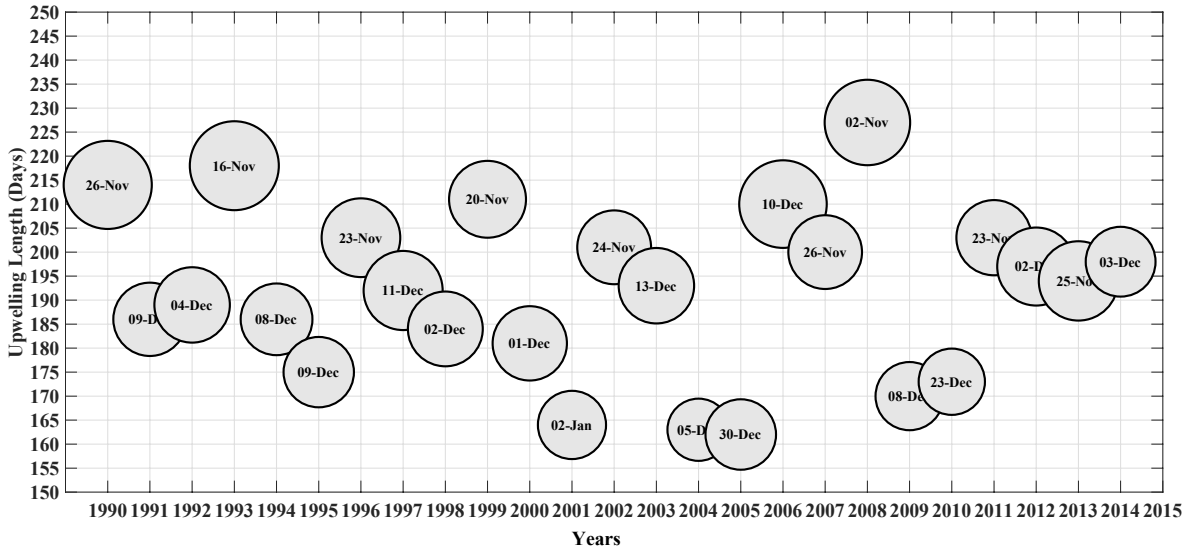


**Figure 6.** Interannual variability of onset date, duration (in days) and area occupied (circle size) of upwelling on the Senegalese Petite-Côte for the period 1990-2015.

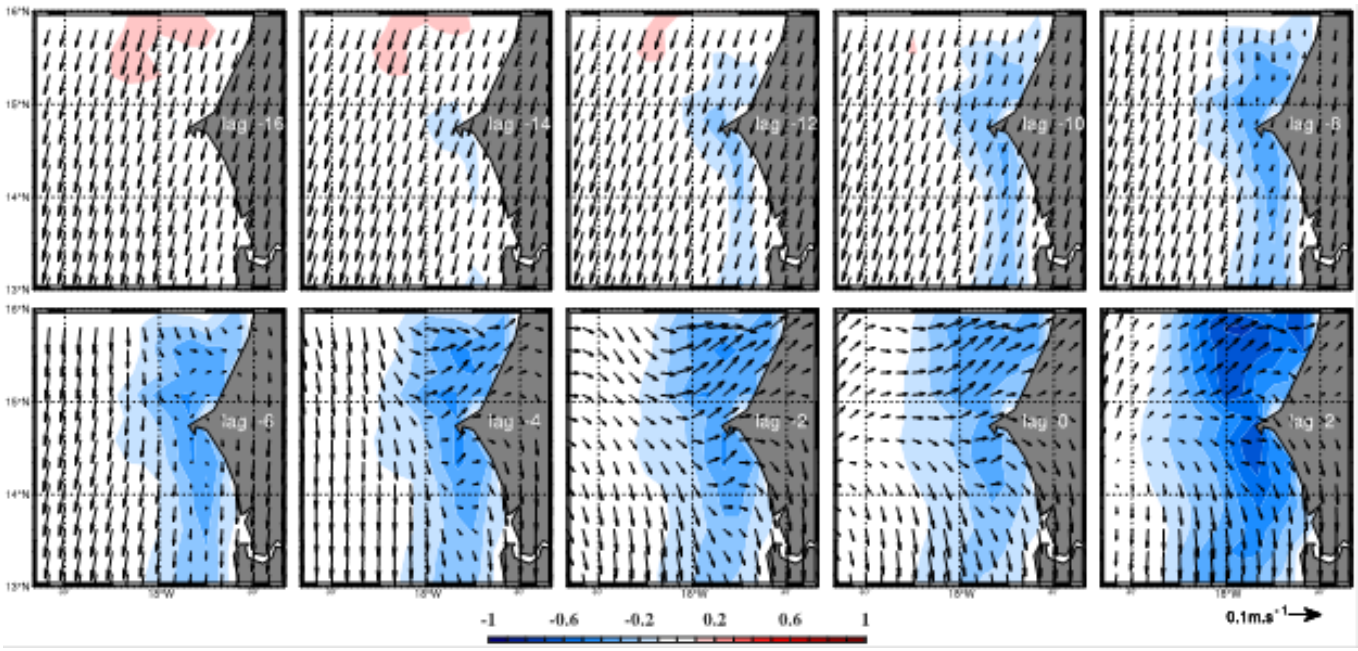


**Figure 7.** Temporal evolution of sea surface temperature for an early upwelling year. Arrows represent surface wind anomalies for an early upwelling year.

of the upwelling, even if the values are low of the order of $1.10^{-8}$ $m.s^{-1}$. Starting date of the vertical velocities (at lag -22) together with that of the negative SST (lag -14) clearly shows that the ocean takes 7 days to react to wind favorable to the upwelling (Figure 8). Maximum values of the vertical velocity (~ $8.10^{-8}$ $m.s^{-1}$) are observed at about two weeks before the upwelling onset along the entire coastal edge. These upwellings are also located within a few tens of kilometers of the coastline in agreement with the SST anomalies in Figure 7. We also note that the upwelling is almost spatially in homogeneous, probably due to the configuration of the continental slope.

The horizontal currents show a strengthening two weeks before the onset of the upwelling. The strengthening of the zonal current is more intense to the

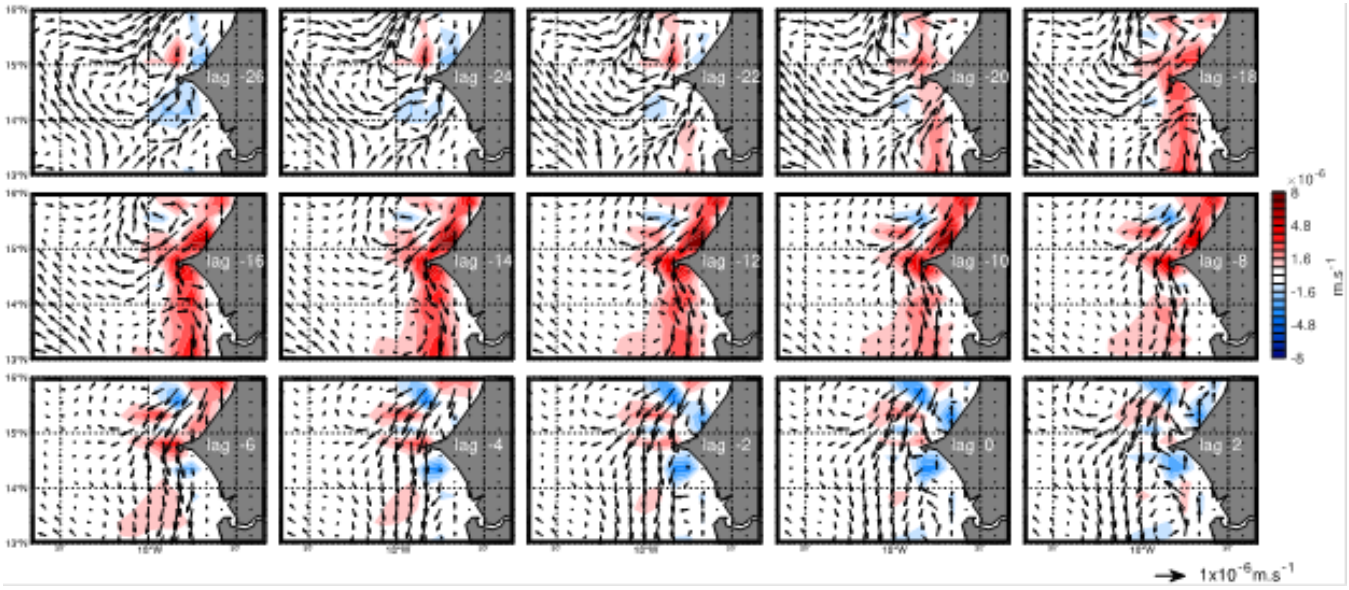


**Figure 8.** Averaged temporal evolution of vertical velocity (color) and horizontal current anomalies (arrows) integrated from the surface to 50m for an early upwelling year.

north of the Petite-Côte and is directed offshore in accordance with Ekman's theory. Moreover, the strengthening of the zonal current coincides with a strengthening of the meridional current. The latter is often associated with the coastal upwelling jet (Figure 8). It is thought that the strengthening and weakening in the intensity of the coastal jet are tightly correlated to the variation winds which, in turn, trigger early upwelling formation. A striking future about the Senegalese upwelling is that the region is one of the richest in biodiversity and fisheries resources on the planet.

## Correlation between variables

We calculated the lagged correlations between the composite SST index and the composite indices of the different variables for an early upwelling year. We clearly observed that for an early upwelling year, the SST is highly correlated with all variables 8-10 days before the onset of the upwelling (Figure 9). The exception is for the zonal current where the maximum correlation is observed two weeks before the onset of the upwelling. Correlation between SST and the costal jet is positive and denotes that the coastal jet becomes stronger carrying the colder northern waters southward, which participates on the early of the upwelling formation (Figure 9).

## Conclusion

In this study, we were interested in looking at the atmospheric and oceanic mechanisms that drive the onset dates of coastal upwelling in the Petite-Côte which is located south of the Senegalese coast. Indeed, the region presents a strong interannual variability in terms of upwelling onset date, its duration and its intensity. To answer to the questions we are interested in, we used daily data outputs from the NEMO model in its version 3.6 and NOAA's OISST sea surface temperature observations. The methodology used in this study is mainly based on a composite analysis which is a statistical method widely used in the scientific community.

We began by describing the average wind conditions (intensity, direction and frequency) in the region. The results show that the winds in the Petite-Côte are mainly from the North. From North to North-East from October to May, the Eastern component disappears in summer in favor of the Western component. Winds from the south are weak in this area (Figures 3 to 4). The coastal upwelling index ($TI_{pc}$) and the surface area ($S_{pc}$) show a very marked seasonal cycle. Indeed, our results show that upwelling in the Petite-Côte starts on average on December 3 and ends on June 13 with intense activity in April-May, peaking in mid-May (Figure 5). Moreover, the observation of the starting dates of the upwelling shows a strong interannual variability (Figure 6).

To understand this strong interannual variability, we performed a composite analysis using the earliness of the upwelling onset dates as the basic criterion to isolate early and late onset years. From the 26 years of data (1990-2015), we were able to isolate 3 early and 3 late years from the previously defined criterion (Table 2).

Our results show that for an early upwelling year, there is a strong cooling several days before the onset of upwelling. This cooling is due to the strengthening of

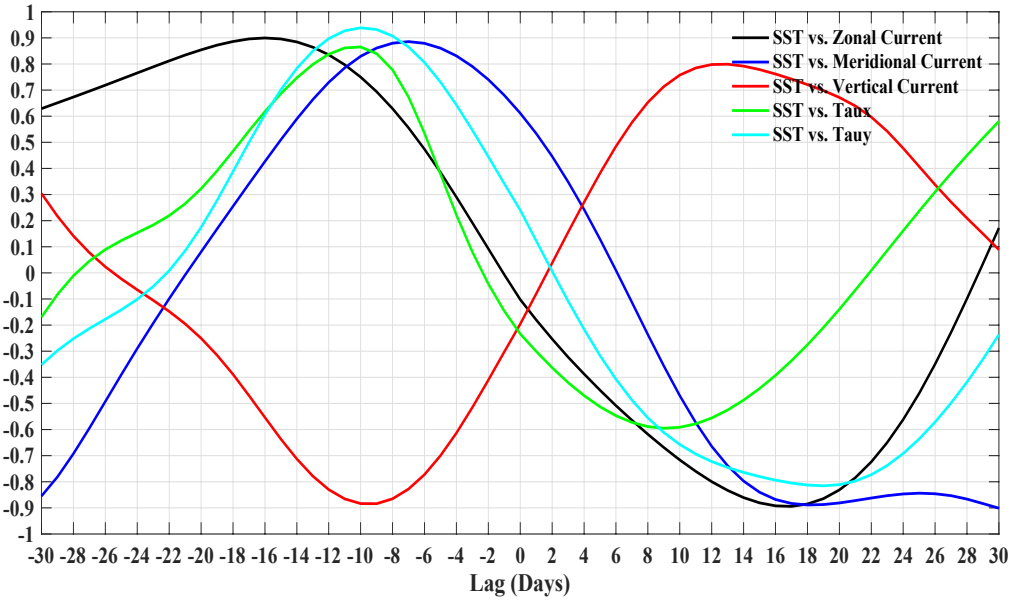


**Figure 9.** Lagged correlations between SST and the different variables for early upwelling year.

northeast to north winds favorable to the upwelling. The offshore surface current increases as well as the coastal upwelling jet which is abnormally intense several days before the onset of the upwelling. This strong cooling of the SST is also associated with intense vertical velocity (up to $8.10^{-6}$ $m.s^{-1}$).

Our results show and highlight that the relationship between the different variables is complex and deserves further analysis. For example, a year can be early in terms of upwelling onset date but its duration does not reach the climatological mean. On the other hand, upwelling onset dates seem to be related, beyond the Ekman transport, to the local strengthening of the coastal jet. These results must be verified by numerical modeling based on sensitivity experiments on the coastal jet. The validation of these results, by modeling, will bring a step further towards the predictability of the upwelling. The latter is necessary because it will allow a better management of the resource and will constitute a real tool for decision support.

## CONFLICT OF INTERESTS

The authors have not declared any conflict of interests.

### REFERENCES

Bricaud A, Morel A, Andre JM (1987). Spatial/temporal variability of algal biomass in the mauritanian upwelling zone, as estimated from CZCS data, Advances in Space Research 7(2):53-62.

Caniaux G, Giordani H, Redelsperger JL, Guichard F, Key E, Wade M (2011). Coupling between the Atlantic cold tongue and the West African monsoon in boreal spring and summer. Journal of Geophysical Research: Oceans 116(C4):1-17.

Dee DP, Uppala SM, Simmons AJ, Berrisford P, Poli P, Kobayashi S, Andrae U, Balmaseda MA, Balsamo G, Bauer DP, Bechtold P, Beljaars ACM,van de Berg L,Bidlot L, Bormann N, Delsol C, Dragani R, Fuentes M, Geer AJ, Haimberger L, Healy SB, Hersbach H, Hólm EV, saksen L, Kållberg P, Köhler M, Matricardi M, McNally AP, Monge-Sanz BM,Morcrette JJ, Park BK, Peubey C, de Rosnay P, Tavolato C, hépaut JN, Vitart F (2011). The ERA-Interim reanalysis: Configuration and performance of the data assimilation system. Quarterly Journal of the Royal Meteorological Society 137(656):553-597.

Demarcq H, Faure V (2000). Coastal upwelling and associated retention indices derived from satellite SST. Application to Octopus vulgaris recruitment. Oceanologica Acta 23(4):391-408.

Dussin RB, Barnier B, Brodeau L, Molines JM (2014). The making of Drakkar forcing set DFS5, DRAKKAR/MyOcean Report 05:10-14.

Faye S, Lazar A, Sow BA, Gaye AT (2015). A model study of the seasonality of sea surface temperature and circulation in the Atlantic North-eastern Tropical Upwelling System. Frontiers in Physics 3:76.

Herbland A, Voituriez B (1974). La production primaire dans l'upwelling mauritanien en mars 1973. Cah ORSTOM sér Océanogr 12(3):187-201.

Hernandez O, Jouanno J, Durand F (2016). Do the Amazon and Orinoco freshwater plumes really matter for hurricane-induced ocean surface cooling? Journal of Geophysical Research: Oceans 121:2119-2141.

Huntsman SA, Barber RT (1977). Primary production off north-west Africa: The relationship to wind and nutrient conditions. Deep-Sea Research 24(1):25-33.

Jacox MG, Edwards CA, Hazen EL, Bograd SJ (2018). Coastal upwelling revisited: ekman, bakun, and improved upwelling indices for the U.S. West Coast. Journal of Geophysical Research: Oceans 123(10):7332-7350.

Large WG, Yeager S (2009). The global climatology of an interannually varying air-sea data set. Climate Dynamics 33(2-3):341-364.

Lathuilière C (2008). Echanges côte-large et propriétés biogéochimiques dans les regions d'upwelling de bord Est. Theses, Université Pierre et Marie Curie - Paris VI.

Levitus S, Conkright ME, O'Brien T, Boyer TP,Stephens C, Johnson D, Baranova O, Antonov J, Gelfeld R, Rochester J, Forgy C (1998). World Ocean Database. Introduction, vol. 1. U.S. Govt. Print. Off, Washington, DC. 346 p.

Madec G (2014). "NEMO ocean engine" (Draft edition r5171), Note du Pole de modélisation 27, Inst. Pierre-Simon Laplace, France, ISSN No. 1288-1619.
Madec G (2008). NEMO ocean engine. Note from the Pole of Modeling, Institut Pierre Simon Laplace (IPSL), France, No 27, ISSN No (1288-1619):31-39.
Madec G, Delecluse P, Imbard M, Levy C (1998). OPA8. 1 ocean general circulation model reference manual. Notes du Pôle de Modélisation IPSL, Pierre Simon Laplace, Paris.
Marin F, Caniaux G, Bourlès B, Giordani H, Gouriou Y, Key E (2009). Why were sea surface temperatures so different in the Eastern Equatorial Atlantic in june 2005 and 2006? Journal of Physical Oceanography 39(6):1416-1431.
Merem EC, Twumasi Y, Wesley J, Alsarari M, Fageir S, Crisler M, Romorno C, Olagbegi D, Hines A, Ochai GS, Nwagboso E, Leggett S, Foster D, Purry V, Washington J (2019). Analyzing the Tragedy of Illegal Fishing on the West African Coastal Region. International Journal of Food Science and Nutrition Engineering 9(1):1-15.
Ndoye S, Capet X, Estrade P, Sow B, Dagorne D, Lazar A, Gaye A, Brehmer P (2014). SST patterns and dynamics of the southern Senegal-Gambia upwelling center. Journal of Geophysical Research: Oceans 119(12):8315-8335.
Polo I, Lazar A, Rodriguez-Fonseca B, Arnault S (2008). Oceanic Kelvin waves and tropical Atlantic intraseasonal variability. 1: Kelvin wave characterization. Journal of Geophysical Research: Oceans 113(C7):1-18.
Rebert JP (1978). Variability of Surface Conditions in the West African Upwelling, in Symp. Canary Current: Upwelling and Living Matter (No. 100).
Roy C (1989). Fluctuations of winds and upwelling variability off the coast ofSenegal, Oceanologica Acta 12(4):361-369.
Teisson C (1983). Le phénomène d'upwelling le long des côtes du Sénégal: caractéristiques physiques et modélisation. Doc CRODT-ISRA (123).
Van Camp L, Nykjaer L, Mittelstaedt E, Schlittenhardt P (1991). Upwelling and boundary circulation off northwest Africa as depicted by infrared and visible satellite observations. Progress in Oceanography 26(4):357-402.

Vol. 15(12), pp. 540-559, December 2021
DOI: 10.5897/AJEST2021.3068
Article Number: 00D0FD468360
ISSN: 1996-0786

http://www.academicjournals.org/AJEST

African Journal of Environmental Science and Technology

*Full Length Research Paper*

# Characterizing groundwater vulnerability in developing urban settings using DRASTIC-$L_uP_a$ approach: A case study of Aba City, Nigeria

**Uche Dickson Ijioma[1*], Frank Wendland[2,3] and Rainer Herd[1]**

[1]Brandenburgische Technische Universität, Cottbus-Senftenberg, Germany.
[2]Forschungszentrum Jülich, Institute of Bio- and Geosciences (IBG)-3 Agrosphere, 52425 Jülich, Germany.
[3]Department of Hydrological System Analysis, Brandenburgische Technische Universität, Cottbus-Senftenberg Germany.

Received 13 September, 2021; Accepted 23 Novemver, 2021

**The impact of certain unregulated land-use activities harms the quality of water resources and reduces the sufficiency of drinking water in many developing countries. This study aimed to capture the impact of such activities and evaluate the specific groundwater vulnerability using a modified DRASTIC approach. The DRASTIC-$L_uP_a$ was proposed and implemented for Aba City, Nigeria by incorporating land-use and the impact of pumping layers to the "intrinsic" DRASTIC parameters. The results of the analysis revealed that the area classified as "low" was 15 and 79.1% as "medium" and 5.9% as "high" vulnerability classes for the DRASTIC. Whereas for the DRASTIC-$L_uP_a$ model 3.2% for "low", 54.3% for "medium", 41.8% for "high" and 0.7% for "very high" were found. The transitions in the vulnerability classes of areas displaying "high" and "very high" found in the DRASTIC-$L_uP_a$ model represent the impact of urban hotspots observed in the area. This result implies that groundwater protection measures should be implemented in the area designated with "low" and "medium" vulnerability classes and used for abstracting clean water for drinking purposes. The proposed model enhances the predictability and guarantees better transferability of the approach in urban settings with similar urban trends.**

**Key words:** Drinking water, DRASTIC, groundwater, groundwater vulnerability assessment, Nigeria.

## INTRODUCTION

Groundwater remains the source of water for about half of the world's population (Kemper, 2004). Studies have shown that in developing countries groundwater is used mainly for domestic and agricultural purposes (Doungmanee, 2016; FAO, 2020). With changing climate, rapid economic and population rise observed in these countries, the groundwater has been under severe stress due to unregulated withdrawals. Again, further reduction in access to groundwater has continued due to anthropogenic contaminations resulting from poor urban

*Corresponding author. E-mail: u.d_ijioma@yahoo.com or UcheDickson.Ijioma@b-tu.de. Tel: +4915211326235.

implementation. Therefore, it is necessary to develop strategies to guarantee the sustainable use of this "invisible public good". The management of groundwater resources can be performed either by planned physical monitoring or through computational modelling if sufficient data is available (Jang et al., 2017). The principle of digital risk management practices suggests identifying areas with high vulnerability potentials to reduce frequent monitoring and costs. This is because sampling and monitoring activities consume a lot of time and are expensive to execute over a large area.

The concept of groundwater vulnerability assessment is one of the management approaches that evaluate the physical properties of aquifers and ensure the sustainable use of the resource. Most vulnerability assessment methods bring natural (e.g., hydrogeological parameters) and/or human-induced activities that deteriorate groundwater qualities together to evaluate the contamination risk (Vrba and Zoporozec, 1994). When the vulnerability is influenced by only hydrogeological factors, it is described as "intrinsic vulnerability". Whereas if it is caused by hydrogeological and human-induced components, then it is referred to as "specific vulnerability" (Frind et al., 2006). The knowledge of the vulnerability types helps to plan monitoring activities to protect the groundwater quality (Saatsaz et al., 2011; Jang et al., 2017).

In different parts of the world, several methods have been developed to evaluate the vulnerability of groundwater to contamination. The assessment method may be objective or subjective depending on the data requirement (Sorichetta, 2010). The objective methods use numerical data, while the subjective ones employ qualitative parameters that influence the hydrological complex (UNESCO, 2004; Sorichetta, 2010). The suitability of each approach depends on factors such as the study objectives, availability of the input data, financial budget, as well as, technical competence required to execute the method (Jang et al., 2017). Some examples of objective methods are process-based models such as SWAT, GLEAMS, HSPF, and MODFLOW (Jang et al., 2017). These models follow some numerical principles and require extended input data to predict groundwater vulnerability.

Again, some statistical methods have been used for groundwater vulnerability assessments. These assessment methods are objective just like the numerical process-based counterparts. Some examples of statistical approaches include the Bayesian theorem (Arthur et al., 2007; Sorichetta, 2010) or log-linear weight of evident (WofE) (Massetti et al., 2008; Sorichetta, 2010) and logistic regression methods (Mair and El-Kadi, 2013; Adiat et al., 2020).

Most groundwater vulnerability assessment studies in developing countries utilize subjective methods. These indexed-based methods are most commonly used because organizing the data is easier and the execution is straightforward compared to the process-based and statistical methods. Some examples include the DRASTIC (Aller et al., 1987), GOD (Foster, 1987), SEEPAGE (Moore and John, 1990), SINTACS (Civita et al., 1991), AVI (Van Stempvoort et al., 1993), EPIK (Dörfliger and Zwahlen, 1998; Doerfliger et al., 1999), COP (Vias et al., 2006), etc.

The DRASTIC is the most widely applied subjective method and will be considered in this study. It has the main advantage of predicting precisely degrees of vulnerabilities in complex geological features, using intrinsic properties of the aquifer. The DRASTIC approach has been modified in many studies to improve its predictive capability and address specific vulnerability issues (Jasem, 2010; Moustafa, 2019; Jhariya et al., 2019). The modification in the method can be done to capture the impact of human activities on the groundwater quality. This can be achieved by incorporating additional human-induced settings that can influence the groundwater quality, besides the DRASTIC parameters (Secunda et al., 1998; Ijeh 2013; Amadi et al., 2014; Singh et al., 2015; Kumar and Krishna, 2019).

Most of Global South's developing urban areas are described by increasing population and economic trends. Weak institutions, as well as the lack of maintenance and expanding existing infrastructures, have led to certain unregulated land-use activities and poor environmental practices that have been reported by Egboka et al. (1989) and Ijioma (2021b). These practices complicate urban hydrology (Wakode, 2016), and worsen the quality of the groundwater, as well as its management. This study aimed to characterize the vulnerability of groundwater in such developing urban settings, by enhancing the predictability of the DRASTIC approach. The specific objectives were (a) to identify appropriate anthropogenic layers that influence the hydrologic settings, (b) add these layers into the DRASTIC model, (c) evaluate the difference between the classical DRASTIC and the proposed modified model, as well as (d) recommend the applicability and transferability of the proposed method in the context of other developing urban settings.

## MATERIAL AND METHODS

### Study area

This study is focused on Aba City, a commercial hub in Abia State, southeast Nigeria (Figure 1a and b). The estimated number of people living in the area is over one million since the last population census of Nigeria was conducted in 2006 (baseline data source was obtained from the Department of Health in the local government areas making up Aba City). The area covers about 236 $km^2$ and it is situated in the rainforest agro-ecological zone of Nigeria. There are two main climate seasons, the rainy season between April and October and the dry between November and March, in the area. The average annual temperature is 27.6°C and the average annual rainfall between 1980 and 2019 is 2450 mm/annum. This amount of annual rainfall showed that the area is

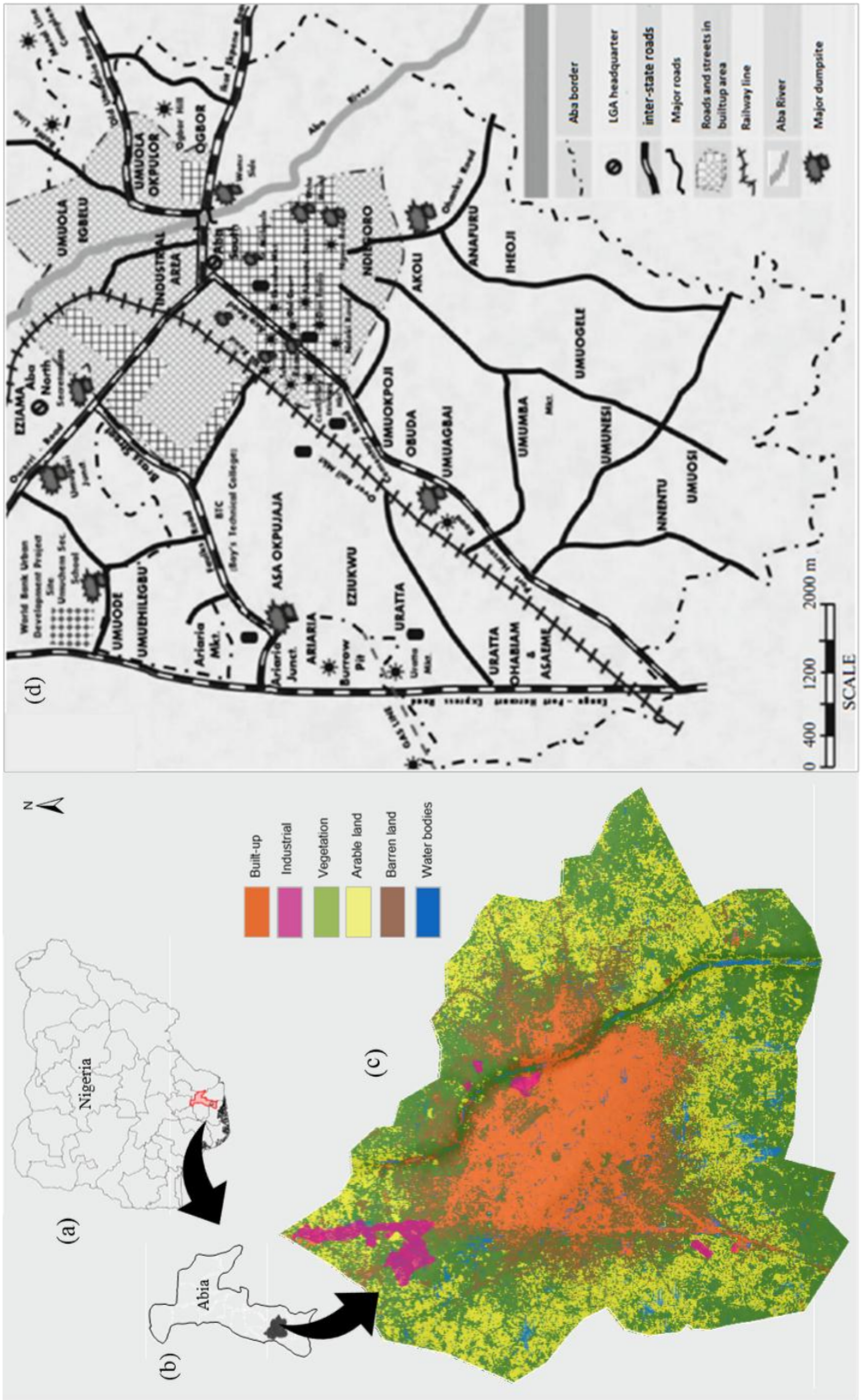


**Figure 1.** Geographical location of the study area showing map of (a) Nigeria and (b) Abia State, (c) land-use distribution in Aba for 2017 and (d) a sketch showing some poor environmental practices within Aba City.
Source: (a) - (c) adopted from Ijioma (2021a), (d) modified from Agharanya and Dim (2018).

ultra-humid. The regional actual evapotranspiration lies between 800 and 1000 mm/annum (Hayward and Oguntoyinbo, 1987). The current water supply system in the area is privately controlled (Ijioma, 2021b). This is because the public supply system operated by state-owned water boards is dysfunctional in most urban parts of Nigeria (Macheve et al., 2015). Groundwater is obtained from private tube wells and it serves as the main source of water for domestic, commercial and industrial uses. However, the installation of these tube wells is poorly regulated, indiscriminate and takes place without licensing. Again, there is no central sewage system to manage the residential, municipal and industrial effluents. This has led to the use of cesspools, septic systems, and the discharge of effluents from both commercial and industrial facilities directly into the aquifer. These types of effluent disposal systems form alternative groundwater recharge sources that can harm the quality. A high chemical and poor bacteriological loading in the densest urbanized parts have been reported in Ijioma (2021b). With the growing population, economic and urbanization trends come with environmental challenges arising from poor handling of municipal wastes in the area. The waste management practices are crude and ineffective in handling tons of refuse generated. The wastes generated are not separated, and collection buckets are sporadically seen over-whelmed in different parts of the area (Figure 1d) and borrow pits are used as landfills. This type of developing urban scenario is not peculiar to Aba City alone, but it is common in many developing urban settings.

## Hydrogeology and lithography of the area

The Benin formation constitutes the parent geology, which is composed of the coastal plain sand. The lithological characterization in this study was derived from three borehole hydrogeological investigations up to the first 100 m depths in different parts of the area (Figure 2). The borehole log hydrogeological investigation revealed the different layers and textures. The strata are made up of medium to coarse to very coarse sand, as well as very fine gravels fairly distributed throughout the area. The groundwater elevation tables range between 26.3 and 30 m in the tube wells. The results imply that the elevation of the water table is deep, and groundwater abstraction is facilitated with submersible motor (SUMO) pumps in the tube wells for the water supply. The average result of the pump test revealed an estimated aquifer yield at 4.5 l/s.

## Groundwater vulnerability assessment based on the DRASTIC concept

The concept of groundwater vulnerability assessment assumes that the susceptibility of the aquifer depends on the extent of physical protection, which the groundwater gets from the covering layers. The DRASTIC method assumes that the contamination of groundwater begins at the surface, and it is conveyed by rainwater through the unsaturated zone to the groundwater in the saturated zone. The acronym DRASTIC represents seven hydrometeorological and geological parameters, which include depth to the water table [D], net recharge rate [R], aquifer media [A], soil media [S], topography [T], the impact of the vadose zone [I] and hydraulic conductivity [C]. The method addresses generally two sets of potential contamination sources: general and agriculture. However, this study deals with the general contamination potential since the aquifer in the area is minimally influenced by agricultural land use. The evaluation procedure assigns each parameter with a weight from 1 to 5. Parameters with higher contamination potentials are assigned higher values. Each parameter has a range, which is interpreted as the extent to which they can influence the quality of the groundwater. These ranges are assigned rating values from 1 to 10. The ranges, rating, and weights for each of the intrinsic aquifer parameters were predefined in Aller et al. (1987) for the DRASTIC (Table A-1 in Appendix 1). The DRASTIC index [*DVI*] is calculated as the sum of the products of the weight and rating for the DRASTIC parameters as expressed in Equation 1.

$$DVI = \sum_{i=1}^{j} w_i * r_i \quad (1)$$

where $j$ = total number of hydrogeologic settings (parameters) considered, $i$ = ith parameter, $w$ = weight assigned to ith parameter, $r$ = rating of the ith parameter.
Equation 1 can be rewritten in a simpler algebra expression as in (Equation 2).

$$DVI = D_wD_r + R_wR_r + A_wA_r + S_wS_r + T_wT_r + I_wI_r + C_wC_r \quad (2)$$

Equation 2 expresses the intrinsic properties of the aquifer since only hydrogeological parameters were considered. To modify the expression, the influence of land use [$L_u$] and the impact of the active pumps [$P_a$] layers were introduced. These mappable layers were identified because they can influence the quality of groundwater in a poorly regulated environment. The modified expression addressed the specific groundwater vulnerability given by Equation 3.

$$DVI_m = DVI - R_wR_r + ([R_m]_w\,[R_m]_r + [L_u]_w{*}\,[L_u]_r + [P_a]_w{*}\,[P_a]_r) \quad (3)$$

where $DVI_m$ = DRASTIC-$L_uP_a$.

For the modified model, the weight, range, and ratings of the land use map were adopted from Kumar and Krishna (2019). The calculated minimum and maximum indices of the DRASTIC and DRASTIC-$L_uP_a$ models lie between 24 - 220 and 34 - 340, respectively. The indices are categorized into five vulnerability classes by dividing them equally. The categorization of the classes has been summarized in Table 1. Each vulnerability class describes the susceptibility of the groundwater to contamination. This means the higher the index, the more vulnerable is the groundwater to contamination. The indices are dimensionless for both models.

The high rating suggests that the range make the aquifer more vulnerable to contamination. This makes the method less subjective and easy to implement with the ratings and ranges already predefined and provided for different scenarios. Then, adopting, reproducing and transferring the model becomes simple to apply in different local situations.

## Creating thematic/rating maps

The sources and data types used to create the thematic maps for the groundwater vulnerability assessment models are summarized in Table 2. All the maps produced from vector data were converted into raster and the grid sizes resampled equally.

### *Rating maps for the intrinsic properties*

The DRASTIC method utilizes intrinsic hydrogeologic properties as input data for its assessment. The combined impact of these properties contributes to the overall vulnerability of the groundwater. The creation of the thematic/rating maps is described in the following.

**Depth to the water table [D]:** The water-table elevation map of the

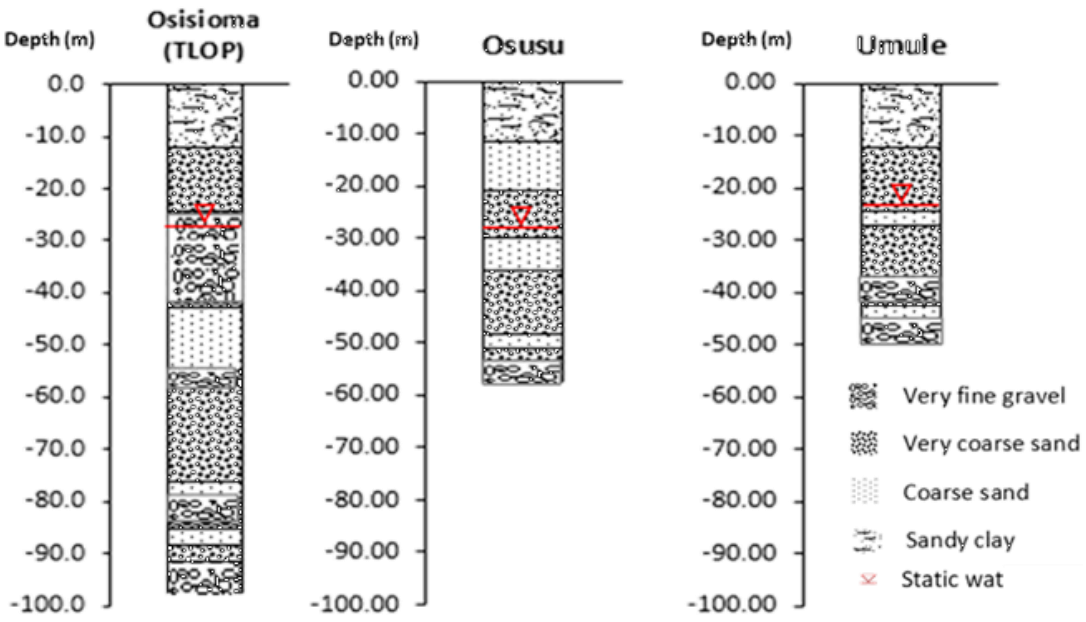


**Figure 2.** Hydrogeological investigations showing the lithography of three borehole sites in Aba City. Source: Ijioma (2021b).

**Table 1.** Vulnerability class designations for the DRASTIC and DRASTIC- $L_uP_a$ indices.

| Designation | Vulnerability indices | |
|---|---|---|
| | DRASTIC | DRASTIC-$L_uP_a$ |
| Very low | 24 - 60 | 34 - 95 |
| Low | 61 - 120 | 96 - 157 |
| Medium | 121 - 160 | 158 - 219 |
| High | 161 - 200 | 220 - 281 |
| Very High | 201 - 220 | 282 - 340 |

area was created from borehole dippings of selected wells based on availability. The data was augmented with records from local drillers in the area. The depth to the water table map was obtained by subtracting the water-table elevation map from the reference elevation map extracted, that is, SRTM DEM for the area (DEM resolution ≈ 30 m). The reference DEM served as a standard surface above sea level for the water table elevation map correction (Adams, 2013).

**Net groundwater recharge rate [R]:** The net groundwater recharge rating map was based on the effective groundwater infiltration rate described in Bazimenyera and Zhonghua (2008) and Sorichetta (2010). The concept employed the water balance method and utilized data from the hydrological parameters (e.g., rainfall, evapotranspiration and runoff coefficients). The land-use map identified four important classes, which include the built-up, barren-land, arable-land, and broadleaf vegetated land for this evaluation. The net recharge rating for each land-use class was calculated according to Equation 4:

$$N_r = (P_a - ET)(1 - R_r) \quad (4)$$

where $N_r$ = Net infiltration rate; $P_a$= Average annual rainfall (mm/annum); $ET$ = Average annual (upper and lower limits) evapotranspiration (mm/annum); $R_r$ = Surface runoff coefficient for different ground surface; (1- $R_r$) = infiltration coefficient.

The surface run-off coefficients corresponding to the identified land use classes were adapted from Jinno et al. (2009) and used to calculate the net recharge in each land-use class. Intrinsically, the following assumptions were made in the estimation of the net recharge rating map.

(1) The rainfall distribution was uniform throughout the area;
(2) Groundwater recharge is only rainfed and all infiltrated rainwater constitute recharge;
(3) Impervious land surface reduces the net recharge rate, and
(4) The surface runoff coefficient is inversely proportional to the infiltration coefficient.

**Aquifer media [A]:** The lithographical information of the boreholes in Figure 2 was used to characterize the aquifer media in the area. The results revealed that the aquifer media consist mostly of medium-coarse-grained sand to very fine gravel. The geology of the area is simply coastal plain sand and the lithology confirmed the

**Table 2.** Hydrogeological settings and data types used for the groundwater vulnerability assessments (modified from Ijioma, 2021b).

| Data output layer | Data type | Sources | Format |
|---|---|---|---|
| Depth to the water table | Borehole log, SRTM DEM | Field measurement, reports from AIRBA*, USGS Earth Explorer (https://earthexplorer.usgs.gov/) | Raster |
| Net recharge rate | Land use map, meteorological data, runoff coefficient | NRCRI meteorological station Umudike, Jinno et al. (2009) | Raster |
| Aquifer media | Shapefile, borehole lithograph | - | Vector |
| Soil media | Shapefile | - | Vector |
| Topography (Slope) | SRTM DEM | USGSA Earth explorer (https://earthexplorer.usgs.gov/) | Raster |
| Impact of vadose | Shapefile, borehole Lithograph | - | Vector |
| Hydraulic conductivity | Shapefile, point data pump test data, sieve analysis | Adamu et al. (2019); Agharanya and DIM (2018) | Vector |
| Impact of active pump surface | Shapefile, well abstraction rates (point data) | - | Raster |
| Land use map | Landsat 8 OLI/TIR imagery | USGSA Earth explorer (https://earthexplorer.usgs.gov/) | Raster |

same. It was assumed that the aquifer is the same throughout the area and a uniform surface was created in this respect.

**Soil media [S]:** The soil media rating map was derived from documented field investigations that have characterized the soil in parts of the study area (Adindu et al., 2013; Adamu et al., 2019). The USDA classification of the soil texture at the sites of these studies revealed that the soil predominantly comprises sandy-silty-clay (sandy loam) sand type. When the study area was extracted from the soil map of Nigeria (ESDAC, 1990) a uniform distribution was observed throughout the area. The rating was assigned based on the recommendations of Aller et al. (1987) in Table A-1.

**Topography/Slope [T]:** The topography rating map was derived from the extracted filled SRTM DEM for the study area. The slopes of the filled DEM were generated in the GIS platform and distributions were reclassified. The outcome of the reclassification followed the recommendations of Aller et al. (1987) as described in the appendix (Table A-1).

**Impact of the vadose zone [I]:** The vadose zone is defined as the geological overburden above the saturated zone. It is part of the geological overburden under the soil, but on top of the saturated zone. It determines to what extent contaminants attenuation happen before they reach the saturated. The lithography information showed that the vadose consists of materials mostly sandy clay, as well as medium to coarse-grain sand and very fine gravel with silty facies in the area.

**Hydraulic conductivity [C]:** The data used to create the rating map was collated from documented field experiments. These include laboratory methods - sieve analysis (Agharanya and Dim, 2018), pump test (Adamu et al., 2019) and analysis of soil texture or grain sizes (Ijioma, 2021b) conducted at sites in different local government areas that make up the study area.

***Anthropogenic-based thematic/rating maps***

It has been observed that unregulated human activities in urban settings of many developing countries harm groundwater quality (Ijioma, 2021a). Two additional rating maps were identified and integrated into the DRASTIC model to enhance the reliability of the vulnerability assessment for Aba City. The parameters captured the impact of poor land-use practices, which is common in many developing countries. The modification incorporates both the land-use ($L_u$) map with a special focus on some identified contamination hotspot activities and the impact of active pumps ($P_a$) as part of the rating maps to implement the proposed DRASTIC-$L_uP_a$ model.

**Land-use [$L_u$]:** The land use map was derived from the Landsat imagery of the area for 2017 using remote sensing techniques. The supervised classification approach based on the maximum likelihood method was used for the characterization as described in Ijioma (2021b). Rasterized polygons of the industrial zones were created and joined to the land map. One of the major urban land-use activities in the built-up parts that can influence groundwater quality is the use of septic drains. This is found in most built-up parts since the area has no central sewerage system to handle the municipal effluent. These two urban features characterize important potential contamination sources in the land-use rating map that harm the groundwater quality.

**Impact of active pumps [Pa]:** The active pumps can affect the lateral and vertical movements of the groundwater within the aquifer and this could harm the quality of the groundwater if poor environmental management practices prevail around the radius of influence of the pump. The impact of the active pump rating map was created using extraction data of pumps for domestic, industrial and commercial activities within the study area. The pump selection was based on availability and accessibility since these are not monitoring wells. Data for 234 pumps were collected and these pumps were categorized into subclasses according to their daily withdrawal rates. The impact of the active pump rating map was created using the ordinary kriging interpolation of the pumps points and their daily withdrawal rates.

***Implementing the groundwater vulnerability assessment models***

The implementation of the vulnerability models followed a GIS-based approach. The GIS platform serves as a

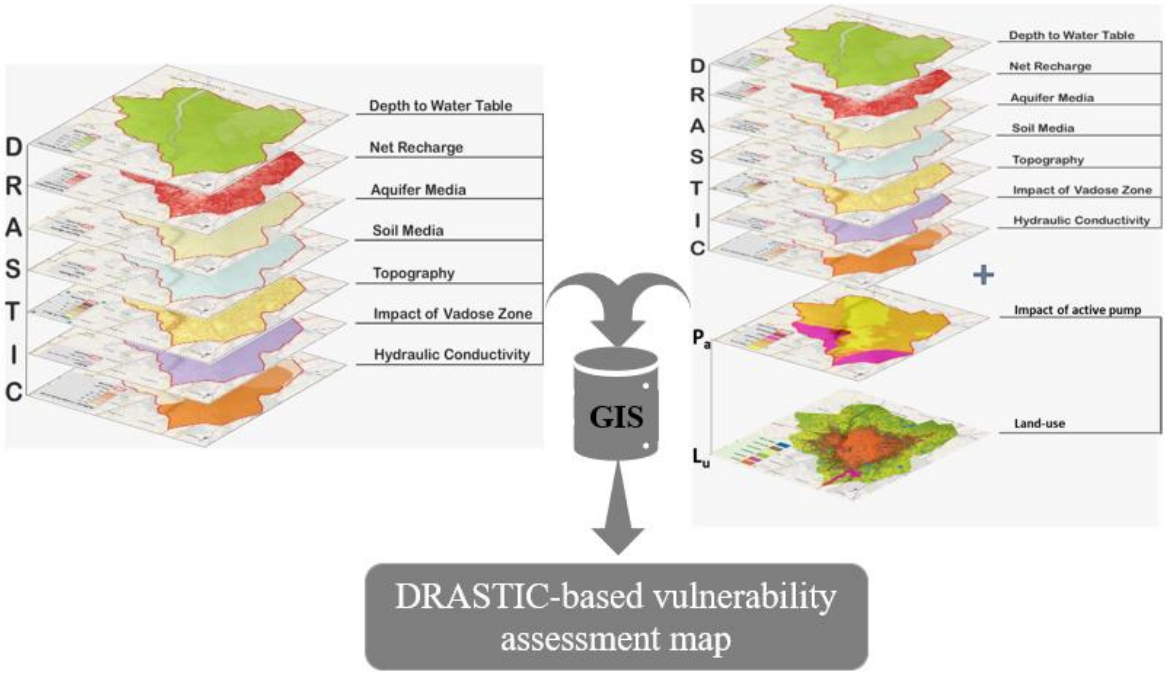


**Figure 3.** A schematic illustration showing different thematic layers used in implementing the DRASTIC and DRASTIC-$L_uP_a$ models.
Source: Modified from Ijioma (2021b).

database to store and process the thematic/rating maps. Figure 3 schematically demonstrates the overlaying of the different rating maps required for each model. The weights and rates for each thematic parameter were appropriately assigned to the different raster pixels on the rating maps. The implementations of the models were executed with the raster calculator function in the spatial analyst toolbox of ArcGIS 10.7 following Equations 2 and 3 for DRASTIC and DRASTIC-$L_uP_a$ respectively.

### *Validating the impact of active pumps on groundwater quality*

Eight water quality indicators were used to develop a groundwater quality index distribution map (Figure 4a) using the geometric weighted sub-index aggregation method. The procedures for the water quality index map derivation are described in Ijioma (2021b).

The map revealed that the groundwater has been contaminated with petroleum products and unfit for drinking in the northwestern parts. This portion of the area was selected to validate the impact of pumping on the hydrogeologic setting since the quality of the groundwater in the remaining parts is evenly spread and acceptable for drinking. The influence of pumping activities caused a 2-dimensional flow (that is, lateral and perpendicular) of the groundwater and around the pump. During pumping, a cone of depression and zone of influence is formed (Figure 5). The empirical estimation of the radius of influence R for an unconfined aquifer was done according to Weber (1928) (equation 5).

$$R = 3\sqrt{K_f h_o \frac{t}{n}} \quad (5)$$

where R = radius of influence (m), $K_f$ = hydraulic conductivity (m/s), $h_o$ = piezometric head before the pumping started (m), $t$ = time of pumping (s), and $n$ = effective porosity (dimensionless ratio representing fractional volume).

Three tube wells were identified in the area where petroleum hydrocarbon product contamination has been observed in the groundwater (Figure 4c). The time ($t$) taken for the pumps to fill the overhead reservoir ($V$) and the depth to the water table elevation ($h_o$) were measured before pumping.

## RESULTS AND DISCUSSION

The rating values used to create the thematic maps for the DRASTIC and DRASTIC-$L_uP_a$ models are summarized in the Appendix (Table A-2). The results of the rating maps are discussed subsequently.

### Intrinsic thematic maps

### *Depth to the water table [D]*

The implication of the depth of the water table parameter to the overall DRASTIC vulnerability assessment shows that the deeper the water table, the lower the chances of the groundwater being contaminated or vice versa. The result of the derived rating map (Figure 6) showed that the rating in the area lies between 1 and 7. The dominant rating depth of the water table lies between classes 1 and 2 in most parts of the study area. Some parts in the southwestern corridor were shallower with a rating of 3, making this part more vulnerable.

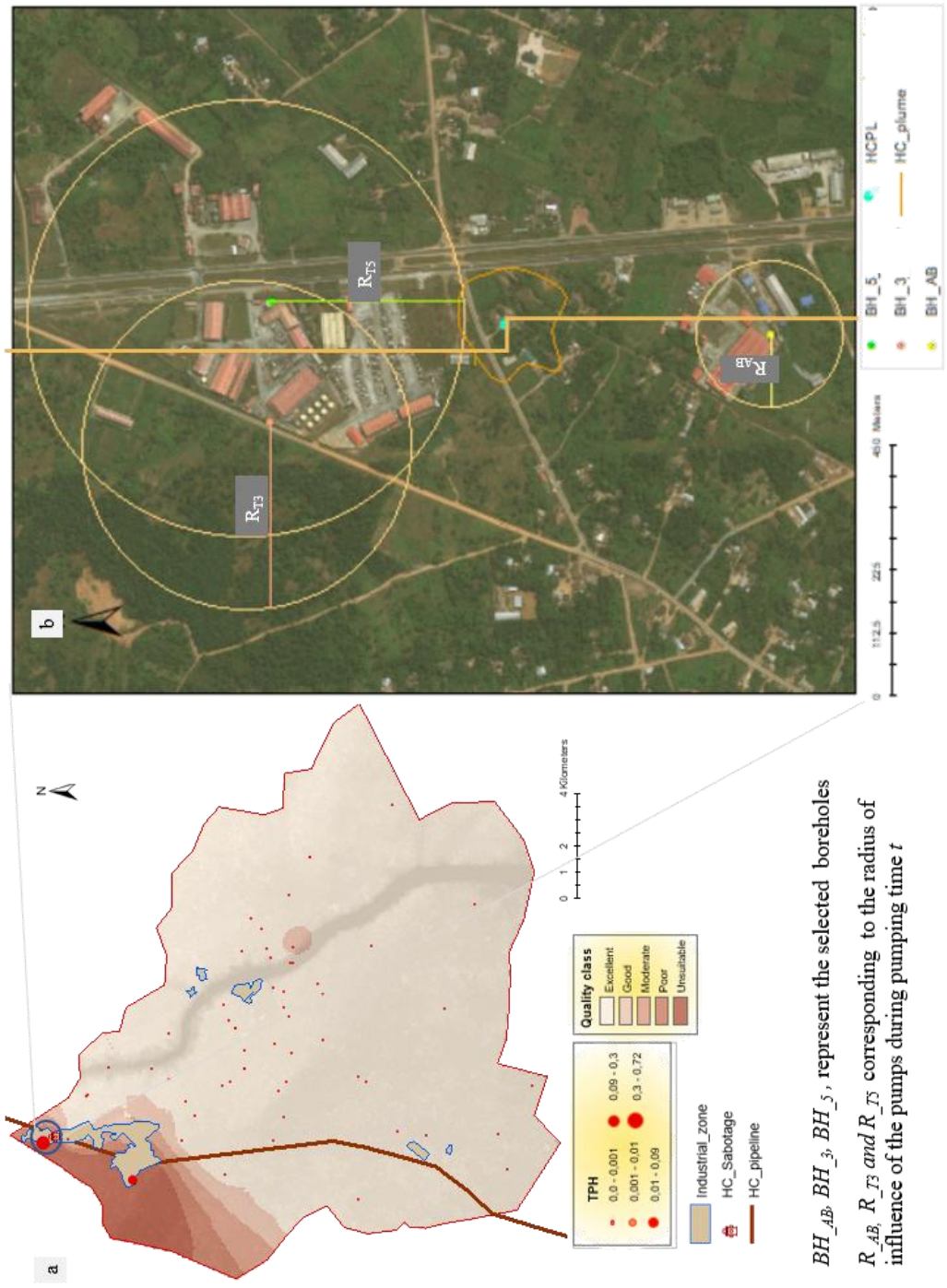


**Figure 4.** Illustration to validate the impact of active pumps on groundwater quality. (a) Quality index map distribution and a selected contaminated site in one of the industrial estates where petroleum hydrocarbon pipeline was vandalized. (b) Satellite image of the selected boreholes pumps estimating their zone of influence from a contamination plume.
Source: Modified from Ijioma (2021b).

***Net groundwater recharge rate [R]***

The net groundwater recharge rate indicates the ease with which contaminants can be transported vertically from the surface to the groundwater. The result of the net recharge distribution in the rating maps is summarized in Table 3. The DRASTIC approach suggests that the higher the net recharge rate, the more likely is that

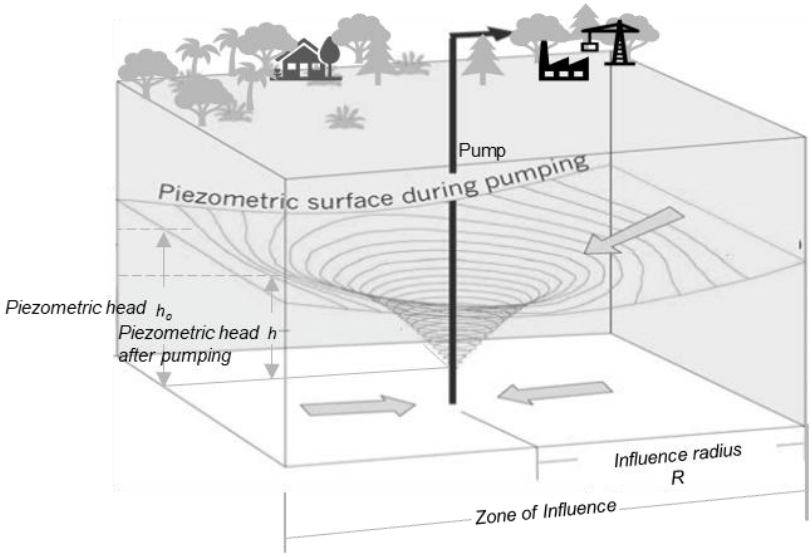


**Figure 5.** Illustration of cone of depression and a pump's zone of influence in a homogenous aquifer.
Source: Modified from Fileccia (2015).

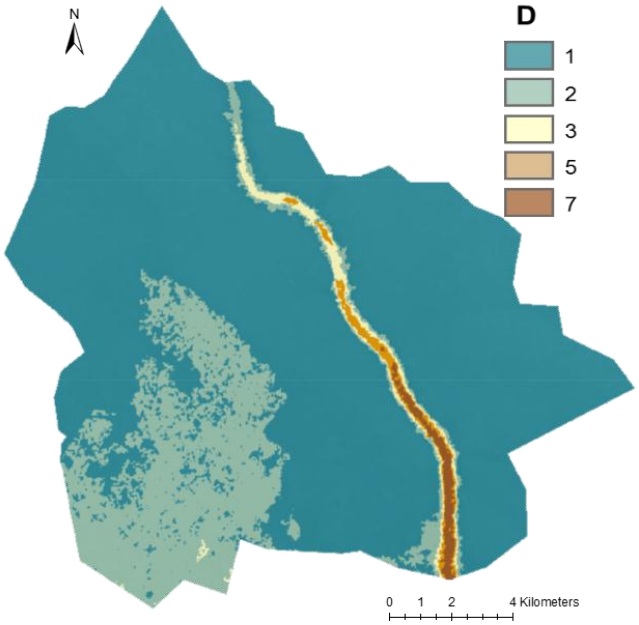


**Figure 6.** Depth to the water table rating map [D].

contamination at the surface reaches the groundwater table faster. The land-use classes influence the ratings in the area. The order according to contamination susceptibility of the aquifer based on the land-use class is as follow: vegetated > arable > built-up > barren land as summarized in Table 3. Considering the impact of some practices in the built-up parts which contribute to groundwater recharge in the area, the rating of the net recharge map was modified [$R_m$] to account for these practices. The rating map illustrations (Figure 7a and b), revealed that groundwater recharge occured mostly within the vegetated and arable land classes. This makes these parts the most susceptible in the area with ratings of 9 and 8 assigned to them in both [R] and [$R_m$] maps respectively. In the [R] map, the barren land and built-up were the least vulnerable parts with ratings of 3 and 1,

**Table 3.** Summary of results of the water balance equation and net recharge distribution.

| | | | | |
|---|---|---|---|---|
| Average annual rain ($P_a$) [mm] | | 2143 | | |
| Evapotranspiration (ET) [mm] | | Lower limit ($ET_l$)[1] 800 - 1000 | | Upper limit ($ET_o$)[2] 1449.8 |
| Effective rain (P-ET) [mm] | | 1243 | | 693.2 |
| Land use | Area ratio | Recharge coeff. (1-$R_f$) [mm] | Net recharge [mm] | Rating |
| Arable land | 0.17 | 0.9 | 97.5 - 118.5 | 6 |
| Vegetation | 0.39 | 0.85 | 210.7 - 407.1 | 9 |
| Built-up | 0.36 | 0.2 | 46.3 - 89.5 | 3 |
| Barren land | 0.09 | 0.4 | 22.2 - 42.9 | 1 |

[1]$ET_l$ is the evapotranspiration values from literature based on the regional basin according to Hayward and Oguntoyinbo, (1987) and Ophori (2007). The average of the range (900 mm) was used in the calculation.[2]$ET_o$ was estimated from the FAO's ET calculator. It represents the reference evapotranspiration.

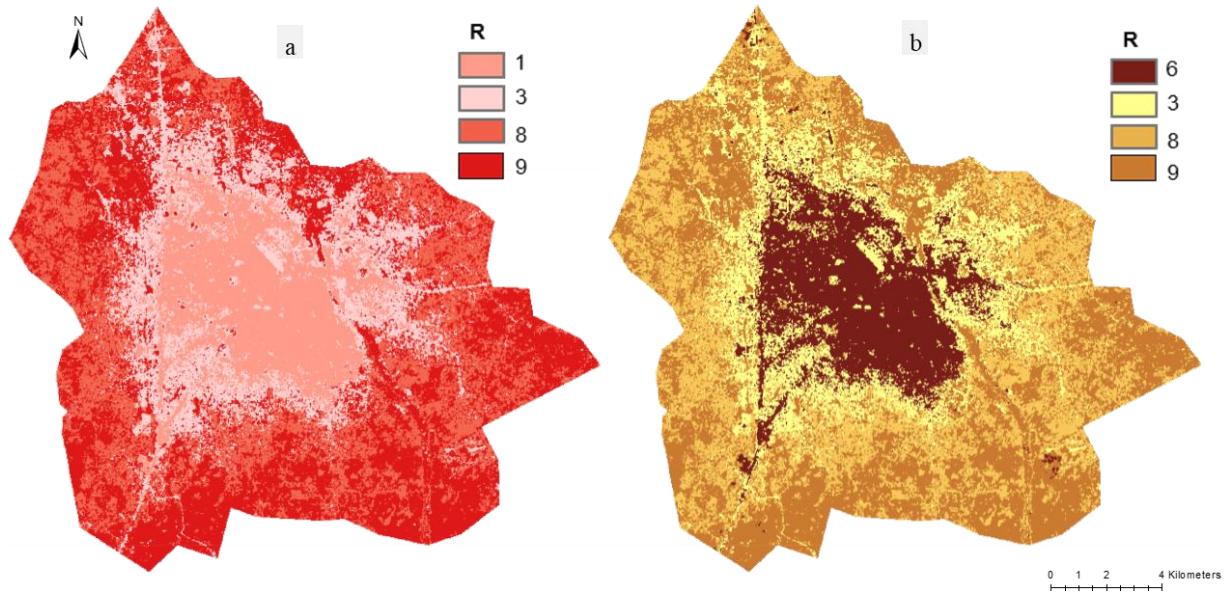


**Figure 7.** Rating maps of (a) net recharge [R] and (b) modified net recharge [$R_m$].

whereas a rating of 6 was assigned to the built-up class in the [$R_m$] map. This higher rating in the built-up class of $R_m$ is because of the harmful impact of some practices already observed and reported in the groundwater quality.

### *Aquifer media [A]*

The aquifer media describes rock types that store groundwater in the saturated zone. The lithology of the boreholes in the area suggests that the aquifer media lie between medium-grained to very fine gravelly materials. Rocks that are porous and unconsolidated have higher capacities to store and transmit groundwater compared to consolidated rock materials, making them more vulnerable to contamination. These sand types make the groundwater moderately prone to contamination because of the medium to high aquifer porosity. Therefore, a uniform rating of 8 was assigned to the aquifer media based on the ranges described in Aller et al. (1987).

### *Soil media [S]*

The soil media is the topmost part of the vadose. The porosity of the soil media determines the extent of its

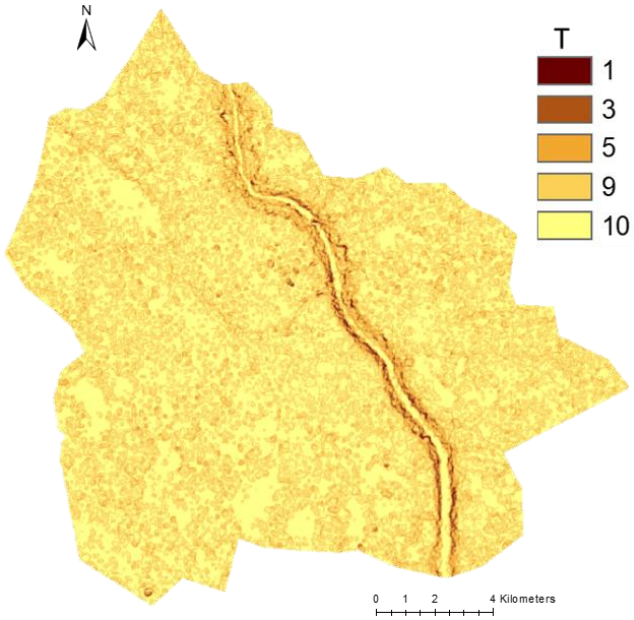


**Figure 8.** Topography rating map [T].
Source: Modified from Ijioma (2021b).

water holding capacity and the ease, with which contaminants can be transmitted from the surface to the saturated zone. The DRASTIC concept assumes that a more porous soil medium is more susceptible to aquifer contamination than the less porous ones. This implies that soil media with clayey or silty materials have a higher water holding capacity. It takes a long time for a surface contaminant to be transmitted through it than with soils that have sandy textures. Since the soil medium is uniform through the area, a single rating of 6 was assigned to represent the soil medium. This implies that the rate of vertical transmission of rainwater is moderated because of the significant clay-silt proportion in the loam soil found in the area.

### *Topography/Slope [T]*

The topography of the area is described by the slope rating map (Figure 8). The DRASTIC concept assumes that flat landforms do not encourage storm runoffs. This means that surface contamination will have more time to percolate through the unsaturated to the saturated zone. When compared with a steep or sloppy landform, rapid run-off reduces the risk of groundwater contamination but heightens the chance of surface water contamination risk. The analysis of the results showed that most parts of the study area are predominantly flat (Ijioma 2021b). These parts have been rated between 9 and 10. The steep sloppy parts occurred along the shoulder of the Aba River with ratings lying between 1 and 3. The predominant flat areas make the groundwater to be more vulnerable.

### *Impact of the vadose zone [I]*

The vadose characteristics were assumed to be the same throughout the area and a rating of 6 was assigned to the rating map. The DRASTIC approach suggests that an aquifer overlaid by a silty and clayey vadose zone require more time for a surface contaminant to travel through the unsaturated zone to the aquifer. In this case, there is sufficient time for attenuation in the vadose media. The top sandy clay layer in the upper parts of the vadose in the area slows down the transfer of rainwater and facilitates an extended attenuation time for any contaminants in the unsaturated zone. This gives the aquifer moderate protection from certain surface contaminants.

### *Hydraulic conductivity [C]*

The concept of DRASTIC assumes when the conductivity is high, there is a higher chance of contaminants transmission in the saturated zone. The hydraulic conductivity $K_f$ values ranged from $1\times10^{-3}$ to $9.6 \times 10^{-2}$ m/s, with an average of $1.52 \times 10^{-3}$ m/s have been reported in the area. Based on these values a uniform rating of 10 was assigned throughout for the rating map. The implication of the assigned $K_f$ value means a high contamination risk for the aquifer.

The hydraulic conductivity describes the ease with which water moves laterally through the aquifer. The transmission of contaminants depends on the porosity of the aquifer materials, and it is a function of time.

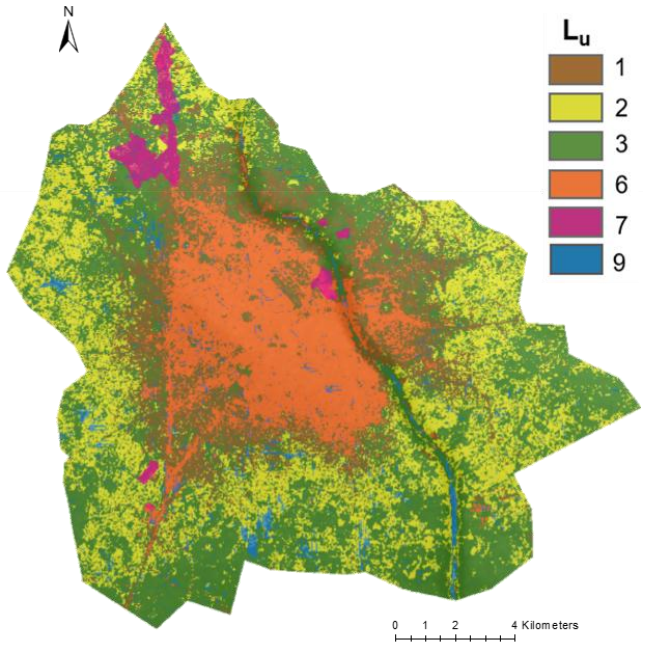


**Figure 9.** Land-use rating map.

**Table 4.** Summary of pump subclasses categorization, average withdrawal, designated and impact rating.

| Important urban subclasses | Daily withdrawal ($m^3$) | Rating | Impact designation |
|---|---|---|---|
| Large scale breweries and manufacturing industries | > 400 | 10 | Extreme |
| Medium-scale manufacturing | 100 - 400 | 8 | High |
| Hotels with swimming pool | 100 - 300 | 8 | High |
| Water bottling | 50 - 100 | 6 | Medium |
| Hotels and restaurants | 15 - 50 | 5 | Medium |
| Pumps on residential blocks | 1 - 9 | 2 | Low |

Source: Ijioma (2021b).

## Anthropogenic thematic/rating maps

### *Land-use [$L_u$]*

The ratings for the identified land-use classes follow the order: water class (9) > industrial (7) > built-up (6) > vegetated (3) > arable (2) > barren land (1) based on the 2017 map (Figure 9). The surface water and pond areas are the most vulnerable parts due to the lack of physical protection with a rating of 9. The industrial zones were assigned a high rating of 7 because this land use practice is a point source. It has been observed that most industries commonly use cesspits to drain their effluents without prior treatment in the area. The use of septic drains and other similarly identified activities form parts of the contamination hotspots that harm groundwater in the area (Ijioma, 2021b). These practices culminate in the high ratings within the impervious built-up areas. This is because such urban activities harm the quality both chemically and bacteriologically as reported in Ijioma (2021a, b).

### *Impact of active pumps [Pa]*

The impact of active pumps depends on the daily withdrawal rates and the land-use activity for which the pump serves. Table 4 summarized some important urban sub-classes, of the pumps, average daily withdrawals and their corresponding impact ratings. The spatial distribution of the 234 pumps and categorization are depicted in Figure 10a. Most of the pumps are used for domestic and small-scale commercial purposes are rated low between 2 and 5. The industrial pumps found in large scale manufacturing facilities such as the breweries companies have the highest impact ratings (between 8

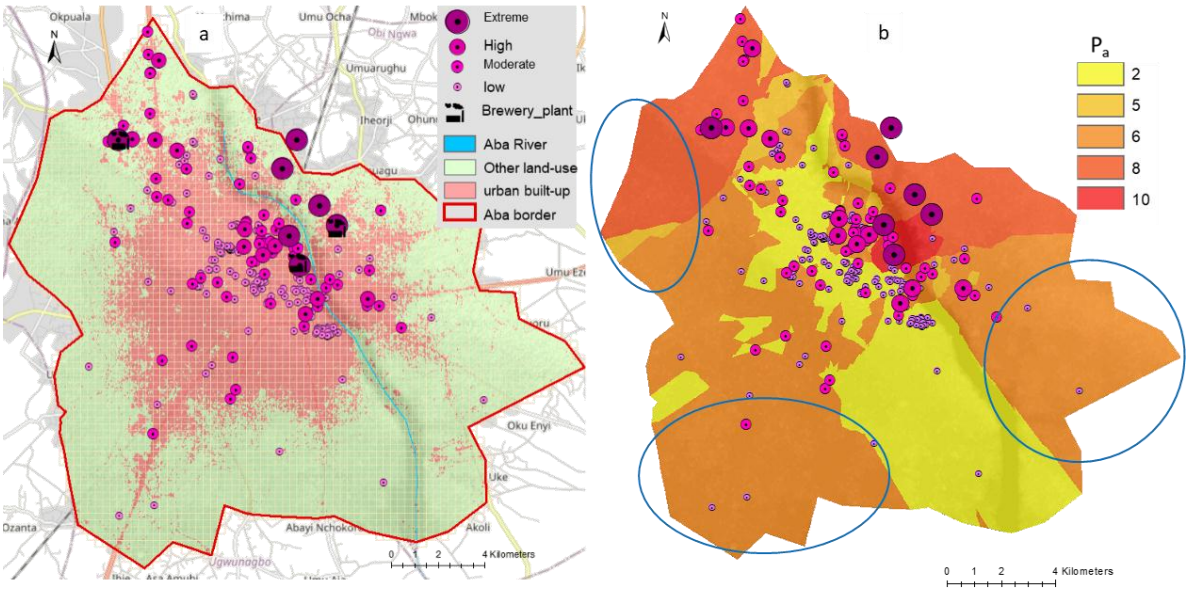


**Figure 10.** Maps of impact of active pumps distribution (a) showing subclasses of pumps and (b) rating map [$P_a$]. Source: Modified from Ijioma (2021b).

and 10). Some skewed rating values were observed on the kriging map of the active pumps (Figure 10b). Some anomalies were identified within the blue elliptical shapes, where there are scanty or no pumps because the kriging interpolation assigned rating values according to the pumps closest to these parts. These values were overall high and underscores the predictions of the rating map. This is because there are insignificant land-use activities taking place in these parts.

## Comparison of results between DRASTIC and DRASTIC-$L_uP_a$ methods

The results of the DRASTIC and DRASTIC-$L_uP_a$ vulnerability assessments maps are illustrated in Figures 11a and b, respectively and summarized in Table 5. The indices classification of the DRASTIC model revealed only three vulnerability classes (low, medium and high) and four classes (low, medium, high and very high) for the DRASTIC-$L_uP_a$. Figure 11a revealed that the area designated with “low” vulnerability make up 15%, 79.1% for “medium”, and 5.9% for “high” vulnerability classes in the DRASTIC model. Relating Figure 11a results with the land use map, the model suggests that the groundwater in most parts of the densely built-up areas is classified as “low” vulnerability. The vegetated and arable lands in the peri-urban parts were classified as “medium” vulnerability. The Aba River and some parts in the southwestern corridor were designated “high” vulnerability. The lack of physical protection over the river makes it highly vulnerable.

In general, the “medium” class represents, the intrinsic baseline vulnerability class in the area. This baseline vulnerability class corroborates with the results of the DRASTIC studies carried out within the regional basin (Ibe et al., 2003; Ijeh, 2013; Edet, 2014; Amadi et al., 2014; Mgbolu et al., 2019). The analysis of the DRASTIC-$L_uP_a$ model (Figure 11b) showed the following designation, 3.2% - “low”, 54.3% - “medium”, 41.8% - “high” and 0.7% - “very high” classes of the total area. In both models, the “medium” vulnerability class remained the predominant category. It was found that appreciable changes in the vulnerability classes happened when the results of the two models (DRASTIC and DRASTIC-$L_uP_a$) were compared. The impact of the anthropogenic (that is, modified net recharge rate, land-use and impact of active pumps) layers were the cause of the spatial transitions in the vulnerability classes. The analysis of the comparison revealed that the low vulnerability class of the DRASTIC, especially in the densely built-up parts was reduced by 11.8% in the DRASTIC-$L_uP_a$. The classified “medium” vulnerability parts in the DRASTIC method was reduced by 24.8%, however, the “high” and “very high” vulnerability classes in the DRASTIC-$L_uP_a$ increased by 35.9 and 0.7%, respectively. These transitions represent the specific vulnerability in the groundwater in these parts. However, part of the transitional effect was drawn from the impact of the active pumps rating map as identified within the ellipses (Figure 11b). There are little or no explainable land-use or physiological differentiation in the identified parts that might be responsible for the shift in the vulnerability. Therefore, it was found that the anomalies in the [$P_a$] rating map worsen the informative values of the DRASTIC-$L_uP_a$ model for these parts.

Despite the observed differences in both models, the

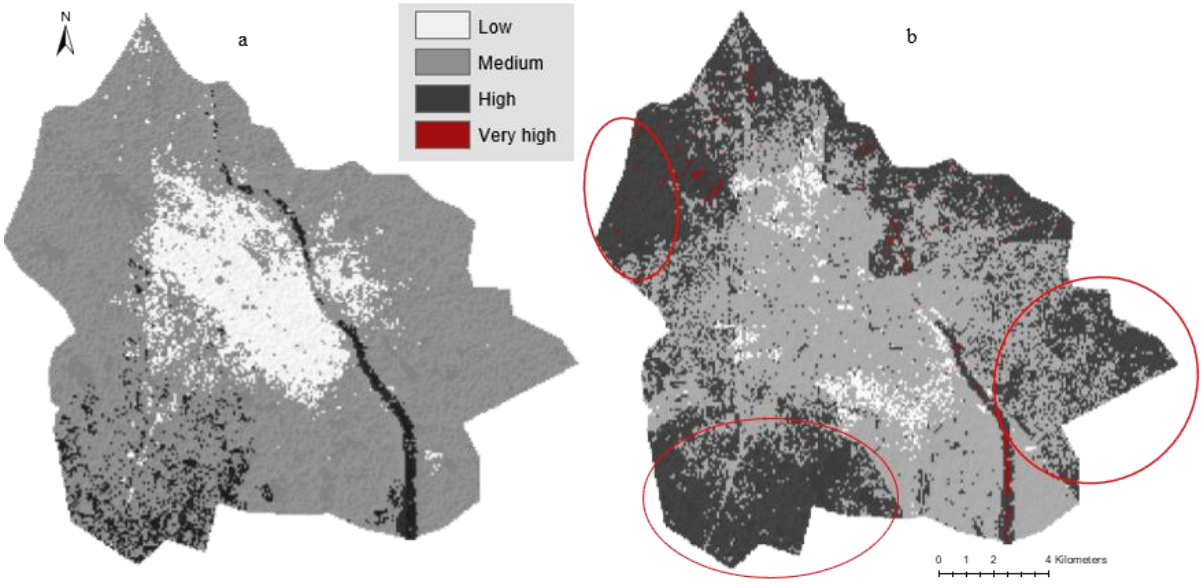


**Figure 11.** The vulnerability assessment maps showing the results of (a) DRASTIC and (b) DRASTIC-$L_uP_a$ models for the area.

accuracy was not validated. This is because the average chemical quality of the groundwater remained within the recommended limits in most parts of the area. However, some spatial changes were observed in the quality of the groundwater especially within the densest urbanized parts (Ijioma, 2021a). Yet, most anthropogenic-linked indicators in groundwater are within the recommended limits for drinking water in the area. Again, the high volume of rainwater received in the area has a considerable diluting effect on the groundwater, keeping the quality indicators in check. As the population continue to grow, the harmful impact of land use on the groundwater quality will become conspicuous and dangerous for human consumption.

## Sensitivity of the intrinsic parameters in the vulnerability map

The result of the DRASTIC method revealed that the depth to water table (D) and net recharge rating (R) were the most sensitive parameters that influenced the differentiation in the outcome of the classical vulnerability assessment map. The net recharge rating caused the most significant changes due to the anthropogenic impact of the urban land use causing low infiltration in parts of the dense built-up parts. The urban land use introduced surface sealing in the densely built-up parts and barren land surrounding the built-up parts. The areas designated with “low” groundwater vulnerability class were surrounded by the predominant “medium” vulnerability class (Figure 11a). Ibe et al. (2003) in their assessment of part of the regional basin in Owerri reported that the groundwater vulnerability was mostly influenced by intrinsic factors such as porosity, the depth to the water table, and topography. In addition, the parts designated “high” vulnerability observed in the southwestern area were caused by changes in the depth to the water table and this agrees with the findings of Ibe et al. (2003). Again, the low reference elevation in some parts of the southwestern area makes the groundwater table elevation higher and more vulnerable than the other parts of the study area. However, the mix in the composition and lithographical arrangement of the geological materials throughout the study area explained the moderate protection in the aquifer and the “medium” baseline vulnerability designation on the groundwater.

## Validating the impact of active pumps on groundwater quality

The validation of the accuracy for the impact of pumping was based on the premise that a large volume of groundwater abstracted exacerbates the quality of the groundwater if there is a nearby contamination source. The presence of total petroleum hydrocarbon (TPH) in the tube wells were determined to demonstrate the influence of daily withdrawals on the quality of groundwater. Table 6 summarized the results of the pumping, the radius of influence estimations and the impact on the groundwater quality. The findings revealed that pumps with high withdrawal generate a wider radius of influence. The radii of influences of the pumps were

**Table 5.** Analysis of the spatial distribution of the vulnerability classes in the DRASTIC and DRASTIC-$L_uP_a$ assessment methods.

| Vulnerability class | DRASTIC | | DRASTIC-$L_uP_a$ | | Differences in vulnerability (%) |
|---|---|---|---|---|---|
| | Area ($km^2$) | Area (%) | Area ($km^2$) | Area (%) | |
| Very low | 0.0 | 0 | 0.0 | 0 | 0.0 |
| Low | 35.5 | 15.0 | 7.7 | 3.2 | -11.8 |
| Medium | 187.4 | 79.1 | 128.7 | 54.3 | -24.8 |
| High | 14.1 | 5.9 | 99.0 | 41.8 | 35.9 |
| Very High | 0.0 | 0 | 1.5 | 0.7 | 0.7 |

**Table 6.** Estimation of the pumps' radii of influence and their impact on the groundwater quality.

| Hydraulic property | Tube-wells | | | Remark(s) |
|---|---|---|---|---|
| | $BH_{T3}$ | $BH_{T5}$ | $BH_{AB}$ | |
| Storage capacity *V* ($m^3$) | 190 | 380 | 60 | Field measurement |
| Time *t* (s) | 42222 | 84444 | 13333 | Pumping time measured |
| Height *h* (m) | 29.1 | 29.3 | 29.4 | Field measurement |
| Radius of influence, *R* (m) | 253 | 358 | 143 | - |
| TPH in water sample (mg/l) | 0.5 | 0.7 | ND | - |
| Pump rate ($m^3/s$) | | $4.5 \times 10^{-3}$ | | Field measurement |
| Hydraulic conductivity $K_f$ (m/s) | | $1.5 \times 10^{-3}$ | | Agharanya and Dim (2018) |
| Effective porosity [*n*] | | 0.26 | | Agharanya and Dim (2018) |

ND = Not detected.
Source: Modified from Ijioma (2021b).

arrayed in descending order of magnitude: $BH_{T5}$ ($R_{T5}$ = 358 m), > $BH_{T3}$ ($R_{T3}$ = 253 m) > $BH_{AB}$ ($R_{TAB}$ = 143 m). The estimated radii are directly proportional to the volume of the overhead storage volume for each pump and the time required to fill the tanks. The closer a pump's zone of influence to the contamination plum, the easier it is for the groundwater to be contaminated. The results revealed that $BH_{T5}$ with the largest storage volume and radius of influence has interacted with the petroleum product plume. A concentration of TPH = 0.74 mg/l was found in the sample of $BH_{T5}$. This concentration of TPH impacts taste and odour on the groundwater because the value is above the WHO limits for drinking water quality. This was followed by $BH_{T3}$, with TPH concentration = 0.54 mg/l in the groundwater sample. Although $R_{T3}$ did not directly interact with the hydrocarbon plume, however, there was an intersection between $R_{T3}$ and $R_{T5}$. This interaction might be responsible for the contamination found in the $BH_{T3}$ sample. However, no TPH concentration was detected in the $BH_{AB,}$ because the storage tank capacity was not large enough to cause a change in the natural flow of the groundwater. This demonstration can validate the impact of active pumps on the DRASTIC-$L_uP_a$ model in this part of the study area, where contamination has already been observed. The transitioning of groundwater vulnerability from "medium" to "high" and "high" to "very high" classes were also seen in these parts. However, these vulnerability classes were not captured in the DRASTIC model.

## Conclusion

The vulnerability characterization carried out for the main drinking water source in Aba Nigeria, suggests that the intrinsic properties of the aquifer provide moderate protection to the groundwater. Based on the DRASTIC model, the densely residential and commercial parts predicted as having "low" vulnerability were assumed because of the artificial surface sealing in these parts. This sealing offered extra protection to the aquifer and slow down the leaching of potential surface contaminants. However, the "low" vulnerability prediction within the densest residential parts cannot explain the observed gradual deterioration in the groundwater quality. Therefore, the assessment of groundwater vulnerability within developing urban areas where urban land-use and other poor environmental practices, which can harm the groundwater should be re-evaluated. The DRASTIC-$L_uP_a$ model was proposed to adapt the impact of anthropogenic parameters such as some urban land activities and active pumps around contaminated areas into the DRASTIC approach. The identified anthropogenic layers account for the observed transitions in the

vulnerability classes, between both models. This modification in the DRASTIC approach enhanced the predictability of the model especially within the densely residential and commercial parts making the DRASTIC-$L_uP_a$ model easily transferrable to many developing urban areas with similar urbanization patterns as found in Aba City. One of the practical implications of the DRASTIC-$L_uP_a$, model is that it identified areas that can be protected and used for safe drinking water abstraction in the study area. Based on this fact, parts of the area classified as “low” to “medium” vulnerability that is not affected by the densely urban built-up parts can be delineated and protected for source water extraction. As part of the study limitations coarse resolutions in some, rating maps created some anomalies in form of discontinuity or missing pixels observed in models’ outcomes. For instance, the DEM and Landsat imagery (approximately 30 m) influenced the output of the depth to the water table, land-use and net-recharge rating maps. A finer resolution of these data can be used when implementing the model for a small area coverage as Aba. Again, the impact of low data density in parts of the impact of active pumps rating map worsen the informative values and reliability of the results in parts of the modified model.

## CONFLICT OF INTERESTS

The authors have not declared any conflict of interests.

## ACKNOWLEDGEMENTS

The authors appreciate Nkene L. Enukeme, and Chidozie Okoroama, for making their facilities available during the hydrological field investigation in Aba. They thank the management and Department of Chemistry, Abia State Polytechnic Aba for granting research stay during the field campaign period in Aba Nigeria. The financial support from the Chair of Raw Materials and Resource Management, Brandenburg University of Technology Cottbus-Senftenberg Germany is appreciated.

## ABBREVIATIONS

**AVI,** Aquifer vulnerability index; **COP,** concentration of flow, overlaying layer and precipitation; **DEM,** digital elevation model; **DRASTIC,** depth to the water, net recharge rate, aquifer material, soil type, topography, impact of vadose and hydraulic conductivity; **DRASTIC-$L_uP_a$,** depth to the water, net recharge rate, aquifer material, soil type, topography, impact of vadose, hydraulic conductivity, land-use and impact of active pumps; **EPIK,** Epikarst, protective cover, infiltration conditions, Karst network development; **GLEAMS,** groundwater loading effects of agricultural management systems; **GOD,** groundwater hydraulic confinement, aquifer overlaying strata resistivity and depth to the water table; **HSPF,** hydrological simulation program Fortran; **MODFLOW,** MODular groundwater FLOW model; **SEEPAGE,** system for early evaluation of pollution potential from agricultural groundwater environments; **SINTACS,** Soggienza-depth to groundwater (S); Infiltrazione - effective Infiltration (I); Non saturo - unsaturated zone attenuation capacity (N), Tipologia della copertura - Soil overburden attenuation capacity (T); Acquifero - Saturated zone features (A), Conducibilità - Hydraulic Conductivity (C), and Superficie topografica - Topographic surface slope (S); **SRTM,** shuttle radar topographic mission; **SWAT,** soil and water analysis tool; **TPH**, total petroleum hydrocarbon; **WQI,** water quality index.

## REFERENCES

Adams R (2013). Water-table elevation and depth to the water table. Minnesota: Minnesota Department of Natural Resources.

Adamu N, Ezeribe IE, Oyedeji OA (2019). Engineering properties of the soils around Aba, Southeast Nigeria. Retrieved on November 11, 2019, from Academia: https://www.academia.edu/8259145/Engineering_properties_of_the_Soils_around_Aba_South_East_Nigeria

Adiat KAN, Akeredolu BE, Akinlalu AA, Olayanju GM (2020). Application of logistic regression analysis in prediction of groundwater vulnerability in a gold mining environment: a case of Ilesa gold mining area, southwestern, Nigeria. Environmental Monitoring Assessment doi: 10.1007/s10661-020-08532-7

Agharanya UP, Dim CI (2018). Water quality assessment and resource potentials: the case of Aba urban and its environs, Niger Delta basin. Water Resource Journal 45(2):250-267.

Aller L, Bennett T, Lehr JH, Petty R, Hackett G (1987). DRASTIC: A standardized system for evaluating ground water pollution potential using hydrogeologic settings. US Environmental Protection Agency. Washington, DC, 455.

Amadi AN, Olasehinde PI, Nwankwoala HO, Dan-Hassan MA, Okoye NO (2014). Aquifer vulnerability studies using DRASTICA model. International Journal of Engineering Science Invention 3(3):1-10.

Arthur J, Wood H, Baker A, Cichon J, Raines GL. (2007). Development and implementation of a Bayesian-based aquifer vulnerability assessment in Florida. Natural Resources Research 16(2):93-107.

Bazimenyera J, Zhonghua T (2008). A GIS-based DRASTIC model for assessing groundwater vulnerability in shallow aquifer in Hangzhou–Jiaxing–Huzhou Plain, China. Resource Journal of Applied Sciences pp. 550-559.

Civita M, Forti P, Marrini P, Meccheri M, Micheli L, Piccini L, Pranzini G (1991). Aquifer vulnerability to contamination map of the Apuan Alps. Mem. explic., Monography G.N.D.C.I.– C.N.R. no. 399.

Doerfliger N, Jeannin PY, Zwahlen F (1999). Water vulnerability assessment in Karstic environment: a new method of defining protection areas using a multi-attribute approach and GIS tools (EPIK method). Environmental Geology 39(2):165-176.

Dörfliger N, Zwahlen F (1998). Practical guide: Groundwater vulnerability mapping in Karstic Regions (EPIK); Bern: Swiss Agency for the Environment, Forests and Landscape (SAEFL).

Doungmanee P (2016). The nexus of agricultural water use and economic development level. Kasetsart Journal of Social Sciences pp. 38-45.

Edet A (2014). An aquifer vulnerability assessment of the Benin Formation aquifer, Calabar, southeastern Nigeria, using DRASTIC and GIS approach. Environmental Earth Sciences 71(4):1747-1765.

Egboka BC, Nwankwor GI, Orajaka IP, Ejiofor AO (1989). Principles and problems of environmental pollution of groundwater resources

with case examples from developing countries. Environmental health perspectives 83:39-68.
ESDAC (European Soil Data Centre) (1990). *Soils map of Nigeria*. Retrieved from European Commission Joint Research Centre: https://esdac.jrc.ec.europa.eu/images/Eudasm/Africa/images/maps/download/afr_ngsms1.jpg
Food and Agriculture Organization (FAO) (2020). Water at a glance: the relationship between water, agriculture, food security and poverty. Retrieved December 10, 2020, from FAO WATER: http://www.fao.org/3/ap505e/ap505e.pdf
Fileccia A (2015). Some simple procedures for the calculation of the influence radius and wellhead protection areas (theoretical approach and a field case for a water table aquifer in an alluvial plain). Acque Sotterranee - Italian Journal of Groundwater https://doi.org/10.7343/as-117-15-0144
Foster S (1987). Fundamental concept in aquifer vulnerability, pollution risk and protection strategy in Duijvenbooden V, Waegeningh HG. Vulnerability of soil and groundwater to pollutions. Hague: Committee on Hydrogeological Research pp. 69-86.
Frind E, Molson J, Rudolph D (2006). Well Vulnerability: A Quantitative Approach for Source Water Protection. Groundwater 44(5):732-742.
Hayward D, Oguntoyinbo JS (1987). Climatology of West Africa. New Jersey: Barnes and Noble's Books.
Ibe KM, Nwankwo GI, Onyekuru SO (2003). Groundwater pollution vulnerability and groundwater protection strategy for the Owerri area, Southeastern Nigeria. Water Resources Systems—Water Availability and Global Change. Sapporo: IAHS.
Ijeh IB (2013). Determination of the vulnerability of water supply aquifers in parts of Imo River Basin, South-eastern Nigeria: The case of Benin formation. International Journal of Modern Engineering Research 3(1):291-295.
Ijioma UD (2021a). Delineating the impact of urbanization on the hydrochemistry and quality of groundwater wells in Aba, Nigeria. Journal of Contaminant Hydrology. Doi: /10.1016/j.jconhyd.2021.103792
Ijioma UD (2021b). Evaluation of water situation and development of drinking water management plan for Aba City, Southeast Nigeria. (PhD-thesis) Brandenburg University of Technology Cottbus-Senftenberg Germany. Doi: /10.26127/BTUOpen-5589
Jang WS, Engel B, Harbor J, Theller L (2017). Aquifer vulnerability assessment for sustainable groundwater management using DRASTIC. Water doi:10.3390/w9100792
Jasem AH (2010). Assessing groundwater vulnerability in the Azraq basin area by a modified DRASTIC index. Journal of Water Resources and Protection.
Jhariya DC, Kumar T, Pandey HK, Kumar S, Kumar D, Gautam AK, . . . Kishore N (2019). Assessment of groundwater vulnerability to pollution by modified DRASTIC model and analytic hierarchy process. Environmental Earth Sciences 67(6):1801-1820.
Jinno K, Tsutsumi A, Alkaeed O, Saita S, Berndtsson R (2009). Effects of land-use change on groundwater recharge model parameters. Hydrological Sciences Journal 54(2):300-315.
Kemper KE (2004). Groundwater—from development to management. Hydrogeology Journal 12(1):3-5.
Kumar A, Krishna AP (2019). Groundwater vulnerability and contamination risk assessment using GIS-based modified DRASTIC-LU model in hard rock aquifer system in India. Geocarto International 35(11):1149-1178.
Macheve B, Danilenko A, Abdullah R, Bove A, Moffitt LJ (2015). State water agencies in Nigeria: a performance assessment. Washington, DC: World Bank doi: 10.1596/978-1-4648-0657-5
Mair A, El-Kadi AI (2013). Logistic regression modeling to assess groundwater vulnerability to contamination in Hawaii, USA. Journal of Contaminant Hydrology 153:1-23.
Massetti M, Poli S, Sterlacchini S, Beretta GP, Facchi A (2008). Spatial and statistical assessment of factors influencing nitrate contamination in groundwater. Journal of environmental management 86(1):272-281.
Mgbolu CC, Obiadi II, Obiadi CM, Okolo CM, Rumhe PE (2019). Integrated groundwater potentials studies, aquifer hydraulic characterisation and vulnerability investigations of parts of Ndokwa, Niger Delta basin, Nigeria. Solid Earth Sciences 4(3):102-112.
Moore P, John SX (1990). *SEEPAGE:* A System for Early Evaluation of the Pollution Potential of Agricultural Groundwater Environments. Chester, USA: Geol Tech; USDA, SCS, Northeast Technical Center.
Moustafa M (2019). Assessing perch aquifer vulnerability using modified DRASTIC: a case study of colliery waste in North-east England (UK). Hydrogeology Journal 27(5):1837-1850.
Nwankwoala H (2015). Hydrogeology and groundwater resources of Nigeria. International Journal of Geology and Earth Sciences 4(4):56-76.
Ophori DU (2007). A simulation of large-scale groundwater flows in the Niger Delta, Nigeria. Environmental Geosciences 14(4):181-195.
Saatsaz M, Sulaiman WN, Eslamian S, Mohammadi K (2011). GIS DRASTIC model for groundwater vulnerability estimation for groundwater of Astaneh-Kouchesfahan Plain, Northern Iran. International Journal of Water 6(1-2):1-14.
Secunda S, Collin ML, Mellou AJ (1998). Groundwater vulnerability assessment using a composite model combining DRASTIC with extensive agricultural land use in Israel's Sharon region. Journal of Environmental Management 54(1):39-57.
Singh A, Srivastav SK, Kumar S, Chakrapani GJ (2015.). A modified-DRASTIC model (DRASTICA) for assessment of groundwater vulnerability to pollution in an urbanized environment in Lucknow, India. Environmental Earth Sciences 74(7):5475-5490.
Sorichetta A (2010). Groundwater vulnerability assessment using statistical methods. Milan: University of Milan.
UNESCO (2004). Groundwater Resóurces of the World and their Uses in Zektser IS, Everett LG (Eds) Retrieved from https://unesdoc.unesco.org/ark:/48223/pf0000134433
van Stempvoort D, Evert L, Wassenaar L (1993). Aquifer vulnerability index: a GIS compactable method for groundwater vulnerability mapping. Canadian Water Resources Journal 18(1):25-37.
Vias JM, Andrco B, Perles M, Carrasco F, Vadillo I, Jimenez P (2006). Proposed method of groundwater vulnerability mapping in carbonate (karstic) aquifers: the COP method. Applications in two pilot sites in southern Spain. Hydrogeology Journal pp. 912-925.
Vrba J, Zoporozec A (1994). Guide book on Mapping Groundwater Vulnerability. Hannover: IAH.
Wakode HB (2016). Analysis of Urban Growth and Assessment of Impact of Urbanization on Water Resources- A Case Study of Hyderabad, India. Georesources and Materials Engineering. Aachen: RWTH Aachen University Library. Retrieved 01 08, 2021, from http://publications.rwth-aachen.de/record/570520/files/570520.pdf
Weber H (1928). Die Reichweite von Grundwasserabsenkungen mittels Rohrbrunnen. Berlin: Julius Springer.

**APPENDIX**

**Table A-1.** Assigned numerical range, rating and weight for each hydrogeologic setting in the DRASTIC model.

| Parameter range | Rating |
|---|---|
| **Depth to water table (m)** | |
| 0.0-1.5 | 10 |
| 1.5-4.6 | 9 |
| 4.6-9.1 | 7 |
| 9.1-15.2 | 5 |
| 15.2-22.9 | 3 |
| 22.9-30.5 | 2 |
| >30.5 | 1 |
| **Net recharge rate (mm)** | |
| >254 | 9 |
| 177.8-254 | 8 |
| 101.6-177.8 | 6 |
| 50.8-101.6 | 3 |
| 0.0-50.8 | 1 |
| **Aquifer media** | |
| Karst limestone | 10 |
| Basalt | 9 |
| Sand and gravel | 8 |
| Massive limestone | 6 |
| Massive sandstone | 6 |
| Bedded sandstone, limestone & shale | 6 |
| Glacial till | 5 |
| Weathered metamorphic/igneous | 4 |
| Metamorphic/Igneous | 3 |
| Massive shale | 2 |
| **Topography (% rise of the slope)** | |
| 0-2 | 10 |
| 2-6 | 9 |
| 6-12 | 5 |
| 12-18 | 3 |
| >18 | 1 |
| **Hydraulic conductivity (m/day)** | |
| >86 | 10 |
| 45-85 | 8 |
| 30-45 | 6 |
| 13-30 | 4 |
| 4.5-13 | 2 |
| 0-4.5 | 1 |
| **Impact of vadose zone** | |
| Karst limestone | 10 |
| Basalt | 9 |
| Sand and gravel | 8 |
| Metamorphic/Igneous | 4 |
| Sand and Gravel with significant silt and clay | 6 |

**Table A-1.** Contd.

| | |
|---|---|
| Bedded limestone, sandstone, shale | 6 |
| Sandstone | 6 |
| Limestone | 6 |
| Shale | 3 |
| Silt/Clay | 3 |
| Confining layer | 1 |
| | |
| **Soil media** | |
| Thin or absent | 10 |
| Gravel | 10 |
| Sand | 9 |
| Peat | 8 |
| Shrinking and/or aggregated clay | 7 |
| Sandy loam | 6 |
| Loam | 5 |
| Silty loam | 6 |
| Clay loam | 3 |
| Muck | 2 |
| Nonshrinking and non-aggregated clay | 1 |
| | |
| **Impact of active pump ($m^3$)** | |
| >400 | 10 |
| 100-400 | 8 |
| 50-100 | 6 |
| 15-50 | 5 |
| 0-15 | 2 |
| | |
| **Assigned weight** | **Weight** |
| Depth to water-table [D] | 5 |
| Net recharge rate [R] | 4 |
| Aquifer media [A] | 3 |
| Soil Media [S] | 2 |
| Topography [T] | 1 |
| Impact of vadose [I] | 5 |
| Hydraulic Conductivity [C] | 3 |
| Impact of pumps [$P_a$] | 5 |
| Land use [LU] | 5 |

The units of some of the hydrogeologic settings, such as D, R, C and $P_a$ are expressed in SI units.
Source: Aller et al. (1987).

**Table A-2.** Summary of ratings for the DRASTIC and DRASTIC-$L_uP_a$ parameters.

| Intrinsic properties | Rating |
|---|---|
| ***Depth to water-table (m)*** | |
| 6.0-9.1 | 7 |
| 9.2-15.2 | 5 |
| 15.2-22.9 | 3 |
| 23.0-30.5 | 2 |
| > 30.5 | 1 |
| ***Topography (%)*** | |
| 0-2 | 10 |
| 3-6 | 9 |
| 7-12 | 5 |
| 13-18 | 3 |
| >18 | 1 |
| ***Net recharge [R] (mm)*** | |
| 21-43.3 | 1 |
| 46.9-83.8 | 3 |
| 112.2-214 | 6 |
| 138.9-268 | 9 |
| ***Impact of vadose*** | |
| Sand & gravel with silt | 6 |
| ***Aquifer media*** | |
| Sand & gravel | 8 |
| ***Hydraulic conductivity (m/s)*** | |
| $> 10^{-3}$ | 10 |
| ***Soil media*** | |
| Sandy loam | 6 |
| ***Impact of pump ($m^3$)*** | |
| 1-10 | 2 |
| 11-50 | 5 |
| 51-100 | 6 |
| 101- 400 | 8 |
| >400 | 10 |
| **Anthropogenic properties** | |
| ***Land-use map*** | |
| Barren land | 1 |
| Arable land | 3 |
| Vegetated | 3 |
| Built-up | 6 |
| Water bodies | 9 |
| ***Net recharge [$R_m$] (mm)*** | |
| 21-43.3 | 6 |
| 46.9-83.8 | 3 |
| 112.2-214 | 6 |
| 138.9-268 | 9 |

Source: Ijioma (2021b).

Vol. 15(12), pp. 560-568, December 2021
DOI: 10.5897/AJEST2020.2942
Article Number: E81841368402
ISSN: 1996-0786

http://www.academicjournals.org/AJEST

African Journal of Environmental Science and Technology

*Full Length Research Paper*

# *Uroclhoa mosambincensis*: A potential native phytoremediator for soils contaminated with arsenic

**Sónia Isabel Ventura Guilundo[1*], Marta Alberto Aduge[1], Edmilson Enes Manuel Simango[1], Domingos Maguengue[1], Esnaider Rodríguez Suárez[2], Célia Marília Martins[1] and Orlando António Quilambo[1]**

[1]Biology Science Department, Eduardo Mondlane University (DCB-UEM), Maputo, Mozambique.
[2]Chemical Department, Eduardo Mondlane University (DQ-UEM), Maputo, Mozambique.

Received 6 November, 2020; Accepted 7 October, 2021

**Industrial development has caused the contamination of the environment, leading to biodiversity loss and human health concerns. The use of native plants and/or their associated microbiota is a sustainable solution for reducing or transforming contaminants into less harmful forms. This study was conducted to evaluate the remedial potential of *Uroclhoa mosambincensis* in soils contaminated with arsenic. In a greenhouse experiment, seedlings of *U. mosambincensis* were divided into four treatments of increasing arsenic concentration. It was found out that in *U. mosambicensis,* although most physiological parameters were affected, in 200 mg.kg$^{-1}$ arsenic trioxide concentration ($As_2O_3$) an increase in 23.3% of leaf biomass was observed. Chlorophyll A was not significantly affected by the presence of arsenic. It was also verified that the increase in arsenic concentration stimulated the removal of arsenic from soil to plant tissues at a percentage of 10.8, 27.7 and 30.2 higher in each treatment. This indicates the arsenic accumulator character of *U. mosambicensis* and its potential use for remediation of soils contaminated with arsenic.**

**Key words:** Accumulation, arsenic trioxide, metalloid, phytoremediation.

## INTRODUCTION

The intensification of industrial, agricultural and urbanization activities has increased the risk of soil pollution by heavy metals (Saxena et al., 2019) and metalloids including arsenic (As) (Yan et al., 2020). The most common forms of As found in plant tissues and in the soil are trivalent (III) and pentavalent (V) As. Trivalent As (III) is 60 times more toxic than inorganic pentavalent (V) form (Zmozinski, 2014; Abbas et al., 2018; Jinadasa and Fowler, 2019).

The toxicity of trivalent As is because it is retained in the body through the connection with sulfhydric groups (De Carvalho, 2004). In humans, doses between 10 and 50 µg. l-1 and > 50 µg. l-1 can be lethal (WHO, 2016), acting as a neurotoxic agent, and long-term exposure, even at low doses, has a carcinogenic effect (Flanagan et al., 2012; Khalid et al., 2017; Shahid et al., 2018; Alam et al., 2019). Various conventional physical-chemical techniques have been used to reduce the availability of As in the environment, such as soil washing by high pressure, gas extraction from the soil, carbon adsorption,

*Corresponding author. E-mail: siventura84@gmail.com.

chemical oxidation, the electro-osmotic method, the thermal method *in situ* and *ex situ*, etc. (Wuana and Okieimen, 2011; Sharma et al., 2018). However, these methods are quite costly and also have undesirable effects on the environment (Wuana and Okieimen, 2011). Alternatively, phytoremediation, which is the use of plants, fungi and associated bacteria, in the recovery of polluted soil, water and air (Greipsson, 2011; Sharma and Pandey, 2014), have proven effective in reducing contaminant concentrations (Lambers et al., 2008; Ma et al., 2016) or in the transformation of contaminants into forms less harmful to living beings, especially in the trophic chain (Andrade et al., 2009; Sharma and Pandey, 2014).

In phytoremediation it is necessary to use plants that have certain characteristics, such as good absorption capacity, a deep root system, an accelerated growth rate, easy harvesting and high tolerance to the contaminant (Oliveira et al., 2007). Thus, in the present study, the potential of *Uroclhoa mosambicensis*, which is a grassy species abundant in the Beleluane Industrial Park, was evaluated to restore As-contaminated soils.

## MATERIALS AND METHODS

The study was formally authorized by the local authorities. The soil and plant material samples were collected at the Beleluane Industrial Park, located near the Matola River, at latitude 25° 91361 and longitude 32° 41940 (Figure 1).

A transect was done and every 5 m a grid with dimensions of 1 m × 1 m was made. Soil was collected at a depth of 30 cm and placed in polyethylene bags for further physical-chemical parameters analysis and As quantification using the X-ray fluorescence (XRF) method (Kodom et al., 2012; Marchand et al., 2016).

Eighty seedlings of *U. mosambinsensis* (the most abundant species) were collected and grown in a greenhouse. Polyethylene pots containing 1 kg of soil from the sampling site, each one with two seedlings, were used and divided into four treatments: 0, 50, 200 and 800 $mg.kg^{-1}$ of $As_2O$, following a completely randomized arrangement. The plants were acclimatized (watered with tap water) for 15 days, after which different amounts of As were added. The plants were harvested 35 days after contamination to assess their physiological and biochemical response to different concentrations of As. The content of As and other chemical elements in soil and plant tissues was also determined.

Different techniques were used to determine the physical and chemical parameters of the soil. The calcium (Ca) and magnesium (Mg) contents were determined by ammonium acetate and the sodium (Na) and potassium (K) contents were determined by the flame photometry method (Barnes et al., 1945). Organic matter and carbon (C) were determined by the wet combustion method (Walkley and Black, 1934). The concentration of nitrogen (N) was determined by the method of Kjeldahl (Bremner and Mulvaney, 1982). The texture was determined by the pipette method (Gee and Bauder, 1986). The phosphorus content was determined by the method of Olsen et al. (1954) and the particle density by the pycnometer method. The cation exchange capacity was determined by the method using ammonium acetate and calcium chloride (Raij and Küpper, 1966).

To determine the dry weight of roots and shoots, three plants were harvested per treatment and dried at 80°C in the greenhouse for 48 h. After drying, the material was weighed on the analytical balance.

The determination of chlorophyll A and B was done using a spectrophotometer. An amount of 0.1 g of fresh leaves of *U. mosambicensis* was weighed and crushed in 10 ml of 99% ethyl alcohol and the material was stored at 17°C for 24 h.

The extracts were centrifuged for 10 min at room temperature and readings were carried out using 99% alcohol as a solvent. Wavelengths of 664 and 649 nm were used for chlorophyll A and chlorophyll B, respectively, according to the following formulas (Lichtenthaler and Buschmann, 2001):

chlorophyll A = 13.36 × A664.1 - 5.19 × A648.6
chlorophyll B= 27.43 × A648.6 - 8.12 × A664.1

The XRF technique was used to determine the As content; the dry plant material was ground in a ball mill until a homogeneous powder had been formed, which was read with the aid of a computer (Kodom et al., 2012; Marchand et al., 2016; Byers et al., 2019).

### Data analysis

The data were analyzed using the STATISTICA version 8.0 program. The difference between treatments was determined using *one-way* ANOVA at a significance level of 5%.

## RESULTS AND DISCUSSION

### Characteristics of the soil

The chemical characteristics of the soil are shown in Table 1. The soil of the industrial area has a sandy texture characterized by a higher concentration of calcium and ion exchange. Soil texture is one factor among others that can affect As mobility and availability (Marquez-Garcia et al., 2012; Abbas et al., 2018).

Sandy soils have greater availability of As, due to the lower presence of iron and aluminium oxides and hydroxides compared to clayey soils (Sheppard, 1992; Karimi and Alavi, 2016).

The As trioxide, which has greater mobility and toxicity, was used as a contaminating agent, because this compound under anaerobic conditions is most abundant and most soluble in relation to pentavalent As. The toxicity of As trioxide is 60 times greater than its pentavalent form (Abbas et al., 2018) owing to the reaction with sulfhydryl groups of enzymes and proteins, which causes the inhibition of cellular functions, contributing to the death of tissues (Jinadasa and Fowler, 2019).

### Effects of different arsenic concentrations on growth

The effect of different arsenic concentrations on the leaf, stem, roots and total plant biomass is as shown in Figure 2A, B, C and D. In general, it was found that As caused reduction of growth parameters in *U. mosambinsencis* when compared with the control treatment, and this negative effect was reported in other studies (Finnegan and Chen, 2012; Abbas et al., 2018; Nabi et al., 2021).

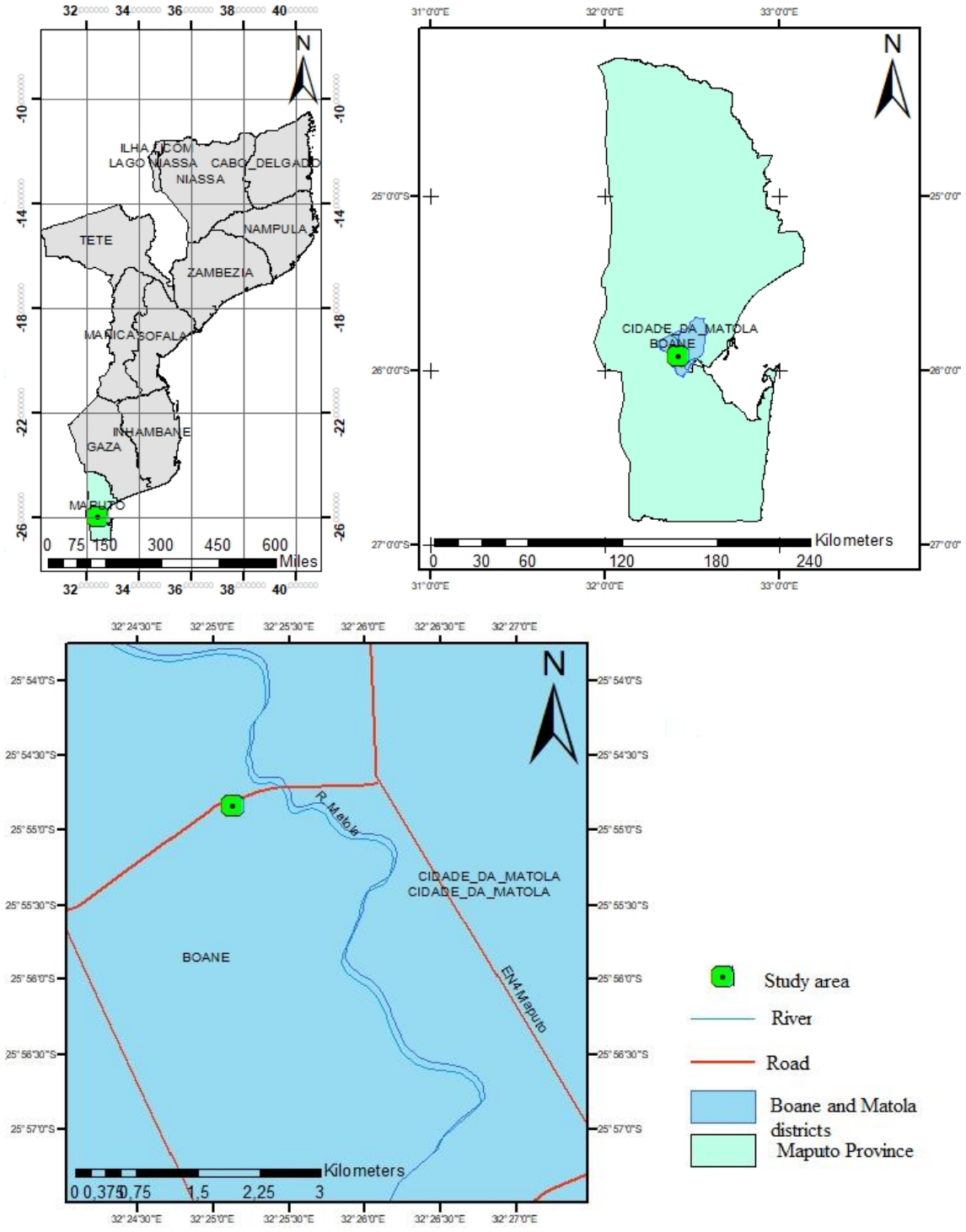


**Figure 1.** Location of the Beleluane Industrial Park.

Despite this general tendency, there was an indication that the concentration of 200 mg.kg$^{-1}$ $As_2O_3$ was the optimum level of arsenic absorption by *U. mosambinsencis*. This idea is supported by the increase of the leaf dry weight in 23.3% after the addition of 200 mg.kg$^{-1}$ $As_2O_3$ concentration ($p \leq 0.05$), suggesting that the 200 mg.kg$^{-1}$ $As_2O_3$ concentration had a stimulating effect on the production of leaf dry weight, as found by Sushant and Ghosh (2010) in a study in which the increase in As concentration increased the leaf biomass

**Table 1.** Physical and chemical characteristics of the soil of Industrial Park.

| Physical and chemical characteristics of the soil | Value |
|---|---|
| Ca | 12 |
| Mg | 0.8 |
| Na | 0.10 |
| K | 0.48 |
| Cationic exchange capacity (meq.kg$^{-1}$) | 13.6 |
| N | 0.04 |
| P | 5.73 |
| C | 0.57 |
| Organic matter | 1.12 |
| Electric conductivity (ms.cm$^{-1}$) | 0.209 |
| pH (KCl) | 7.37 |
| pH ($H_2O$) | 8.80 |
| Sand % | 79.54 |
| Clay % | 15.10 |
| Silt % | 5.36 |
| Structure | Sandy |

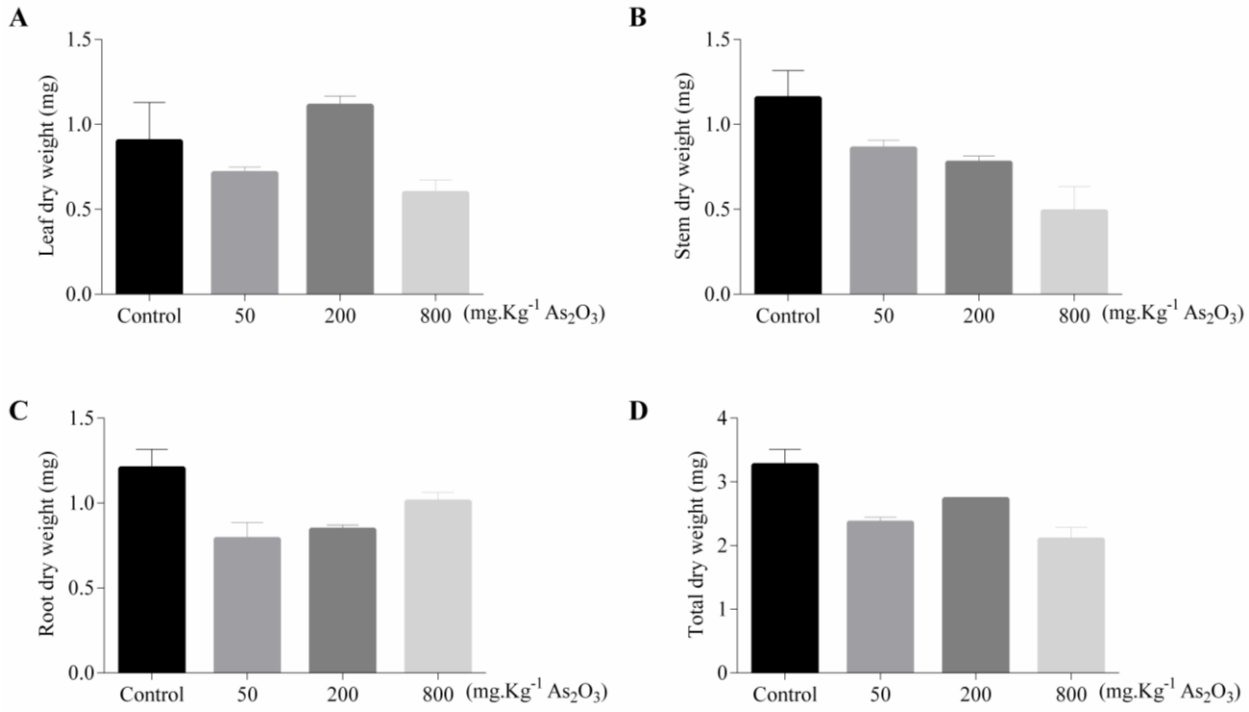


**Figure 2.** Effect of different As concentrations on the leaf, stem, roots and total plant dry weight is presented A, B, C and D. Data refer to the average of three replicates ± standard deviation.

in *Allium cepa*. Less reduction of root and total dry weight was also observed in the concentration when compared with the other treatments with arsenic in this study. Probably, the arsenic did not affect the root directly but interfered with the nutrients translocation to aerial parts as defended by Rehmus et al. (2014) in a study about the effect of aluminium on seedling of forests plants, in which it was verified that the root biomass increased or was not significantly affected while the shoot's biomass was reduced. It was verified that Al caused the reduction of

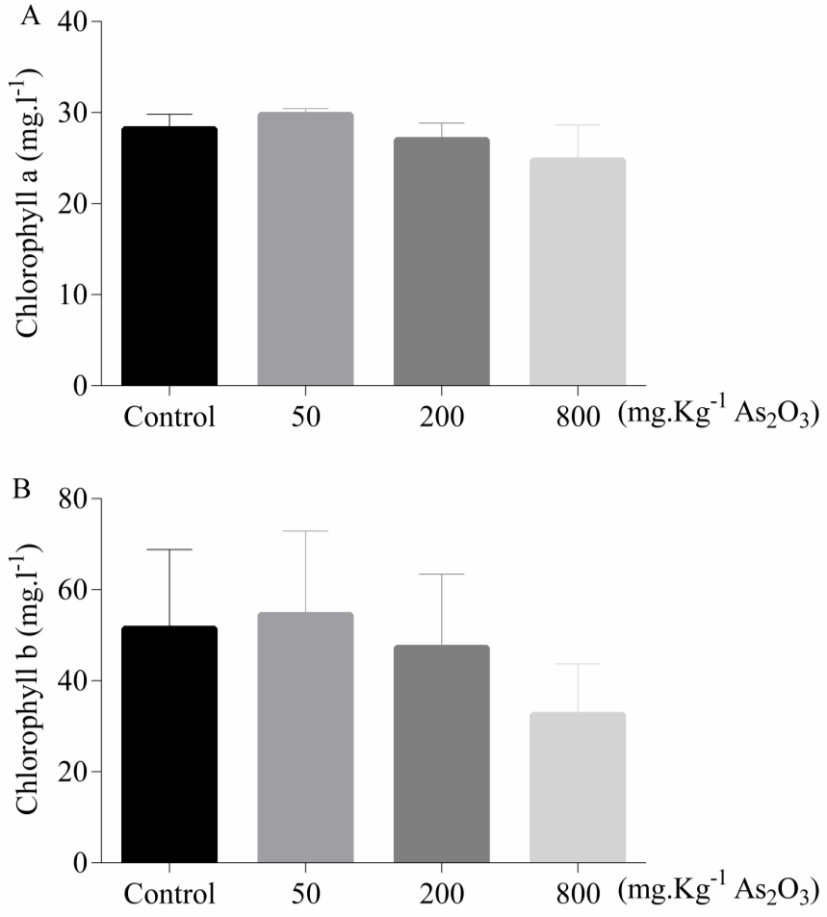


**Figure 3.** Effect of different As concentrations (0.0, 50, 200, 800 mg.kg$^{-1}$ $As_2O_3$) on chlorophyll A (A) and chlorophyll B (B) content of *Uroclhoa mosambincensis*. The bars represent the mean of three individual plants ± SD.

the macronutrient calcium in the shoots. In the present study, it was also verified that for some nutrients as potassium, calcium, chlorine among other, increase in the plant tissues was observed with the increase of $As_2O_3$ concentration, but it was not possible to verify if the nutrients were accumulated in roots or aerial parts of *U. mosambicensis.*

The stem biomass decreased 25.2, 32.2 and 57.4%, respectively with an increase in As concentration ($p \leq 0.05$). A decrease by 34.7, 30.6 and 17.4% was observed in root biomass and by 27.6, 16.3 and 35.9% in total plant biomass in all As concentrations when compared with control treatment. This is in line with Melo et al. (2018), who observed a decrease by 63 and 59% in roots, and 60 and 63% in shoots of *Anadenanthera peregrina*. But an increase of root biomass was also found with the increase of arsenic and the opposite behavior in stem biomass. These results may be explained by the high toxicity of arsenic on the growth of many plants (Várallyay et al., 2015; Mawia et al., 2021). The response to the presence of As varies with the physical-chemical characteristics of the soil, the species of plant and different mechanisms of absorption, as well as toxicity and detoxifications (Abbas et al., 2018).

In a study in which several trace elements such as As were used in different plants, including *Medicado sativa* and *Phaseolus vulgaris*, it was demonstrated that the biomass was reduced in contaminated soils. Contrary to what happens with other trace elements, As is not used as a nutrient by plants and its phytotoxic effect is well known (Melo et al., 2018).

## Effect of different concentrations of arsenic on chlorophyll content

Figure 3A and B shows that chlorophyll B decreased by 36.6% in 800 mg.kg$^{-1}$ $As_2O_3$ concentration ($p<0.05$); however, chlorophyll A content was not significantly affected by the addition of As, indicating that *U. mosambincensis* in the presence of As is able to maintain photosynthetic activity, suggesting a tolerance mechanism.

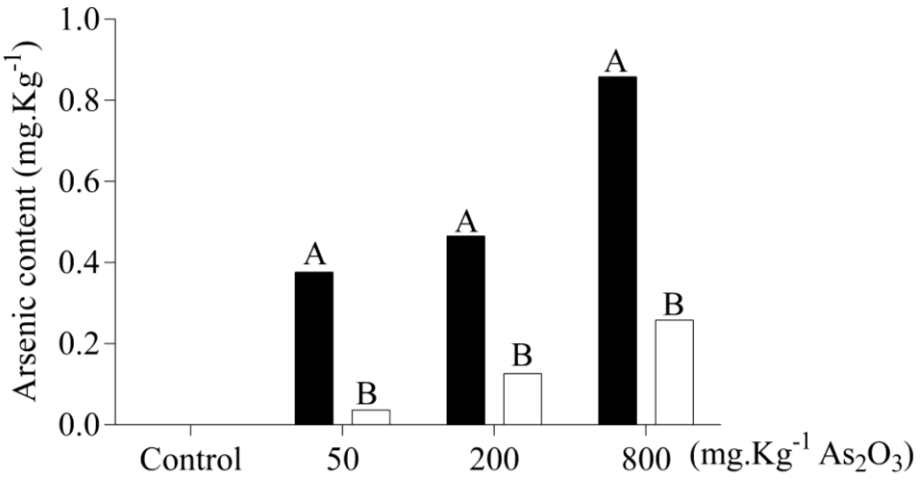


**Figure 4.** Arsenic concentrations in soil (A) and plant tissue (B) of *Uroclhoa mosambincensis*, submitted to different treatments (0.0, 50, 200, 800 mg.kg$^{-1}$ $As_2O_3$).

The chlorophyll A and B content in 50 mg.kg$^{-1}$ treatments was 5.8% higher compared to the control. Several studies have shown that the synthesis of photosynthetic pigments in different species is influenced in a different way by contamination with As (Abbas et al., 2018). In *A. cepa* it was shown that the increase in As concentration has a stimulating effect varied by 60 to 113% and by 14.6 and 59%, on the synthesis of chlorophylls A and B, respectively (Sushant and Ghosh, 2010). However, it was found that rice plants were sensitive to contamination with As, which caused a reduction by 57.3 and 50.2% in chlorophyll A and B, respectively (Miteva et al., 2005; Rahman et al., 2007). It is suggested that the reduction in the average levels of chlorophyll in plants under the effect of As is due to the destruction of the structure of chloroplasts by the metalloid (Miteva et al., 2005). In this study, it was not possible to establish a relation between the chlorophyll content and the biomass, except in stem dry weight where the increase of As concentration reduced the chlorophyll B content and consequently the biomass.

## Arsenic concentration in the soil and in the plant

Figure 4 represents the arsenic accumulation in soil and plant tissue after 35 days of experiment. In the control, no As concentration was detected in either soil or plant tissue; however, from 50 to 800 mg.kg$^{-1}$ $As_2O_3$ concentrations, the As content increased by 10.8, 27.7 and 30.2%, respectively. This result indicates that with the increase in As concentration, the stimulus for the plant to remove As from the soil increases, resulting in its accumulation in plant tissues, which is a strong indication that *U. mosambicensis* is an accumulator species.

This fact is also supported by Melo et al. (2009), using different As concentrations, they observed an increase of As in *Ricinus communis* and *Helianthus annus* tissues by 85.31 and 79.69%, in Oxisol and 32.31% and 26.03% in Entisol, respectively. This was also proven by Melo et al. (2018), observing an expressive translocation of As was observed to the aerial part of the plant *Anadenanthera peregrina*.

On the other hand, *U. mosambicensis* can be considered an accumulator, since it was found that it grows in As-contaminated soils with a concentration of 800 mg.kg$^{-1}$ $As_2O_3$ (Da Silva, 2012), showing no evident signs of phytoxicity. This fact is confirmed by Melo et al. (2018), indicating that plants growing in contaminated soil with a concentration limit of 400 mg.kg$^{-1}$ of As showed tolerance. However, other authors consider As hyperaccumulating plants as those that are able to naturally accumulate more than 1000 mg.kg$^{-1}$ of As in dry matter (Ma et al., 2001; Gonzaga et al., 2006, 2008).

The accumulation capacity found in *U.mosambicensis* is in line with the findings of Zhao et al. (2009), who reported that As (III) is as a rule accumulated by hyperaccumulative plants. This is probably due to the fact that plants have developed different mechanisms to circumvent the toxicity caused by this metal, including compartmentalization, protein synthesis of As binding proteins and synthesis of compatible solutes (Abbas et al., 2018). On the other hand, studies carried out on *Arabidopsis thaliana* and *Brassica juncea* have proven that the accumulation of As (III) in the roots and aerial parts of plants is coordinated by sulfhydryl groups such as glutathione and phytoquelatins. Singh et al. (2006) observed that a higher level of ascobarte-glutathione pool conferred protection form oxidante in arsenic hyperaccumulator P. vittata.

Table 2 represents the concentration of some elements in soil and plant tissue after 35 days of experiment. The soil exhibited a high concentration of silicium (Si), iron (Fe), manganese (Mn) and aluminium (Al) in both the

**Table 2.** Macro, micro and other element concentrations in soil and plant tissue of *Uroclhoa mosambincensis*, under different treatments (0.0, 50, 200, 800 mg.kg$^{-1}$ $As_2O_3$ concentration).

| Element | | 00 mg.kg$^{-1}$ $As_2O_3$ | | 50 mg.kg$^{-1}$ $As_2O_3$ | | 200 mg.kg$^{-1}$ $As_2O_3$ | | 800 mg.kg$^{-1}$ $As_2O_3$ | |
|---|---|---|---|---|---|---|---|---|---|
| | | **Soil** | **Plant** | **Soil** | **Plant** | **Soil** | **Plant** | **Soil** | **Plant** |
| Macro | K | 5.475 | 9.936 | 5.329 | 9.101 | 5.451 | 6.769 | 5.865 | 9.172 |
| | Ca | 1.187 | 4.117 | 1.7000 | 4.788 | 1.19 | 3.766 | 1.723 | 5.469 |
| | S | 0 | 0.785 | 0.742 | 0.668 | 0 | 0.785 | 0 | 0.78 |
| Micro | Cl | 0.53 | 6.503 | 0.91 | 6.164 | 0.755 | 4.84 | 0.554 | 7.483 |
| | Fe | 8.271 | 3.425 | 8.905 | 4.103 | 8.434 | 2.704 | 9.081 | 5.781 |
| | Mn | 0.299 | 0.18 | 0.301 | 0.199 | 0.319 | 0.171 | 0.344 | 0.257 |
| | Cu | 0.061 | 0.147 | 0.064 | 0.121 | 0.072 | 0.437 | 0.167 | 0.278 |
| | Zn | 0.009 | 0.079 | 0.011 | 0.048 | 0.009 | 0.08 | 0.01 | 0.089 |
| | Br | 0 | 0.038 | 0 | 0.043 | 0 | 0.028 | 0 | 0.042 |
| | Ni | 0 | 0.031 | 0 | 0.034 | 0 | 0.028 | 0 | 0.044 |
| | Si | 68.205 | 5.942 | 67.489 | 5.446 | 68.768 | 4.572 | 67 | 7.78 |
| | Sr | 0.024 | 0.017 | 0.026 | 0.018 | 0.028 | 0.015 | 0.032 | 0.027 |
| | Zr | 0.165 | 0.016 | 0.142 | 0.024 | 0.222 | 0.024 | 0.167 | 0.042 |
| | V | 0 | 0.016 | 0 | 0.013 | 0 | 0 | 0 | 0.046 |
| | Al | 14.079 | 0 | 12.727 | 0 | 12.902 | 0 | 13.166 | 0 |
| | Rb | 0.036 | 0.016 | 0.037 | 0.022 | 0.04 | 0.011 | 0.038 | 0.028 |
| Plastic and others | | 0 | 68.392 | 0 | 68.452 | 0 | 75.016 | 0 | 31.234 |

control and the As treatments. However, *U. mosambicensis* tissue presented high concentrations of plastic and other elements such as potassium (K), calcium (Ca), chlorine (Cl), cupper (Cu), bromide (Br) and nickel (Ni).

The difference in the nutrient content between the soil and the plant is probably due to the main factors that affect the transfer of As from the soil particles to the roots of the plants, namely the concentration of As in the soil solution, bioavailability, mass flow soil solution, pH reduction, the adsorption/desorption ratio and reduction of redox potential interaction with other ions, among others (Dabrowska et al., 2011).

It was also observed that the macro K element concentration in plants tissue decreased with As application when compared with the control. The same pattern was observed in soil, with the exception of the 800 mg.kg$^{-1}$ $As_2O_3$ treatment. Similar results were obtained in a study with *R. communis* in which Mn, Fe and Cu concentrations decreased with an increase in As, probably owing to the stress effect caused by high As concentrations (Melo, 2009).

The microelement concentrations showed a different pattern; Fe increased in all As treatments when compared with the control. No Ni was detected in soil, but it appeared in all As treatments. This phenomenon was also observed in a study with the species *R. communis*, in which an increase in As concentration caused an increase in some nutrients in the plant tissues (Melo, 2009). The aluminium (Al) was only detected in soil, but was not found in plant tissue in all treatments, showing the high ionic strength and capacity of this element to compete aggressively for access through the root (Taiz and Zieger, 2014).

## Conclusion

*U. mosambicensis* has proven to have the potential to grow in soils contaminated with As. The leaf biomass was 23.3% higher in the 200 mg.kg$^{-1}$ $As_2O_3$ concentration. The stem biomass decreased with an increase in As concentration. A decrease of 34.7, 30.6 and 17.4% in root biomass and a decrease of 27.6, 16.3 and 35.9% in total plant biomass in all 50, 200, and 800 mg.kg$^{-1}$ $As_2O_3$ concentrations were observed. The chlorophyll A content was not affected by different As concentrations. As accumulation was found in plant tissues at a percentage of 10.8, 27.7 and 30.2 higher than in soil in all treatments, suggesting *U. mosambicensis* as an As accumulator and its potential use for remediation of soils contaminated with As.

## CONFLICT OF INTERESTS

The authors have not declared any conflict of interests.

**REFERENCES**


Abbas G, Murtaza B, Bibi I, Shahid M, Niazi NK, Khan MI, Amjad M, Hussain M (2018). Arsenic Uptake, Toxicity, Detoxification, and Speciation in Plants: Physiological, Biochemical, and Molecular Aspects. International Journal of Environmental Research and Public Health 15(1):59.

Alam MZ, Hoque MA, Ahammed GJ, McGee R, Carpenter-Boggs L (2019). Arsenic accumulation in lentil (*Lens culinaris*) genotypes and risk associated with the consumption of grain. Scientific Reports 9:9431.

Andrade MG, Melo VF, Gabardo J, Souza LCP, Reissmann CB (2009). Metais Pesados em Solos de área de Mineração e Metalurgia de Chumbo: Fitoextração. Revista Brasileira de Ciências do Solo 33:1879-188.

Barnes BR, Richardson D, Berry JW, Hood RL (1945). Flame Photometry: a rapid analytical procedure. Industrial Engineering Chemistry Analytical Edition 17(10):605- 611.

Bremner JM, Mulvaney CS (1982). Nitrogen-Total - Methods of Soil Analysis. Madison. American Society of Agronomy Publishing.

Byers HL, McHenry LJ, Grundl TJ (2019). XRF techniques to quantify heavy metals in vegetables at low detection limits. Food Chemistry1:30.

Da Silva JF (2012). Prospecção De Plantas Fitorremediadoras Em Solos Contaminados Por Metais Pesados. Tese de Doutoramento. Universidade Federal Do Amazonas, Manaus.

Dabrowska BB, Vithanage M, Gunaratna KR, Mukherjee AB, Bhattacharya P (2011). Bioremediation of Arsenic in Contaminated Terrestrial and Aquatic Environments. Netherlands. Springer Publishing.

De Carvalho LM, Nascimento PC, Bohrer D (2004). Especiação Analítica de Compostos de Arsénio Empregando Métodos Voltâmetricos e Polarográficos: Uma Revisão Comparativa de Suas Principais Vantagens e Aplicações. Química Nova 27(2):261-269.

Finnegan PM, Chen W (2012). Arsenic toxicity: the effects on plant metabolism. Frontiers in Physiology 3(182):1-18.

Flanagan SV, Johnston RB, Zheng Y (2012). Arsenic in tube well water in Bangladesh: health and economic impacts and implications for arsenic mitigation. Bull World Health Organization 90:839-846.

Gee GW, Bauder JW (1986). Particle-size analysis. In Klute A. editors. Methods of soil analysis. 2nd ed. United States of America: American Society of Agronomy. Soil Science Society of America pp. 383-411.

Gonzaga MIS, Santos JAG, Ma LQ (2006). Arsenic phytoextraction and hyperaccumulation by fern species. Scientia Agricola 63(1):90-101.

Gonzaga MIS, Santos, JAG, Ma LQ (2008). Phytotoextraction by arsenic and hyperaccumulator *Pteris vittata* L. from six arsenic-contaminated soils: Repeated harvests and arsenic redistribution. Environmental Pollution 154(2):212-218.

Greipsson S (2011). Phytoremediation. Nature Education Knowledge 3(10):7.

Jinadasa BKKK, Fowler SW (2019). Critical Review of Arsenic Contamination in Sri Lankan. Journal of Food Quality and Hazards Control 6(4):134-145.

Karimi N, Alavi M (2016). Arsenic contamination and accumulation in soil, groundwater and wild plant species from Qorveh County, Iran. Biharean Biologist 10(2):69-73.

Khalid S, Shahid M, Dumat C, Niazi NK, Bibi I, Bakhat HFSG, Abbas G, Murtaza B, Javeed HMR (2017). Influence of groundwater and wastewater irrigation on lead accumulation in soil and vegetables: Implications for health risk assessment and phytoremediation. International Journal of Phytoremediation 19(11):1037-1046.

Kodom K, Preko K, Boamah D (2012). X-ray Fluorescence (XRF) Analysis of Soil Heavy Metal Pollution from an Industrial Area in Kumasi, Ghana. Soil Sediment Contamination 21(8):1006-1021.

Lambers H, Chapin FS, Pons TL (2008). Plant Physiology Ecology. United States of America. Springer.

Lichtenthaler HK, Buschmann C (2001). Chlorophylls and carotenoids: Measurement and characterization by UV-VIS spectroscopy. Current Protocols in Food Analytical Chemistry 1(1):F4-3.

Ma LQ, Komar KM, Tu C, Zhang W, Kennelley ED (2001). A fern that hyperaccumulates arsenic. Nature pp. 409-579.

Ma Y, Oliveira RS, Freitas H, Zhang C (2016). Biochemical and Molecular Mechanisms of Plant-Microbe-Metal Interactions: Relevance for Phytoremediation. Frontiers in Plant Science 7:1-18.

Marchand L, Sabaris CQ, Desjardins D, Oustrière N, Pesme E, Butin D, Wicart D, Mench M (2016). Plant responses to a phytomanaged urban technosol contaminated by trace elements and polycyclic aromatic hydrocarbons. Environmental Science and Pollution Research 23(4):3120-3135.

Marquez-Garcia B, Pérez-López R, Ruíz-Chancho MJ, López- Sanchez LF, Rúbio JF, Abreu R, Nieto MM, Cordoba JM (2012). Arsenic speciation in soils and *Erica andevalensis* Cabezudo and Rivera and *Erica australis* L. from São Domingos Mine area, Portugal. Journal of Geochemical Exploration 119:51-59.

Mawia AM, Hui S, Zhou L, Li H, Tabassum J, Lai C, Wang J, Shao G, Wei X, Tang S, Luo J, Hu S, Hu P, Meharg AA, Hartley-Whitaker J (2021). Arsenic uptake and metabolism in arsenic resistant and nonresistant plant species. New Phytologist 154(1):29-43.

Melo EEC (2009). Fitorremediação de Arsénio: Disponibilidade do metalóide no solo e seu acúmulo em girassol e mamona. Tese de Doutoramento. Universidade Federal de Lavras, Lavras.

Melo RF, Dias LE, Assis IR, Anjos N (2018). Efeito de doses de fósforo na mobilidade do arsênio e no desenvolvimento de duas essências florestais. Revista Brasileira de Geografia Física 11(2):401-414.

Miteva E, Hristova D, Nenova V, Maneva S (2005). Arsenic as a factor affecting virus infection in tomato plants: changes in plant growth, peroxidase activity and chloroplast pigments. Scientia Horticulturae 105(3):343-358.

Oliveira DM, Cara DVC, Xavier PG, Paula MS, Sobral LGS, Lima RB, Loureiro A (2007). Série Tecnológia Ambiental Fitorremediação: O Estado da Arte. CETEM/ MCT. Rio de Janeiro 39(2):50-53.

Olsen SR, Cole CV, Watanabe FS, Dean LA (1954). Estimation of available phosphorus in soils by extraction with sodium bicarbonate. – USDA Circular No. 939, U. S. Department of Agriculture. Washington DC.

Rahman MA, Hasegawa H, Rahman MM, Islam MN, Miah MAM, Tasmen A (2007). Effect of arsenic on photosynthesis, growth and yield of five widely cultivated rice (*Oryza sativa* L.) varieties in Bangladesh. Chemosphere 67(6):1072-1079.

Raij BV, Küpper A (1966). Cation exchange capacity of soils. A comparative study of methods. Bragantia 25(2):30:327-336.

Rehmus A, Bigalke M, Valarezo C, Castillo JM, Wilcke W (2014). Aluminum toxicity to tropical montane forest tree seedlings in southern Ecuador: response of biomass and plant morphology to elevated Al concentrations. Plant Soil 382(1):301-315.

Saxena G, Purchase D, Mulla SI, Saratale GD, Bharagava RN (2019). Phytoremediation of Heavy Metal-Contaminated Sites: Eco-environmental Concerns, Field Studies, Sustainability Issues, and Future Prospects. Reviews of Environmental Contamination and Toxicology 249:71-131.

Shahid M, Dumat C, Niazi NK, Natasha KS (2018). Global scale arsenic pollution: increase the scientific knowledge to reduce human exposure. VertigO- la revue électronique en sciences de l´environment 19(3):1-13.

Sharma P, Pandey S (2014). Status of Phytoremediation in World Scenario. International Journal of Environmental Bioremediation and Biodegradation 2(4):178-191.

Sharma S, Tiwari S, Hasan A, Saxena V, Pandey LM (2018). Recent advances in conventional and contemporary methods for remediation of heavy metal-contaminated soils. Biotechnology 8(4):1-18.

Sheppard SC (1992). Summary of phytotoxic levels of soil arsenic. Water, Air and Soil Pollution 64(3):539-550.

Singh N, Ma LQ, Srivastava M, Rathinasabapathi B (2006). Metabolic adaptations to arsenic-induced oxidative stress in *Pteris vittata* L. and *Pteris ensiforms* L. Plant Science 16(2):274-282.

Sushant KS, Ghosh AK (2010). Effect of Arsenic on Photosynthesis, Growth and its Accumulation in the Tissues of *Allium cepa* (Onion). International Journal of Environmental Engineering and Management 1(1):39-50.

Taiz L, Zieger E (2014). Plant Physiology. 6th edition; United States of America Sinauer Associates, Inc. pp. 119-143.

Várallyay S, Bódi E, Garousi F, Veres S, Kovács B (2015). Effect of arsenic on dry weight and relative chlorophyll content in greening maize and sunflower tissues. Journal of Microbiology Biotechnology

and Food Science 4:167-169.
Walkley A, Black IA (1934). An examination of the Degtjareff method for determining soil organic matter and a proposed modification of the chromic acid titration method. Soil Science 37(1):29-38.
World Health Organization (WHO) (2016). Arsenic. World Health Organization.
Wuana RA, Okieimen FE (2011). Heavy Metals in Contaminated Soils: A Review of Sources, Chemistry, Risks and Best Available Strategies for Remediation. International Scholarly Research Network pp. 1-20.
Yan A, Wang Y, Tan SN, Yusof MLM, Ghosh S, Chen Z (2020). Phytoremediation: A Promising Approach for Revegetation of Heavy Metal-Polluted Land. Frontiers of Plant Science 11(359):1-15.
Zhao FJ, Ma JF, Meharg AA, McGrath SP (2009). Arsenic uptake and metabolism in plants. New Phytologist 181(4):777-794.
Zmozinski AV (2014). Desenvolvimento de Métodos para a Determinação de Elementos Traço em amostras de Pescado por Espectrofotômetria Atómica de Massa e Técnicas Acopladas. Tese de Doutoramento em Química. Universidade Federal do Rio Grande do Sul, Porto Alegre.

Vol. 15(12), pp. 569-579, December 2021
DOI: 10.5897/AJEST2021.3008
Article Number: 1D01D1368404
ISSN: 1996-0786

http://www.academicjournals.org/AJEST

ACADEMIC JOURNALS
expand your knowledge

African Journal of Environmental Science and Technology

*Full Length Research Paper*

# The environmental impact of landfill fires and their contaminant plumes at the Chunga landfill site, Lusaka, Zambia

**Muleya Milimo[1*], Hinchliffe Graham[2] and Petterson Michael[2]**

[1]Department of Environmental Science, Faculty of Health and Environmental Sciences, Auckland University of Technology (AUT), Zambia.
[2]Department of Environmental Science, Faculty of Health and Environmental Sciences, School of Science, Auckland University of Technology (AUT), New Zealand.

Received 16 March, 2021; Accepted 6 December, 2021

**The management of solid waste is recognised as a challenging activity with respect to the environment, particularly within rapidly growing urban centres in Lower Income Countries. This paper examines the issue of landfill-waste-generated fires and resultant pollution plumes sourced within the Chunga Landfill Site, Lusaka, Zambia. The authors present the results of a geospatial analysis research programme to map and assess risks posed by landfill combustion. The project identified fires and their plumes in the period 2013 to 2019. Pollution plumes are predominantly oriented East to West but also form plumes blowing towards the South West and North West. The area impacted by landfill plumes increased from 34 ha in 2013 to 133 ha in 2019. There is significant existential and potential human-exposure to these plumes. An estimated 5000 residents live within the areas affected by landfill-combustion-plumes. The authors suggest the following framework for landfill management to be adopted: (1) for waste to be increasingly sorted and segregated with different disposal options developed for different types of waste; ( 2) for methane and gas evacuation pipes to be inserted into the Chunga Site in a systematic rectilinear manner which allows for its safe dispersal: alternately collect the gases as usable biogas; (3) rapid extinguishing of any fires; (4) weekly monitoring of the landfill site by UAV and on-the- ground inspections; (5) active weekly monitoring of air quality; (6) develop a communication strategy that aims to engage local residents and other stakeholders concerning Chunga Landfill waste management; (7) the further drafting of medium-long term waste management policy in Lusaka that takes account of the rapid population growth and increasing landfill requirements.**

**Key words:** Landfill fires, smoke plume, photogrammetry, geospatial mapping, disaster, risk management.

## INTRODUCTION

This paper documents and analyzes photogrammetric, environmental management, and waste management research, focused on Chunga Landfill Site, Lusaka, Zambia. Whilst this paper reports on a case study, the research has international relevance, particularly for Lower to Middle Income countries. Here the authors focus

*Corresponding author. E-mail: milimomuleya@gmail.com.

on the issue of landfill combustion with resultant fires and pollutant plumes containing potentially harmful substances (PHS). This work has revealed the existence of burning waste at Chunga from at least 2013 to the present day. Remote sensing analysis demonstrates that the Chunga Landfill Site experiences multi-centred landfill fires that persist for significant time periods.

Landfill- generated plumes are transported via the predominant winds present within the Chunga locality, with a real and potential impact on a significant population as the plumes travel down-wind. This research has not focused on the human population, in terms of health studies, but rather the objective is to study landfill fires by mapping the plumes created by these fires, highlight the areas impacted by fire-plumes and assess the environmental impact of the plumes.

This paper describes the purpose, methodologies and results from the Chunga Landfill Fires research and sets the issue in context with the challenge of generic waste management within Lusaka, and the wider world.

Waste management is a global challenge. The world production of solid waste has grown from 1 million to 7 million tonnes per day from 1950 to 2020, with an estimated peak of 12 million tonnes per day by 2100 (Hoornweg, 2013). Africa has been identified as a key region for improvement in solid waste management practices given the rapid rate of population growth and urbanization (Hoornweg et al., 2013).

Lusaka is an example of a rapidly growing African city with a population change of 934, 000 in 1996 to 2, 647, 000 in 2019 (PopulationStats, 2020). Management of higher volumes of solid waste associated with rising populations and increasingly urbanised populations is one of the higher magnitude environmental challenges of the $21^{st}$ century.

Low income countries are positioned to see the highest net percentage increase of urban dwellers over the next 50 years.The population of Lusaka was estimated at 2,647,000 in 2019, growing to 5,143,000 by 2034 (PopulationStats, 2020). Increased urbanisation is mainly caused by inward-migration from rural areas, and consequent increasing levels of consumption, have been the main drivers of increased waste production in the city over the last two decades. In 1996, when Lusaka's urban population was at 934, 000, waste production was estimated at 220,000 tonnes per year. This figure increased to 530, 000 tonnes per year in 2011, when the urban population was c. 1.8 million (Edema et al., 2012).

Lusaka developed its first purpose- built waste management landfill disposal site at Chunga, North West of Lusaka city in 2007 as part of its solid waste management strategy (Table 1). Of the total waste produced in Lusaka, it is estimated that c. 40% is collected and deposited at Lusaka's largest landfill site (Luke, 2017). A report by the Zambia Environmental management Agency (ZEMA) has estimated that between 2016 and 2018, an average of 29% of waste was collected and deposited at the landfill with an estimated 1000 tons of waste produced a day (ZEMA, 2019).

Landfill fires are a consequence of the spontaneous combustion of methanogenic landfill deposit material (e.g., rotting organic waste) and occur both within the surface regions and within the main body of landfill deposits. Landfill fires may produce a wide range of potentially harmful substances (PHS) through the burning of chemicals, plastics, and other waste materials. A study by (Weichenthal et al., 2015), on the impact of landfill fires on ambient air quality, discovered that there was a concomitant increase in PHS such as benzene and dioxins/furans. These toxic substances are a health risk to a range of vulnerable populations including Landfill Site workers, and residents living close to Landfill sites, as well as contaminating the surrounding environment and biosphere. According to (Lohmann and Jones, 1998), "*Polychlorinated dibenzo-p-dioxins and -furans (PCDD/Fs) are two groups of persistent, semi-volatile and toxicologically significant trace organic contaminants present in Landfill fire products."* Whilst no studies to date have definitively identified these PHS species at Chunga, their presence is suspected, as there are parallels between fires at Chunga and other, better-studied landfill fire zones, with respect to the character of stored waste and the fires themselves. The uncontrolled combustion of waste containing PHS results in widespread environmental pollution including depositing materials within the soil and deeper geological environments, surface and ground waters, and ingestion by humans, animals and plants (Zhang et al., 2015).

Landfill fires can be classified from a number of analytical viewpoints, according to cause, source, magnitude, and so on. This paper uses a classification system based on how easily fires can be extinguished (Jurbin, 2003):

1) Level one -small easily extinguished garbage fires.
2) Level two -fires that occur on the face of the landfill, on the side where garbage is being actively dumped.
3) Level three - fires are more serious and may take up to a week to extinguish.
4) Level four - fires cover an area of at least one hectare and take more than a week to extinguish (Jurbin, 2003).

The biological decomposition of waste through aerobic or anaerobic processes, produce exothermic reactions yielding extraneous heat for the surrounding environment. Landfills can produce average internal temperatures of 60 to $71^{o}$C (Stearns and Petoyan, 1984).

Through the process of pyrolysis, these exothermic reactions change from biological to chemical transferring heat to the surrounding areas through conduction and/or convection of entrenched fluids within the landfill deposit, and radiation within the immediate vicinity (Jurbin, 2003; Stearns and Petoyan, 1984). Poorly designed and managed Landfill Sites that lack an effective surface cap or seal allow the flow of oxygen into the Landfill deposit

**Table 1.** Types of waste dumped at The Lusaka city dump site (Chunga Landfill) showing the various types of waste that is dumped at the site, excluding hazardous industrial waste (Chishiba, 2002).

| Type of waste | Composition |
|---|---|
| Industrial waste | This comprises waste from construction and demolition processes while also including light industrial waste such as, clothes, ash, and polythene. This type of waste does NOT include hazardous wastes. |
| Green waste | Waste from road maintenance, mainly vegetation and wood. |
| Packaging waste | This includes plastics, cardboard, and aluminium foil. |
| Commercial/ Trade waste | This includes waste from trading institutions such as, shops, offices, hotels, restaurants, and garages. The waste comes in the form of packaging material, paper, and automotive parts. |
| Household and Institutional waste | Waste from households and institutions such as hospitals, schools, prisons etc. |

subsurface, and are consequently placed at higher risk levels with respect to landfill combustion. Sub-surface fires are more difficult to extinguish than surface fires, usually because they are harder to detect, and get to directly, (Øygard et al., 2005), also suggest that sub-surface fires cause fractures and crevices to form within the landfill structure, which affects the structural integrity of the landfill deposit and can become a factor in landfill collapse.

## MATERIALS AND METHODS

### Research site location

The Chunga Landfill Site is located at Latitude 15$^{O}$20'57.55" South, Longitude 28$^{O}$16'04.92" East, at an elevation of 1215m (GoogleEarthPro, 2019). The site covers an area of 24.53 ha and has a fenced perimeter of 2.15km. The Chunga Landfill Site is built upon bedrock geology of metamorphic schists and carbonates with overlying clay-sand-gravel rich loam soils. The presence of large areas of karstic substrate under Lusaka is noted which could allow for the ingress of pollutant fluids from Landfill Sites such as Chunga (Figure 1).

### Types of waste present at Chunga Landfill

#### *Climatic characteristics of study site*

The climatic conditions at Chunga landfill are characteristic of regions located in central Africa. The periods of rain in Zambia occur between November and March annually: however, changes in climate conditions have resulted in extreme weather conditions such as droughts and floods. The highest temperatures are reported in October, averaging24.7ºC. In July, when the study was conducted, average temperatures were recorded at 16ºC. July to September is dry and windy with Easterly winds being predominant.

### Data acquisition

#### *Equipment*

One of the core activities of the Chunga Landfill Research project was the surveying and subsequent production of a 3-dimensional photogrammetric model of the Chunga Landfill Site itself. The following equipment was used for this survey: a DJI Phantom 4 (Figure 2), Unmanned Aerial Vehicle (UAV) or Drone was used to acquire 966 images on the 27$^{th}$ of June 2019, flown at a height of 70m. This UAV has a 12.4 mega pixel (MP) camera and 60 mega bit per second (mbps) facility for video acquisition and covers a range of 6000 m which adequately covered the research area, that has a perimeter of 2, 142 m. The Phantom 4 has a flight time of 25 to 30 min on a fully charged battery. Two additional batteries were used to extend the flight time and ensure full data coverage was collected in one session. The phantom 4 is equipped with a global positioning system (GPS) and Global Navigation Satellite System (GLONASS), providing real time position of images acquired.

### GNSS receivers (EMLID Base and Rover)

As a back up to GPS information recorded by the UAV, two Global Navigation Satellite System (GNSS) receivers were used to record Ground Control Points (GCP) that would improve the absolute position of the landfill if needed. One receiver acted as a Base station (Figure 3) and the second as a rover station. The base station remained in one place and sent corrections to the moving rover. The two GNSS receivers utilized a technique known as Real Time Kinematic (RTK) to achieve centimetre accuracy (Volodina, 2020).

### Data processing

#### *Digital surface model (DSM) processing*

The georeferenced drone images were processed using the photogrammetry software Capture Reality (S.R.O, 2019) to create a Digital Surface Model (DSM). A digital surface model represents the surface elevation of the terrain and includes structures such as buildings and trees, implying that each pixel in the DSM has an elevation "Z" value that is representative of the elevation above bare earth. The analysis of this data type was done by importing the DSM into the GIS program, (Esri$^{TM}$, 2019) ArcMap 10.5.1, for further analysis as it cannot be processed in programs such as Google Earth (Wampler et al., 2013).

### Fire-plume mapping

Google satellite images were obtained between 2007 to 2019. These sequential series of time images allowed the study of plume

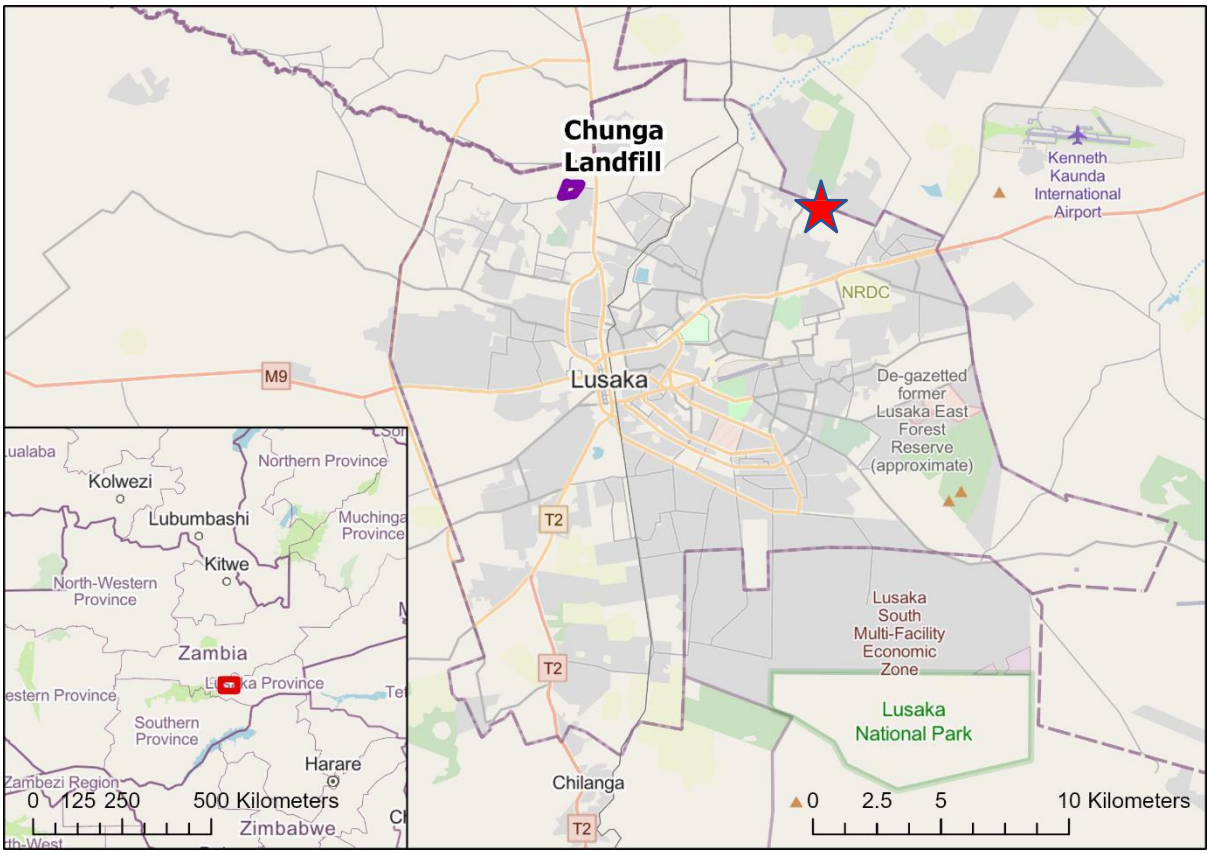


**Figure 1.** Geographical location of research site, Chunga Landfill, in Southern Africa, Lusaka Zambia, located north west of the Lusaka City is the only engineered Landfill in the city (Esri. OpenStreetMap Basemap data © OpenStreetMap contributors, 2021).

**Figure 2.** Phantom 4 (UAV) used for image acquisition at Chunga landfill.

**Figure 3.** An EMLID Rover is held in place to collect GCP at Chunga Landfill.

locations over time to be undertaken. The plumes were mapped and georeferenced. Maps were produced by creating KML polygons around identified fire-plumes. KML is a file format that is used in an Earth Browser such as Google Earth to display geographic data. Polygon shapes were converted to raster polygons, in *ArcMap*, and stacked using the cell statistics tool, that added each raster layer on top of the other, to create a fire-plume density map (Figure 6).

#### Fire-Plume area calculations

A plot of the average area covered by fire-plumes for the years, 2007 to 2019, was created (although fires have only been observed in images from 2013 and later), based on the methods described above. The area affected by fire-plumes was determined by visual observation and measurement, using the measurement tools in Google Earth Pro. The plot shown in (Figure 8) is the result of the examination of 39 images over the 12-year period. Nineteen images did not contain fire-plumes.

## RESULTS

### Digital Surface Model (DSM)

The Chunga Landfill site is shown as a digital surface model (DSM) in Figure 4. The general geomorphology can be expressed as two main ridges with a valley between them. The eastern lobate ridge is the largest and most extensive with a maximum height of c. 1200m, and measures some 320m NNW-SSE by 200m east-west. The western 'ridge' is more nebulous in form with higher areas to the north and southwest. A valley-oriented NNW-SSE separates and drains the two key ridges. In the NW there is a drainage lake, which our research shows does not retain all draining waters from the Landfill site. Overall, the site is higher in the southwest and eastern region and gradually reduces in elevation towards the northwest. This has been designed for drainage of waters towards the drainage lake in the NW of the site. The digital surface model is displayed in Figure 4, with a colour gradient as the topography key. Highest elevations are shown in a brick red colour, with a gradual reduction in colour intensity corresponding to lower elevations. The colour blue represents the lowest topographic regions. The DSM not only allows for analysis of structural elevation but also presents accurate geographical location of the landfill site.

### Fire sources

The research shows that fires at the landfill are mainly visible on the waste heaps to the North (A), North East (B) and North West (C) of the landfill (Figure 5). The Map shows the fires as red borders and the landfill Digital Surface Model (DSM) with the higher elevations appearing as red while lower evelations appear blue to violet. These regions have been mapped to show the main sources that is, combustion of waste mainly at the surface and shallow depth levels. From the DSM we observe that the fires are mainly located on the waste heaps North (A) and North east (B), with a high and lower elevation respectively.

Waste to the North West (C) is also seen as a source of fires yet not the main source of plumes. Imagery from

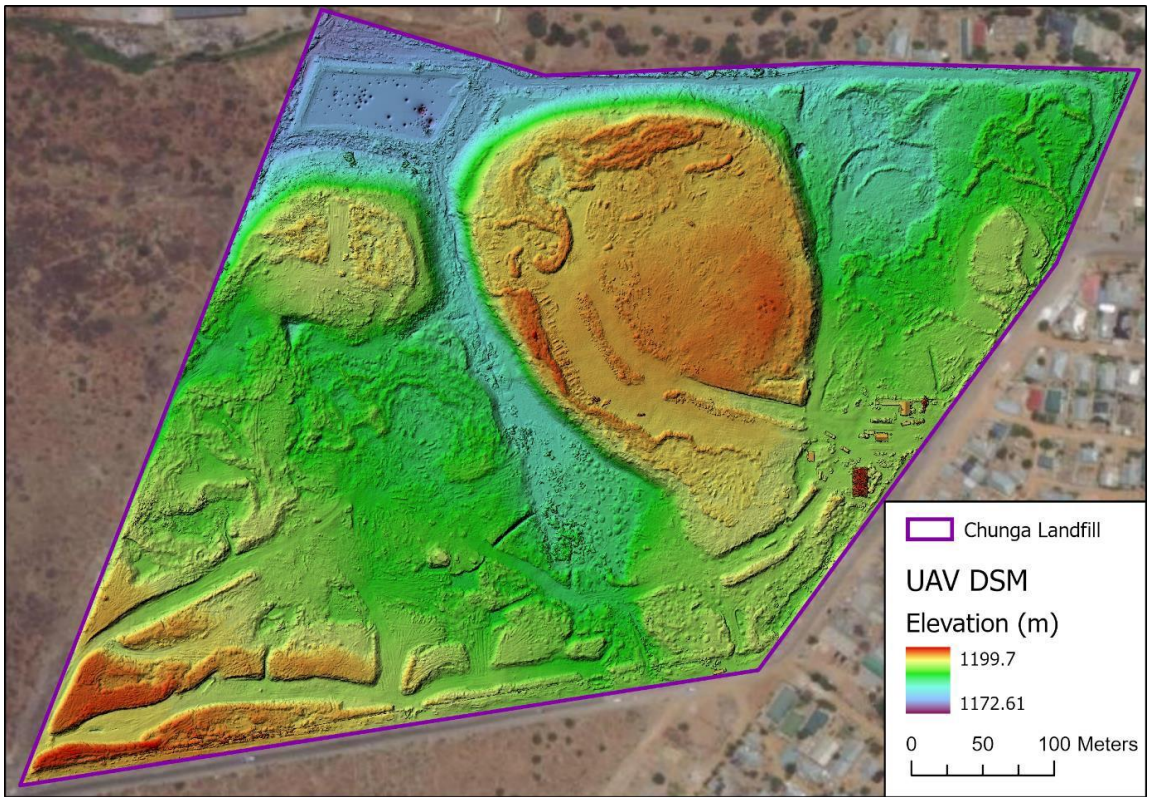


**Figure 4**. Chunga Landfill Digital Surface Model (DSM) showing the general shape and form of the site and changes in elevation based on waste heap elevations and landfill topology. Note the prominent balloon-shaped brick-red coloured ridge on the eastern side and more nebulous ridges on the western side. A broad NNW-SSE trending valley drains much of the landfill. The lowest elevation is in the NW of the site and contains a lake appearing as a deeper blue colour in NW corner (Esri, 2021).

satellite images using Google Earth (GoogleEarthPro, 2019), from 2013 to 2019, were used to record the location and temporal variation in landfill combustion. The fires are interpreted to be level two and level three fires, based on their relative longevity, difficulty to extinguish, and location within the landfill structure. The research also shows that waste heap (A) is the oldest of the fire groupings, followed by waste heap (B) and (C). Figure 5 show that waste heaps (A) and (B) are the major fire sources resulting in plume smoke.

## Plume mapping

Figure 6 displays the geographical extent of the mapped fire-plumes. The bright colours show the highest density of overlapping fire-plume trajectories (between 9 and 14 individual plumes are present within brighter yellow to red regions).

Light green to yellow regions corresponds to 6-9 fire-plume trajectories and green regions 2-4 trajectories. Dark green colour indicates the lowest density of fire-plumes and map and the maximum-peripheral extent of Chunga fire-plumes.

Figure 6 also show that the Chunga fire-plumes can cover three main areas: 1) the Chunga Land Fill site itself; 2) the open ground to the west of the Chunga Landfill Site and 3) a large area of residential properties located around the edges of the open ground area. At least 800 to 1000 individual houses have been estimated to be affected by plumes using the software.

The households are primarily to the North West, west and southwest of the landfill site. Those households immediately west of the plumes are the most exposed to most plumes with those south and north of the plume trail suffering a lesser but significant level of exposure to plume pollution. The map shows households that are exposed to different densities of plume activity (1 - 2 plume events (dark green), and 2 – 4 plume events (green to light green). An aerial image of plumes from the landfill as captured by the Unmanned Aerial Vehicle (UAV) shows thick plumes from multiple focal points being carried by Easterly winds (Figure 7).

## Average plume area

Between 2013 and 2015 there was an increase in plume

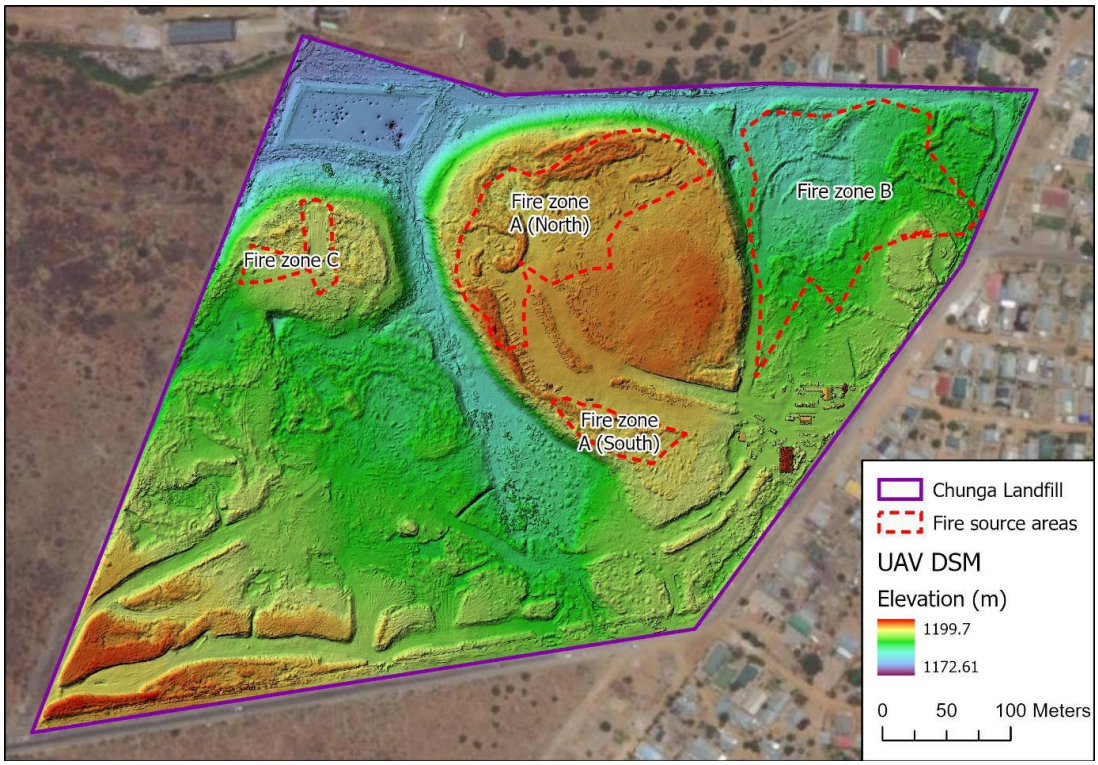


**Figure 5.** A map of Chunga Landfill showing regions where fires have been identified to burn resulting in plume smoke from 2013 to 2019.

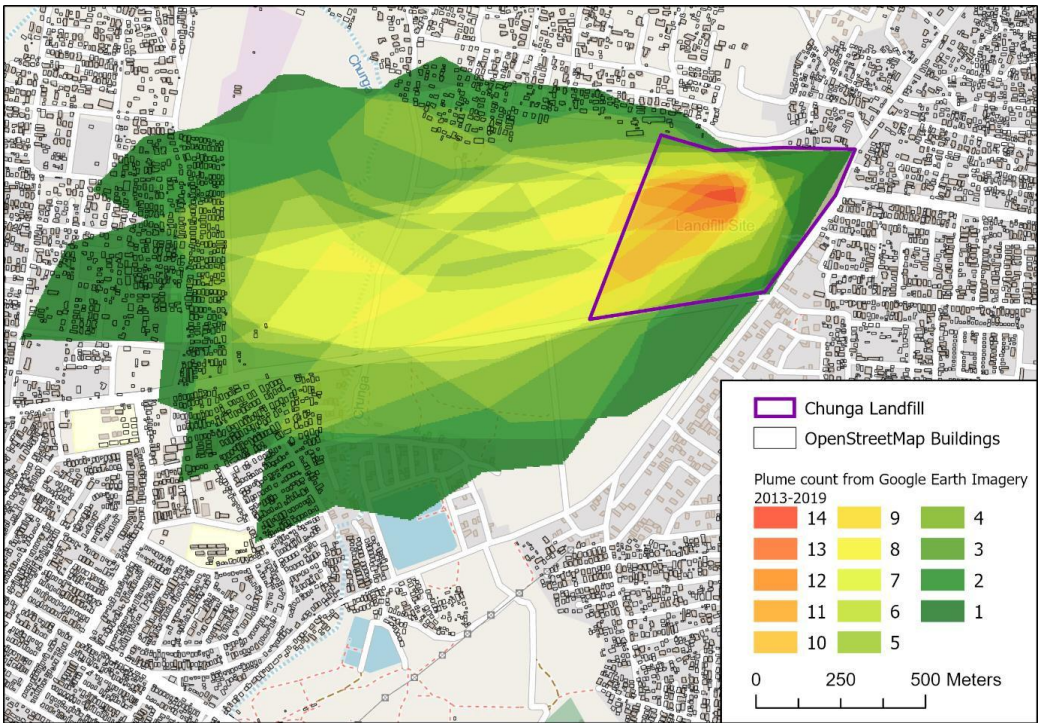


**Figure 6.** A Map of Households Under risk of plume from Chunga Landfill as evidenced by communities under plume layers to the west and south west of the landfill. This map is based on visual observation of plume and also maps plume density. The Map Legend shows plume cover from 2013 to 2019 (Esri. OpenStreetMap Basemap data © OpenStreetMap contributors, 2021).

**Figure 7.** Smoke Plumes from subsurface fires at Chunga landfill resulting from multiple fire focal points across the landfill. The Plume blows primarily west to south west affecting residents of surrounding communities (Aerial Image taken at the landfill site).

activity with an average area cover of 41 ha. There was a noticeable drop in plume coverage between 2015 and 2017, with a drastic increase in plume area between 2017 and 2019. The area covered by plumes increased to 110 ha in 2018, and increased further in 2019 to the highest observed plume cover of 133 ha. Results show that 2013 was the first year we can detect in which smoke plume at the landfill became visible on satellite images and the area covered progressively increased until 2015 when it decreased but as still present. The increased extent of plume coverage in 2018 and 2019 is observed to reach residential properties within the surrounding communities. Figure 8 show that fire plumes were not observed from the data prior to 2013 and have recently increased since 2017.

## DISCUSSION

Fires at the Chunga landfill have been a cause for concern due to their continuous presence over a significant time period the contents of the waste plumes, and the distribution of plumes resulting from these flames. The cause of these fires is mainly attributed to production of methane and other flammable gases from organic waste (Luke, 2017), resulting in plumes that are observed to travel primarily Westwards and South-Westwards from the Chunga site, driven by predominant Easterly winds throughout the year. The analysis of plume data generated from primary research and Google Earth image analysis from 2007 to 2019, and resulting data were used to construct a plume density and direction map (Figure 6). Each plume polygon was examined to interpret which areas produced the highest-lowest density and most frequent plume trajectories over the 13 years of analysis. The region directly west of the landfill has the highest impact with 9 to 14 cumulative polygon segments. It is evident from Figure 6 that the dominant plume direction is just south of west (c. 260º using the metric scale of geographical compass orientation) but varies between SW and just north of west (215º to 280º). These directions result from predominantly easterly winds, measured to move at an average speed of 4.5m/s (Fant et al., 2016). The Lusaka/Zambian Meteorological Office produce data of wind directions for Lusaka and these indicate predominant Easterly winds, with weaker

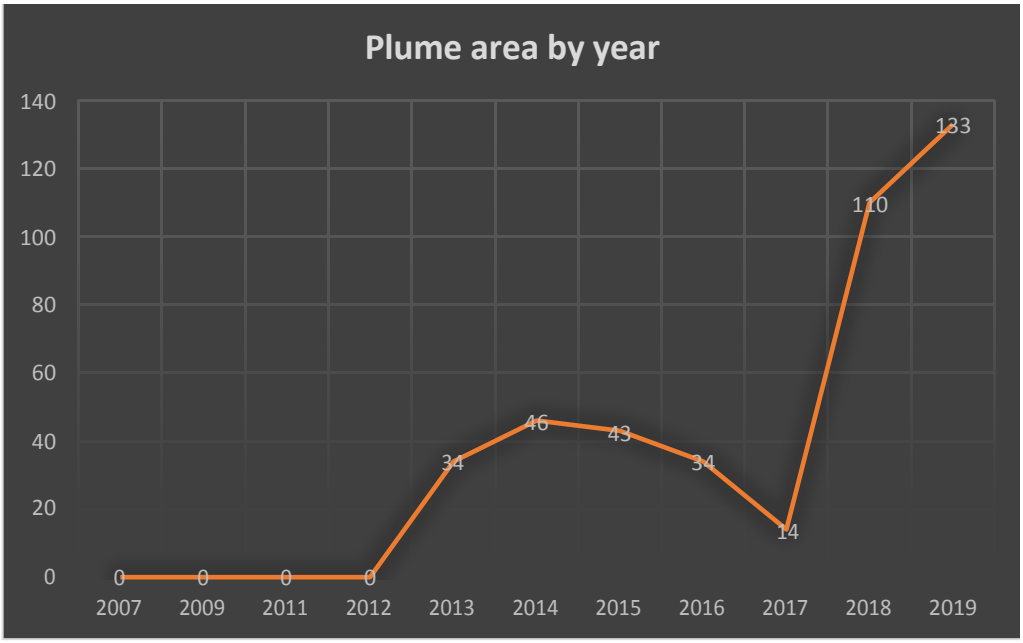


**Figure 8.** The plot of the average smoke plume area resulting from Chunga landfill between 2007 and 2019, showing the first satellite images of plume in 2013 with an average area of 13 (Ha).

southerly and northerly winds blowing during January-March, in addition to the easterly winds (Meteoblue, 2019). This suggests that the footprint of plumes could be more extensive with plumes extending north-south during certain seasons. Our research, however, did not capture north-south plume directions. The contaminant plumes directly affect people at the landfill site, including staff, visitors, and waste pickers. Many other plumes may not have been recorded via the Google photographs, and it has also been theorized that with distal distance from the fire source the plumes will decrease in density, and become less visible to satellite images. Estimates from visible plumes are at the lower end of the likely number of residents impacted by the plumes. However, even if only 800 to 1000 households are directly impacted by fire-plumes, this indicates that a population of c. 4000 -5000 Lusaka residents is at risk to PHS derived from Chunga Land Fill Site Fire- Plumes, using the figure of c. 5 people per household in Lusaka (Zamstats, 2015). This represents a significant public health exposure hazard for the households that are observed under the plume layers created by the landfill fires. Plumes are most dense at proximal locations, and least dense at distal locations.

Residential structures, as far away as 3 km west of the waste site are affected by a single distal plume layer, including a primary school to the south west, Namando Primary school (Figure 6). Houses within 1-2 km west of Chunga are particularly impacted by denser plumes. The plume primarily affects the residents of the low cost, high density Chunga and Lilanda settlements. The effect on public health could be significant, although no studies of impacts have been undertaken. Due to the non-segregation of waste at the Chunga Landfill site, materials that will burn probably include: plastic; cloth; wood; rubber; organic materials; domestic waste; industrial waste; and possibly even chemicals. A wide range of potentially harmful substances that can have an impact on human respiratory systems are present, in addition to potential longer-term medical impacts resulting from the ingestion of heavy metals, organic compounds, and a range of gases. Pollutants could include: benzene; furans/ dioxins; and a range of solid particulate matter in suspension (PM2.5) (Weichenthal et al., 2015). Research by (Weichenthal et al., 2015), found increased concentrations of dioxins/furans and benzene in the atmosphere caused by landfill fires produced at a landfill in Iqaluit Canada. The presence of NO2, (Nitrogen dioxide) O3, (Ozone) and PM2.5.

(Particulate matter of diameter < 2.5 micrometre) was detected. Similar research by (Toro and Morales, 2018), observed an increased PM2.5 concentration of 200µg m−3 after 3 days of monitoring a landfill fire at the Santa Mata landfill in Chile. These toxins pose a health risk to vulnerable populations particularly children, pregnant women, the elderly, and/or individuals with pre-existing chronic respiratory conditions (Krzyzanowski and Cohen, 2008).

For Low Income Countries like Zambia, many individuals from the aforementioned vulnerable populations earn a living from the landfill as waste pickers. Waste pickers earn a living by picking “valuable” and unrecycled waste such as plastic and metals, which they resell to recycling

companies. However, for recyclable materials to effectively reach recycling stations, stake holders such as the Lusaka City Council should upscale efforts to encourage the separation of waste before it reaches the landfill.

This research has implications for policy and management related to landfill sites not only at Chunga, but by extrapolation to other landfill sites in Lusaka and elsewhere. The authors suggest the following framework for landfill management be adopted: 1) for waste to be increasingly sorted and segregated with different disposal options developed for different types of waste. At the very least the more combustible, and organic waste elements should be separated and perhaps composted rather than disposed amongst other waste types. 2) For methane and gas evacuation pipes to be inserted into the Chunga Site in a systematic rectilinear manner to be disposed of in a different manner to other waste types. Alternately these biogases can be collected and used for energy purposes, whilst at the same time reducing contributions to atmospheric greenhouse gases; 3) rapid extinguishing of any fires be that remain following better waste sorting to be undertaken; 4) weekly monitoring of the landfill site by UAV and on-the-ground inspections to be undertaken; 5) active weekly monitoring of air quality and specific analysis of pollutant species to be undertaken by the Lusaka City Council; 6) the design of a communication strategy that aims to engage in more proactive communication and consultations with local residents and other stakeholders in waste management at Chunga; 7) the further drafting of medium-long term waste management policy in Lusaka that takes account of the rapid growth in urbanisation and resultant waste production.

Extinguishing of landfill fires that cause massive plume smoke reduces the risk of respiratory complications in the communities particularly west, south west and North West of the landfill. The authors encourage Landfill Operators put into practice an action framework that effectively deals with landfill fires. It is therefore recommended to improve Landfill Gas Collection to prevent methane release. Methane collected could be used for energy production as demonstrated by Sweden and other Developed and Developing Nations (Finnveden et al, 2007). This has the added advantage of limiting additional greenhouse gas contributions to the atmosphere.

Weekly monitoring is recommended at Chunga landfill using photogrammetry. This would allow the assessment of waste heap slopes, volume, Landfill Fires, smoke plume resulting from fires, and the drainage status. Photogrammetry is cost effective and presents an opportunity for managers to continuously monitor the status, public and environmental impact of Chunga Landfill. They acknowledge that any temporal trends are based on a limited amount of data. The authors' results demonstrate that there is a significant fire-plume issue relating to the Chunga Landfill site, that this hazard varies in intensity, and there is a suggestion that it will become an increasingly important issue as more material is deposited within the Landfill Site.

Future research is needed to understand the impact so far that Chunga landfill has had on soil, air and ground water quality as these aspects are directly related to public health.

Zambia's population is pegged to double over the next decade and hence the need to focus on research into reduced pollution from Landfill waste to improved soil quality for agriculture, clean drinking water and improved air quality for susceptible communities.

## Conclusion

The immediate and most visible risk to the environment and surrounding communities comes from constant smoke plume resulting from landfill fires first recorded in 2013. Results show that between 2013 and 2019, the area covered by smoke plume has increased from an average of 34 ha to 143 ha, respectively. Smoke plume is observed to be carried south west, west and North West of the landfill by primarily easterly winds throughout the year. The landfill is surrounded by high densities communities. The western direction in which plume is carried, at an average speed of 4.5 (m/s), puts these communities in the west, north west and south west are most at risk. The dry season in Lusaka lasts between May to October and therefore, this time of the year results in a greater wind distribution of particulate matter.

## CONFLICT OF INTERESTS

The authors have not declared any conflicts of interests.

## ACKNOWLEDGEMENTS

Milimo Muleya gratefully acknowledges a New Zealand Ministry of Foreign Affairs and Trade (MFAT) Scholarship that funded his research and scholarship at AUT, Auckland, New Zealand.

## REFERENCES

Chishiba J (2002). Environmental monitoring and operations manual for Chunga Waste Disposal Site. Lusaka City Council.

Edema MO, Sichamba V, Ntengwe FW (2012). Solid waste management-case study of Ndola, Zambia. International Journal of Plant, Animal and Environmental Sciences 2(3):248-255.

Esri. (2021). "World Imagery" [basemap]. Scale Not Given. "World Imagery Map". November 10, 2021.

Esri. OpenStreetMap Basemap data © OpenStreetMap contributors, M., Esri Community Maps contributors, Map layer. (2021). "OpenStreetMap Vector Basemap" [basemap]. Scale Not Given. "OpenStreetMap".

EsriTM (2019). ArcGIS Desktop. Retrieved from https://www.esri.com/en-us/arcgis/products/arcgis-desktop/resources

Fant C, Gunturu B, Schlosser A (2016). Characterizing wind power

resource reliability in southern Africa. Applied Energy 161:565-573.
Finnveden G, Björklund A, Reich MC, Eriksson O, Sörbom A (2007). Flexible and robust strategies for waste management in Sweden. Waste management 27(8):S1-S8.
GoogleEarthPro (2019). Lusaka City Dump Site, Lusaka, Zambia. Retrieved from Lusaka City Dump Site, Lusaka, Zambia
Hoornweg D (2013). Waste production must peak this century. Nature. Retrieved from https://www.nature.com/polopoly_fs/1.14032!/menu/main/topColumns/topLeftColumn/p df/502615a.pdf
Hoornweg D, Bhada-Tata P, Kennedy C (2013). Environment: Waste production must peak this century. Nature News 502(7473):615.
Jurbin T (2003). Landfill fires. Canadian Consulting Engineer. https://www.canadianconsultingengineer.com/features/landfill-fires/
Krzyzanowski M, Cohen A (2008). Update of WHO air quality guidelines. Air Quality, Atmosphere and Health 1(1):7-13.
Lohmann R, Jones KC (1998). Dioxins and furans in air and deposition: a review of levels, behaviour and processes. Science of the Total Environment 219(1):53-81.
Luke M (2017). Waste as a Resource: Development Opportunities within Zambia's Waste Value Chain and Management System. Research Gate.
Meteoblue (2019). Wind maps lusaka. Retrieved from https://www.meteoblue.com/en/weather/forecast/windmap/lusaka_zambia_909137
PopulationStats (2020). Lusaka Zambia Population. Retrieved from https://populationstat.com/zambia/lusaka
S.R.O CR (2019). Retrieved from https://www.capturingreality.com/
Stearns RP, Petoyan GS (1984). Identifying and controlling landfill fires. Waste Management and Research 2(1):303-309.
Toro R, Morales L (2018). Landfill fire and airborne aerosols in a large city: lessons learned and future needs. Air Quality, Atmosphere and Health 11(1):111-121.
Volodina K (2020). What Is NTRIP and How to Use It for RTK with Reach.
Wampler PJ, Rediske RR, Molla AR (2013). Using ArcMap, Google Earth, and Global Positioning Systems to select and locate random households in rural Haiti. International Journal of Health Geographics 12(1):3.
Weichenthal S, Van Rijswijk D, Kulka R, You H, Van Ryswyk K, Willey J, Baike M (2015). The impact of a landfill fire on ambient air quality in the north: A case study in Iqaluit, Canada. Environmental Research 142:46-50.
Zamstats (2015). Average Household Size. Retrieved from https://zambia.opendataforafrica.org/dajivbb/living-conditions-statistics#
ZEMA (2019). National Inventories for Location of Dumpsites, Landfills and Related Hotspots in Zambia Retrieved from https://stopopenburning.unitar.org/site/assets/files/1097/zambia_inventory_report.pdf.
Zhang M, Buekens A, Jiang X, Li X (2015). Dioxins and polyvinylchloride in combustion and fires. Waste Management and Research 33(7):630-643.

## Related Journals: